DEVELOPMENT OF A SOLID-GAS COUPLED MODEL FOR THERMALLY THICK BIOMASS COMBUSTION IN PACKED BEDS

Kulupanage Upuli Chathurika Perera

(148022U)

Thesis submitted in fulfillment of the requirement for the Degree Doctor of Philosophy of Engineering in Chemical and Process Engineering

Department of Chemical and Process Engineering

University of Moratuwa

Sri Lanka

January 2020

DECLARATION

“I declare that this is my own work and this thesis does not incorporate without acknowledgement any material previously submitted for a Degree or Diploma in any other University or institute of higher learning and to the best of my knowledge and belief it does not contain any material previously published or written by another person except where the acknowledgement is made in the text".

"Also, I hereby grant to University of Moratuwa the non-exclusive right to reproduce and distribute my thesis, in whole or in part in print, electronic or other medium. I retain the right to use this content in whole or part in future works (such as articles or books)".

Signature: Date:

The above candidate has carried out research for the PhD thesis under my supervision.

Name of the supervisor: Prof. Mahinsasa Narayana

Signature of the supervisor: Date:

ACKNOWLEDGEMENTS

I would like to pay my heartiest gratitude to my supervisor Prof. Mahinsasa Narayana for his guidance and patience he had on me. I would also like to thank Prof. Shantha Amarasingha, Prof. P.G. Ratnasiri and Dr. Maneesha Gunasekara for their valued comments given in the progress review sessions.

Dr. Sanja Gunawardena, Head of the Chemical and process Engineering Department and all the lecturers of the department should be mentioned with sincere gratitude.

I would like to thank all the staff members of Chemical and process Engineering Department for their support in various ways during the research.

I am very much thankful to the Department of Chemical and Process Engineering for providing me with the experimental facilities for the research. Department of Materials Science and Engineering and Department of Mechanical Engineering should be mentioned with gratitude for providing experimental facilities and support in different occasions.

I would like to thank the Vice Chancellor, the Dean, Faculty of Enginnering Technology and the Head, Department of Mathematics and Philosophy of Engineering, The Open University of Sri Lanka for granting me study leave for this research, which otherwise would not have been a reality. I'm also thankful to staff memebrs of the Department of Mathematics and Philosophy of Engineering, The Open University of Sri Lanka.

I would also like to pay my sincere thanks to Mr. Kapila Peiris, Ms. Y.M.M.K. Ranathunga and Mr. Nandana Edirisingha for providing me the necessary data for the research. I wouls also like to pay my sincere gratiutude to Ms. Yamuna Pathiraja and Ms. Niluka Athukorala for being suerities of the bond for study leave.

I am thankful to my friend Dimuthu Rajapaksha for providing me with the experimental data in this research. I am thankful to my colleagues, Thamali Jayawickrama, Niranjan Fernando, Kethaki Wickramarachchi, Chathuranga

Wickramasingha, Gayani Jayathunga and all other friends for their support for me and valuable ideas shared.

Finally, I am very much thankful to my parents and the family for their support to make this research a reality.

Abstract

The aim of this research is to model the moving grate combustion process by Computational Fluid Dynamics (CFD) method by OpenFOAM software. Kinetic data for heterogeneous reactions, specific to local fuel types is essential. Therefore, pyrolysis kinetics of Rubber and Gliricidia was evaluated by two methods; the sequential approach for Kissinger method and Miura and Maki approach for Ditributed Activation Energy Model (DAEM). The activation energy values obtained by the sequential spproach for Kissinger method are 107.9 $kJmol^{-1}$ for Gliricidia and 83.44 $kJmol^{-1}$ for Rubber wood. Obtained activation energy by Miura and Maki approach for DAEM, varies between 190.57 $kJmol^{-1}$ and 230.58 $kJmol^{-1}$ for Gliricidia and between 111.52 $kJmol^{-1}$ and 179.07 $kJmol^{-1}$ for Rubber wood.

A CFD model was developed which describes the wood combustion in fixed grate type packed bed furnaces. Linear rate of mass loss observed in batch type simulations can be used to describe the steady state burning characteristics of a continuously operated furnace which has a feeding rate equal to burning rate. This mass loss rate was used to evaluate Equivalence Ratio (ER) variation for different particle sizes of wood. A sensitivity analysis was conducted to find the effect of moisture content and particle size on ER. It was found that moisture content of wood has more significant effect on ER than the particle size. The optimum equivalence ratio was studied based on the maximum outlet gas temperature with minimum CO fraction for different particle sizes of wood. The optimum ER values obtained were 0.28 for 25 mm sized particles, 0.13 for 38 mm sized particles and 0.18 for 63 mm sized particles.

The model was elaborated to simulate wood combustion in moving grate type furnaces. This heterogeneous model developed within Eulerian framework, includes the grate movement through boundary conditions, which can solve both bed and free board region simultaneously.

Keywords: Computational Fluid Dynamics, packed beds, combustion, moving grate furnaces

TABLE OF CONTENTS

LIST OF FIGURES

LIST OF TABLES

LIST OF ABBREVIATIONS

Abbreviation	Description
CFD	Computational Fluid Dynamics
DAEM	Distributed Activation Energy Method
DNS	Direct Numerical Simulation
DOM	Discrete Ordinates Model
DPM	Discrete Particles Models
DTM	Discrete Transfer Method
ER	Equivalence Ratio
FVM	Finite Volume Method
FWO	Flynn–Wall–Ozawa
KAS	Kissinger–Akahira–Sunose
LES	Large Eddy Simulation
RANS	Reynolds Averaged Navier-Stokes
RTE	Radiative Transfer Equation
TGA	Thermo Gravimetric Analysis

LIST OF NOMECLATURE

Symbol	Description
A	pre-exponential factor (s^{-1})
A_{spec}	volume specific surface area (m^{-1})
A_p	projected area (m^2)
a_g	absorption coefficient of gas (m^{-1})
a_s	absorption coefficient of solid (m^{-1})
C_i	concentration of gases ($molm^{-3}$)
C_1, C_2	constants used in standard k-epsilon equation
C_{pg}	specific heat capacity of gas ($Jkg^{-1}K^{-1}$)
C_{ps}	specific heat capacity of solid ($Jkg^{-1}K^{-1}$)
$D_{a,I}$	effective diffusivity of species i through ash layer (m^2s^{-1})
D_i	binary diffusivity of species i in air (m^2s^{-1})
$D_{k,i}$	Knudsen diffusivity of species i (m^2s^{-1})
$D_{eff,i}$	effective diffusivity of species i (m^2s^{-1})
d_p	particle diameter (m)
$d_{p,o}$	initial particle diameter (m)
d_{pore}	pore diameter (m)
E	activation energy ($Jmol^{-1}K^{-1}$)
E_p	radiation emission from particles (Wm^{-3})
G	radiation intensity (Wm^{-2})
e	emissivity
$H_{g,i}$	heat of reactions gas phase reactions (Jkg^{-1})
H_m	heat of evaporation (Jkg^{-1})
$H_{s,i}$	heat of reactions solid phase reactions (Jkg^{-1})
h	convective heat transfer coefficient ($Wm^{-2}K^{-1}$)
$h_{m,a,i}$	mass transfer coefficient of i^{th} gaseous component through ash layer (ms^{-1})
h_{mi}	mass transfer coefficient of i^{th} gaseous species in boundary layer (ms^{-1})
$h_{mi,eff}$	effective mass transfer coefficient (ms^{-1})
k	turbulent kinetic energy (m^2s^{-2})

k_i	kinetic reaction rate of char with i^{th} gaseous component (ms^{-1})
$k_{i,eff}$	effective reaction rate (ms^{-1})
l_a	ash layer thickness (m)
M_{air}	air molar weight ($kgmol^{-1}$)
M_c	carbon molar weight ($kgmol^{-1}$)
M_i	species molar weight ($kgmol^{-1}$)
m_0	initial mass of sample (kg)
m_f	final mass of sample (kg)
$m_{s,i}$	mass of solid phase constituents in a computational cell (kgm^{-3})
$m_{s,w}$	mass of water in a computational cell (kgm^{-3})
m	mass (kg)
n	reaction order /refractive index
Nu	Nusselt number
P	pressure (Pa)
Pr	Prandtl number
$Q_{rad,g}$	radiation heat source term ($Jm^{-3}s^{-1}$)
R	universal gas constant ($kJK^{-1}mol^{-1}$)
Re	Reynolds number
$R_{g,i}$	gas phase reaction rate i^{th} species ($kgm^{-3}s^{-1}$)
R_{ki}	gas phase kinetic reaction rate of i^{th} species ($kgm^{-3}s^{-1}$)
$R_{mix,i}$	gas phase mixing rate i^{th} species ($kgm^{-3}s^{-1}$)
$R_{s,i}$	solid phase reaction rate ($kgm^{-3}s^{-1}$)
$R_{s,w}$	rate of drying ($kgm^{-3}s^{-1}$)
$S_{g,i}$	summed production rate of i^{th} gas species in gas phase reactions ($kgm^{-3}s^{-1}$)
Sh	Sherwood number
S_{ij}	turbulent stress tensor (Pa)
S_m	momentum resistance source term ($kgm^{-2}s^{-2}$)
$S_{s,i}$	summed production rate of i^{th} gas species in solid phase reactions ($kgm^{-3}s^{-1}$)
T_{evap}	evaporation temperature (K)
T_g	gas phase temperature (K)

T_s	solid phase temperature (K)
t	time (s)
u	velocity (ms^{-1})
u_{bed}	bed velocity (ms^{-1})
u_{grate}	grate velocity (ms^{-1})
V_{cell}	volume of cells (m^3)
X_a	mass fraction of ash
x	conversion
Y_i	mass fraction of gas species i
Y_b	mass fraction of bound water in solid phase
Y_w	mass fraction of water in solid phase

Greek symbols

α	mass fraction
β	heating rate in pyrolysis kinetic determination/solid cell identification factor shrinkage model
γ	factor of bed height change
ε	turbulent dissipation rate
λ_g	thermal conductivity of gas ($Wm^{-1}K^{-1}$)
λ_s	thermal conductivity of solid ($Wm^{-1}K^{-1}$)
μ	viscosity ($kgm^{-1}s^{-1}$)
μ_t	turbulent viscosity ($kgm^{-1}s^{-1}$)
ρ_a	ash density (kgm^{-3})
ρ_g	gas density (kgm^{-3})
ρ_s	solid density (kgm^{-3})
σ	Steffan Boltzmann constant ($Wm^{-2}K^{-4}$)
$\sigma_{i,air}$	collision diameter (A)
σ_ε, σ_k	model constants in standard k-epsilon equation
σ_s	scattering coefficient
τ	stress tensor (Nm^{-2})

ϕ	porosity
ϕ_a	ash layer porosity
$\Omega_{c,i}$	stoichiometric coefficient of i^{th} heterogeneous reaction
$\Omega_{g,i}$	stoichiometric coefficient of i^{th} gas phase reactions
$\Omega_{c,o}$	stoichiometric coefficient of char oxidation reactions
$\Omega_{g,i,o}$	stoichiometric coefficient of i^{th} gas phase oxidation reaction
$\Omega_{i,air}$	collisional integral

LIST OF APPENDICES

Chapter 1

INTRODUCTION

1.1 Introduction

Biomass is an important source of renewable energy. It accounts for the largest share in the industrial energy usage in Sri Lanka in the form of fuel wood. Tea, brick and tile are the main industrial consumers of fuel wood. Current rate of fuel wood consumption, which is 33 kt per day is presumed to make a scarcity in fuel wood in Sri Lanka in future [1]. Rubber wood is the main variety of fuel wood used by industries. Rubber wood has experienced an increasing demand as a timber source in the recent years. Therefore, shifting towards other fuel wood varieties such as Gliricidia, saw dust and cut-offs from saw mills and timber mills can be observed [2]. Increasing demand with limited supply has increased the price of fuel wood and the existing pattern of demand and supply is predicted to create adverse effects on the environment.

The contribution from fuel wood is mainly used for thermal energy production in furnaces by combustion. Larger contribution from fuel wood as a renewable energy source does not itself guarantee efficient and cleaner combustion process. Good example is tea industry, which is one of the largest consumer of fuel wood, where average thermal efficiency of a wood furnace is about 50% [3].

Furnaces used in the industrial sector are of packed bed type due to less processing required and the capability of burning wide variety of fuel wood with different moisture contents. Many of the furnaces are operated manually. Therefore, technological interventions are limited in the field of furnace design and operation.

The fuel wood used in these furnaces is mainly in the form of logs (Figure 1.1). A formal supply method of processed fuel wood has not been observed until recent past. Sustainable Energy Authority of Sri Lanka has initiated a code of practice on Sustainable Growing and Harvesting of Fuel wood. Several large-scale pre-

processing and collection centers have been established closer to end user industries under United Nations Development funds.

Figure 1.1 Packed bed wood burning furnace used in tea industry

With the increasing demand for fuel wood by industries and development of fuel wood supply as a commercial commodity, there exists a requirement to utilize it in a sustainable manner. Sustainable usage of fuel wood in thermal applications is guaranteed by efficient combustion with less pollutant. Good understanding of packed bed combustion is required to control the parameters which affect the combustion and to achieve efficient combustion with less pollutant.

Fuel wood which is in the form of wood logs or wood chips is burnt commericially in packed bed arrangements in boilers or furnaces. A good understanding on the combustion process assists the control of combustion which directs the way to achieve better efficiencies with less pollution. Cost and time requirement for experimental studies of combustion in boilers are high. Changing the independent variables throughout its full spectrum is not practical and full spatial description of the dependent parameters cannot be obtained in experiments. Numerical modelling with Computational Fluid Dynamics (CFD) technique offers an alternative method of

studying relationship between different parameters by providing the details of the parameters within the entire furnace domain.

1.2 Objectives

Being an economical alternative to fossil fuel, fuel wood usage in the industrial sector in Sri Lanka has increased. Initiatives were taken to develop the fuel wood as a commercial energy commodity. With the increasing demand for fuel wood, associated technology for fuel wood conversion must be developed for sustainable utilization. Fuel wood in Sri Lanka is mainly combusted in traditional packed bed furnaces to produce thermal energy. Behaviour of these furnaces is similar to that of moving grate type furnaces. Therefore, the main objectives of this research are, to develop a transient two-dimensional mathematical model for combustion of thermally thick biomass particles under packed bed conditions using CFD approach.

The main objectives are

(i) Evaluation of pyrolysis kinetics of Gliricidia and Rubber wood types

(ii) Development of numerical model to simulate packed bed combustion of thermally thick wood particles

(iii) Analysis of optimum Equivalence Ratio (ER) for different sizes of wood particles

(iv) Development of comprehensive transient mathematical model to solve both gas phase and solid phase in a single domain.

1.3 Thesis outline

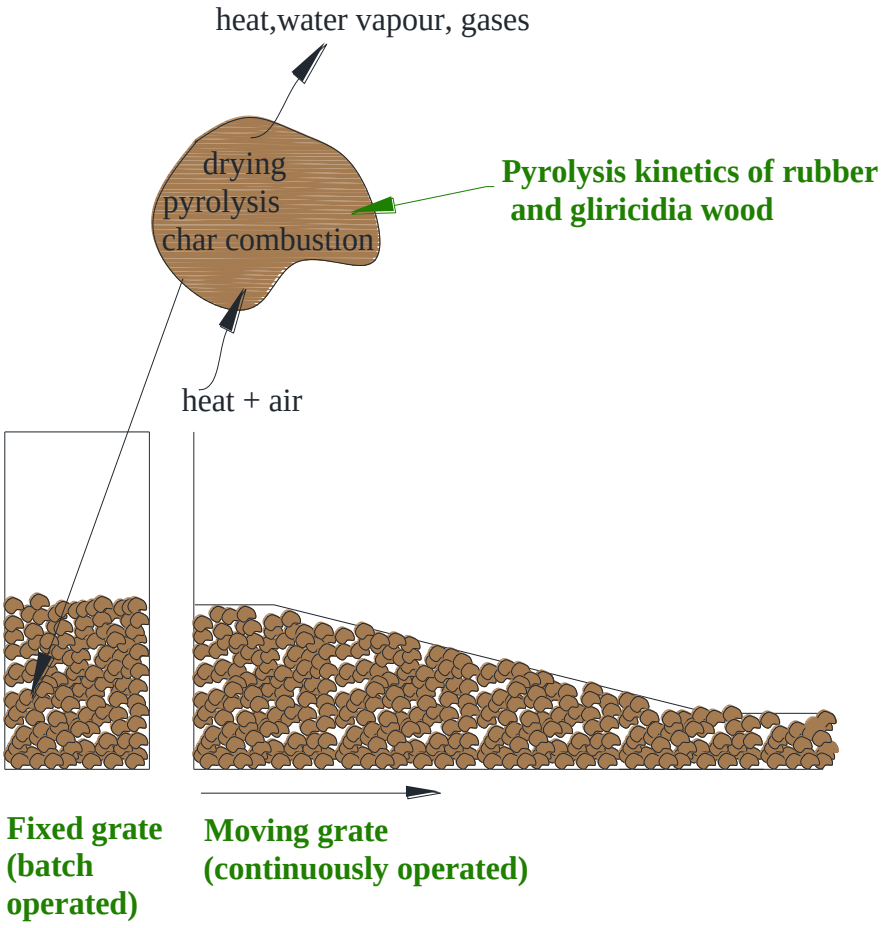

Figure 1.2 Overview of the thesis

Chapter 1 includes a brief introduction on fuel wood usage and industrial applications of packed bed combustion and the background for the research. The final objective of this research is to model wood combustion in moving grate furnaces through CFD approach. In order to achieve this objective, this research was conducted in three main sections, which are presented in separate chapters as described below. Review of packed bed combustion and mathematical modelling of packed bed combustion is presented in Chapter 2.

Kinetic data related to pyrolysis is of vital importance for combustion modelling studies. Therefore, pyrolysis kinetic data was evaluated for Rubber and Gliricidia wood types by Thermo Gravimetric Analysis (TGA) which is described in Chapter 3.

A comprehensive mathematical model was developed to analyse biomass packed bed combustion and solved by a Computational Fluid Dynamics platform (Chapter 4). The model includes description of solid phase thermal conversion, gas phase reactions, effect of turbulence, radiation and bed shrinkage. The packed bed combustion model was validated and model was used to analyse the variation of Equivalence Ratio (ER) with different wood particle sizes in packed bed combustions (Chapter 5). A sensitivity study was carried out to evaluate the effect of particle size and moisture content on ER. Model was further extended to model wood combustion in moving grate furnaces. The simulations on moving grate combustion of wood fuel are included in Chapter 6. Each section of the study, kinetic study of fuel wood types, packed bed combustion model and ER analysis and moving grate combustion model includes separate conclusions related to respective analysis.

Chapter 7 includes overall conclusions of the study and recommendations for future work.

Chapter 2

CFD MODELLING OF WOOD COMBUSTION IN PACKED BED FURNACES

2.1 Packed bed combustion

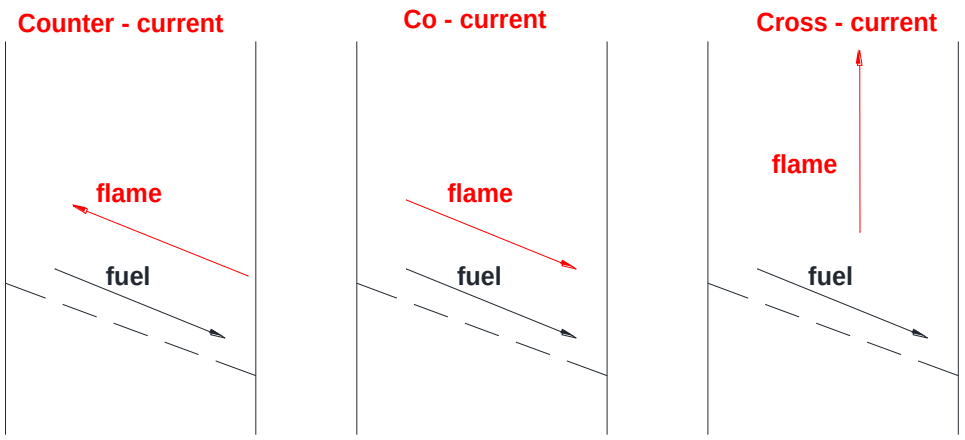

Figure 2.1 Classification of packed bed furnaces according to direction of flame and direction of fuel movement [4]

Fuel rests on a grate and air is supplied under the grate in packed beds. Packed beds can be classified into three categories according to the direction of flue gas flow and fuel movement. In counter-current bed arrangement hot gases pass through the fresh fuel fed into the bed. It vaporises the moisture in fresh fuel. Pre-heated air is used in co-current bed arrangement. Fuels that have low moisture content are suitable for this type of bed arrangements. In cross-current flow arrangement mixture of counter current and co-current flow conditions can occur. Packed bed combustion is the simplest combustion arrangement and requires minimum fuel pre-processing. Larger sized fuel particles can be burnt in packed beds. The particles which are burnt in packed bed furnaces are mainly in thermally thick (Bi>1) regime. Fuels with different compositions can be fired in packed beds. Wood is a made up of cells which mainly contains cellulose, hemicellulose and lignin. In addion to that lower molecular compounds and ash is contained in wood. Wood is an anisotropic material

and its structure affects the transport mehanisms. Therefore, wood combustion is complex and highly variable in nature.

In a packed bed, fuel particles exchange heat with the neighbouring particles by conduction. Flow of gas through the bed carries heat from high temperature zones which heat the low temperature zones by convection. Turbulence flow characteristics affect gas phase reactions. Once the bed and the walls of the combustion chamber reach high temperatures, radiation heat transfer becomes significant.

During thermal conversion, wood particle reduces weight and size. Particles at the bottom of the bed which reduce their size, allow the particles lying on top to move downwards. This movement of wood particles affects the heat and mass transfer process. Irregularity in bed conversion makes the bed porosity to vary within the bed and makes the bed combustion a highly complex process.

Fuel undergoes drying, pyrolysis and char combustion while it stays on the bed. Simultaneous and sequential occurrence of these processes causes irregular conversion of fuel in the packed bed. Volatile gases released by solid phase reactions are burnt in gas phase. These gas phase reactions inturn generate the heat required for solid phase reactions. Modelling packed bed combustion process is a complicated task due to above mentioned phenomenae. Different approaches have been presented in literature to model above mentioned phenomenae. These models will be discussed in following sections.

2.2 Drying

It is reported that freshly cut woody biomass has a moisture content of 30% -60% w/w [5]. Moisture in the wood is in the form of free water or bound water. Liquid water exists in cell cavities are termed as free water. Water attached to cell walls through hydrogen bonds is termed as bound water. When the cell-walls are saturated with water with no free water exists in the cell cavities, moisture content is defined as the Fibre Saturation Point. Free water evaporates in the initial step of drying and then the bound water. Water evaporation ceases at equilibrium moisture content when vapour pressure of water within the wood equals to ambient vapour pressure.

Packed bed combustors have the capability of burning fuels with variety of moisture contents. Since drying is endothermic, an upper limit exists for the moisture content, which is mentioned as 60% of the total mass [6], above which the combustion of fuel can not produce net heat. Different models have been presented in literature to describe drying: Heat sink model, first order kinetic rate model, equilibrium model and transport model [7]. These models are discussed below.

2.2.1 Heat sink model

This model assumes that drying occurs at a pre-defined temperature. Drying rate is controlled by heat transfer. Heat sink drying model assumes drying occurs in an infinitesimally thin layer. Therefore, this model is suitable for the conditions where drying front is significantly smaller than the particle size. Heat sink model has been used to model combustion of thermally thin particles [8] in addition to, thermally thick particles [9], [10]. This model can predict the drying plateau at the evaporation temperature. Sand et al [11] used heat sink model to predict drying rate in which he estimated equilibrium vapour pressure to calculate evaporation temperature for different moisture contents in pyrolysis of wet wood logs .

2.2.2 First order kinetic rate model

First order kinetic rate model assumes that drying rate depends on moisture content and temperature of the particle. This model can be easily implemented and shows numerical stability. Use of kinetic rate model is valid for the experimental conditions under which, kinetic parameters have been obtained. Peters and Bruch [12] compared the results of heat sink model and kinetic rate model with experimental results. He found with the kinetic parameters presented by Chan et al. [13], that kinetic rate model under predicts drying rate. Peters and Bruch [12] further concluded that kinetic rate drying model is unsuitable for larger particles where heat transfer becomes the rate limiting step. Exceptions can be found in literature where kinetic rate evaporation model was used by Lu et al to calculate bound water evaporation rate in thermally thick wood particles [14] .

2.2.3 Equillibrium drying model

This model calculates drying rate based on the vapour - liquid equilibrium of moisture. This model is applied to calculate drying rate at low temperatures. Since the model predictions are based on mass transfer coefficient, it has to be adjusted to match with data obtained under fast drying conditions. This model was used to predict free moisture evaporation of thermally thick wood particles in [14]. Good agreements were made between simulated results and experimental results for wet wood logs. Wurzenberger et al [15] used equilibrium drying model to predict temperature profiles and mass loss profiles of thermally thick particles.

2.2.4 Transport drying model

Transport drying model accounts for detailed transport mechanisms in the drying process. It includes description of the transport of liquid water, bound water and water vapour. This model was used by Grønli [16] and separate conservation equations were solved for free water and bound water.

2.3 Pyrolysis

Biomass thermally converts into gas, tar and char in inert environments which is identified as pyrolysis. Heating rate, temperature variation during pyrolysis, particle size and shape, pressure, moisture content and chemical composition are main controlling factors in pyrolysis [16]. In combustion fuel is rapidly heated to high temperatures, which produces volatiles and char. The released volatiles prevent oxygen from entering to the particle, therefore, create oxygen depleted environment favourable for pyrolysis. Pyrolysis takes place between 200 -500 ^{o}C. Variety of models has been used in literature to describe pyrolysis due to its complex nature. Pyrolysis kinetics are determined based on model fitting or model free methods [17]. A brief discussion on pyrolysis models is included in the following section. Model based methods assume that pyrolysis occurrs according to previously defined reaction mechanism and model free methods do not require prior assumptions on pyrolysis mechanism. Pyrolysis kinetics, which is an essential component in

mathematical modelling was studied by model based and model free methods, is described in Chapter 3

2.3.1 Model based methods

Global one-step model

Global one step model is used to describe decomposition of a single constituent according to reaction R2.1. Mass fraction of char formed by the reaction is described by υ. In this model secondary reactions are ignored. This model have been used in modelling of biomass and wood chip combustion in [18]–[23].

$$\text{Wood} \rightarrow \upsilon \text{ char} + (1-\upsilon) \text{ volatiles} \quad \text{(R2.1)}$$

Competitive reaction models

This model assumes formation of pyrolysis products through independent pyrolysis kinetics according to reaction R2.2. The product fractions are decided by chemical kinetics which has independent reaction rate constants (k_i, i=1,2,3) according to the temperature of the solid. Therefore, product fractions have not to be decided in advance. Effect of tar cracking is incorporated in this reaction mechanism by including additional steps [13]. Variations to this model can be found in [16], [17], [24] and used in modelling thermal conversion of biomass in [11], [12], [25].

$$\left.\begin{array}{l} \text{wood} \xrightarrow{k_1} \text{char} \\ \text{wood} \xrightarrow{k_2} \text{tar} \\ \text{wood} \xrightarrow{k_3} \text{gas} \end{array}\right\} \quad \text{(R2.2)}$$

Pseudo component models

Pseudo component models have been developed to model the reactions of pseudo components (cellulose, hemicellulose and lignin) of biomass at their own reaction rate without any interaction with other pseudo components. Therefore, pyrolysis of constituents of biomass; cellulose, hemicellulose and lignin, occurs independently and the interaction between each component during the conversion is not considered

in the model. Cellulose, hemicellulose and lignin content in wood are important in pseudo component model. Therefore, when the mass fraction of each constituent in the fuel and reaction rate constant of each constituent (k_i,i=4,5,6) is known, this model can be used to calculate pyroysis rate. A general form of the model is presented in equation R2.3. Pseudo component model was used by Mehrabian et al [26] to model thermal conversion of biomass particles.

$$\left.\begin{array}{c} \text{cellulose} \xrightarrow{k_4} (1-\upsilon 1)\text{gas}+\upsilon 1\text{char} \\ \text{hemicellulose} \xrightarrow{k_5} (1-\upsilon 2)\ \text{gas}+\ \upsilon 2\text{char} \\ \text{lignin} \xrightarrow{k_6} (1-\upsilon 3)\text{gas}+\upsilon 3\text{char} \end{array}\right\} \text{(R2.3)}$$

2.3.2 Model free methods

Iso conversional [27], [28] and Distributed Activation Energy Method (DAEM) [29], [30] are model free methods which describe the kinetics of pyrolysis. Since a specific mechanism for pyrolysis kinetics is not assumed in advance, errors added by such an assumption will be avoided. Composition of fuel and pyrolysis product distribution have been taken into consideration in DAEM [30].

2.4 Heterogeneous reactions

Pyrolysis of biomass produces char particles which have porous structure. Char particles react with O_2, CO_2, CO, H_2 and H_2O in the surrounding gas. Heterogeneous reactions mainly occur at the surface of the char. Porous structure of char offers larger surface area for the char reactions. Two factors affect the char reaction rate. One is the availability of gaseous species for the reaction and the other one is the kinetic rate of reaction. Three zones of combustion have been identified according to the supremacy of each process (Figure 2.2).

Zone I: Reaction rate is controlled by the kinetic rate of reaction. Diffusion of the reactive gas species is so fast. The concentration of reactant gas at the surface of the char particle is equal to the concentration of reactant gas in the bulk flow.

Zone II: Reaction rate is controlled both by diffusion rate of reactive gas to the surface of the char particle and the kinetic rate of reaction.

Zone III: Reaction rate is limited by the rate of diffusion of gas species to the surface of the particle. The kinetic rate is so fast. Therefore, reactant gaseous species are consumed at the reactive surface before it gets penetrated the char particle.

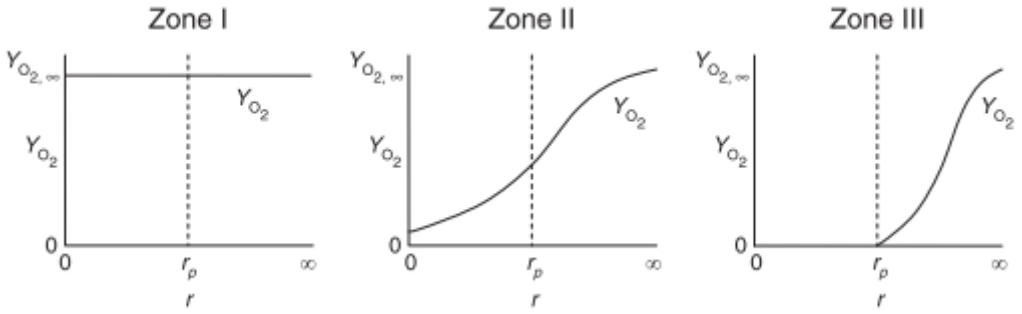

Figure 2.2 Sample oxygen profiles through the char particle boundary layer and the char particle itself during combustion proceeding according to the characteristic burning zones [31].

Zone I combustion is applicable to small particles which burn at low temperatures. Small particle sizes increase the diffusive flux while low temperatures reduce the kinetic rate of reactions. In this type of combustion char particle diameter remains constant while the density reduces evenly throughout particle.

Zone II combustion is applied to conditions where partial penetration of oxygen presents. Char particles which have large internal surface area can have combustion similar to Zone II. Both the particle diameter and density reduce in this combustion regieme.

In Zone III combustion, particle density remains constant while the particle diameter reduces. Combustion of large sized particles in high temperatures occurs in this zone. High temperatures increase surface reaction rate and large sized particles reduce diffusion of oxygen.

Two approaches have been presented in deciding reaction rate of char; apparent kinetic rate and intrinsic kinetic rate. Apparent kinetic rate model is the widely used heterogeneous reaction model. This model does not include the effects of pore structure and char reactivity etc and it is valid for limited pressure and temperature ranges. Intrinsic kinetic rate model requires details on intrinsic reactivity, surface area of pores and local oxidant concentration [7]. These factors vary widely with the type of fuel like biomass. Intrinsic reactivity model better predicts the char reaction rates but requires sufficient data on internal pore structure and reactivity.

2.5 Homogeneous reactions

Volatiles released during pyrolysis and char reactions react with each other in the gas phase. These homogeneous reactions are affected by chemical kinetics and mixing of the reactants. Eddy dissipation, Eddy Break-Up model and laminar flamelet model can be used to describe turbulent non premixed combustion. In Eddy-Break-Up model fuel dissipation rate is described by the turbulent time scale. Therefore, precision of the predictions depends on the turbulent model. Eddy dissipation model has been adapted from Eddy-Break-Up model which utilizes the significance of fine structures on reacting flows [32]. Laminar flamelet model allows incorporating detailed chemistry to turbulent chemistry calculations. Alternative formulations to calculate gas phase mixing rates are used in [23], [33]. Since the predictions of homogeneous reactions are affected heavily by the flow patterns, attention should be given for modelling flow conditions inside the furnace. Therefore, modelling of flow conditions will be discussed in the next section.

2.6 Flow conditions inside the packed bed

Size, shape and orientation of fuel particles affect the flow conditions inside packed beds, hence the combustion in packed beds [34]. Large particles create larger scale turbulence in local bed structure and help cross flow and inflow mixing of gases [35]. Release of gas species may enhance the turbulent effect at low velocities [36]. Increase in flow velocities enhances heat transfer due to turbulence effect [37]. In biomass grate furnaces, flow conditions above the fuel bed lie in the low turbulence

region [38], nevertheless there may be turbulence vortices inside the porous bed [39]. Gas phase reaction rates are influenced by the flow field which is in turn affected by the increased temperatures near the fuel bed. Therefore, a good description of the flow conditions inside the reactor is needed.

Different models have been presented for describing turbulence in packed bed furnaces. Reynolds Averaged Navier-Stokes (RANS), Large-Eddy Simulation (LES) or Direct Numerical Simulation (DNS) equations are presented for turbulent flow calculations [32]. RANS equation calculates effect of turbulence on mean flow properties. The turbulence terms which appear in Navier Stokes equation are solved with turbulence models such as standard k-epsilon model, k-omega model or Reynolds stress model. RANS models like k-epsilon and Reynolds stress model can produce results with good accuracy at less computational time. LES includes the behavior of large eddies in turbulence modelling by filtering off smaller eddies. LES requires higher computer power and is in development stage to be used for industrial applications and for complex geometries. DNS resolves mean flow and all turbulent velocity fluctuations using a computational mesh. Therefore, it requires fine grids with small time steps. DNS requires high computational power which limits its use for non-industrialized applications [32].

2.7 Heat transfer inside the packed bed furnace

Heat transfer in packed beds occurs through conduction, convection and radiation. The particles in the bed exchange heat with neighboring particles through conduction and radiation. Particles exchange heat with gas phase by convection and radiation. Heat transfer inside a furnace depends on the flow conditions, characteristics of fuel and the geometry of the combustor. Heat transfer in packed beds affects the reactions in the combustor. Above mentioned characteristics can be effectively adjusted to optimise the performance of packed bed combustion systems. Optimum combustion of biomass can be achieved through controlling above mentioned characteristics. Therefore, it requires good understanding of the process, which can be achieved through numerical modelling.

Radiation is the principal heat transfer mechanism in furnaces. It is estimated that 20% of reaction heat is directly emitted as radiation energy in combustion. 30% of energy contained in combustion products, is then released as radiation energy [40]. Wood particles in the bed exchange heat through radiation with neighboring particles, reactor walls and flame at the top of the bed. In packed beds radiation heat above the bed can only penetrate a short distance into the bed. It is reported that radiation intensity can be enhanced by 24% by turbulent effects [37]. Therefore, modelling of radiation heat transfer has been treated separately in CFD modelling.

Different approaches have been used in the literature to model radiation effect in combustion. Conservation equation for a radiation beam travelling along a path through a medium is represented by the Radiative Transfer Equation (RTE), Eq. (2.1) [41]. In the above equation I_λ is the spectral radiation intensity, $I_{b\lambda}$ is the spectral radiation intensity for a black body, a_λ is the spectral absorption coefficient of the medium, $a_{\lambda s}$ is the spectral scattering coefficient and $\left(\overrightarrow{S'} \to \overrightarrow{S}, \overrightarrow{\lambda'} \to \vec{\lambda}\right) d\Omega' d\lambda'/4\pi$, represents the probability that radiation of wavelength λ' propagating in the direction $\overrightarrow{S'}$ and confined within the solid angle $d\Omega'$ is scattered to the direction $\overrightarrow{S}$ and wavelength 1.

$$\frac{dI_\lambda}{dS} = -(a_\lambda + a_{\lambda s})I_\lambda + a_\lambda I_{b\lambda} + \frac{a_{\lambda s}}{4\pi}\int_0^\infty \int_0^{4\pi} \Phi\left(\overrightarrow{S'} \to \overrightarrow{S}, \overrightarrow{\lambda'} \to \vec{\lambda}\right) I'_\lambda\left(\overrightarrow{S'}\right) d\Omega' d\lambda' \qquad (2.1)$$

Exact solution for the above RTE equation is only possible under simplifying assumptions such as uniform radiation properties of the medium and uniform boundary conditions. Combustion apparatus are multidimensional and non-homogeneous. The other limitation of RTE is evaluation of different coefficients which depend on wavelength, pressure, temperature, gas composition and type of particles. Therefore, different solution methods have been developed to overcome the above mentioned limitations in RTE and they will be described below [42].

- Directional averaging approximations (2-Flux, 4-Flux, Multi flux, Discrete Ordinates Model (DOM))
- Differential approximations (moment, modified moment, spherical harmonics, etc.);
- Energy balance (zone, Monte Carlo, finite volume, finite element, boundary element, etc.) methods
- Hybrid (discrete transfer, zone-Monte Carlo, ray tracing, etc.) methods.

Directional averaging approximations involve averaging of radiation field related to different directions. Accuracy of these models depends on the selection of solid angle subdivision over which the intensities are integrated to obtain the flux. The other limitation is that the flux in one direction is not coupled with the flux in other directions if the medium is not scattering. Flux models were used in [35], [43]–[46] to model radiation heat transfer in packed bed furnaces. Due to low accuracy the application of the model has been limited.

DOM is also considered to be a multi flux method. Presumptions are not required in DOM on the relationship of radiation intensity with the direction. Two types of RTEs are used in DOM. The first one is the classical approach which approximates the RTE to first order ordinary differential equation. The second approach is named as even parity formulation which is a second order partial differential equation. This method discretises the total solid angle into finite number of ordinate directions. RTE is written for each ordinate. The integrals over these ordinates are replaced by numerical quadrature. Then the RTE is transformed into a transport equation for radiation in spatial coordinates. DOM was used in [39], [47]–[51] for modelling radiative heat transfer in packed bed combustion systems.

Representation of RTE in spherical harmonics forms differential approximation for RTE. First order differential approximations of the radiation models are capable of treating the radiative heat transfer problems in scattered media. P_n approximation is obtained by taking moments of RTE. This results in n^2 number of equations. P_1 approximation produces a single equation. P_1 approximation is widely applicable due to its simplicity and accuracy. Due to the diffusive nature of the radiation energy

transfer in P_1 approximation, it has been identified as well suited for optically thick media where radiation travels short distances. It has been used in the work of CFD modelling of biomass combustion in small scale combustion units [52], [53]. Klason [6] observed that the difference between predicted temperatures from P1 model and Finite Volume Method radiation models was small for biomass combustion in furnaces.

Finite Volume Method (FVM) from the category of energy balance method is suitable for the application of CFD in combustion systems. In FVM radiance in each discrete direction is assumed to be constant as in DOM. Results are obtained by solving for discrete angles which cover a solid angle of 4π sr. Discrete equations are obtained by integrating RTE in each control volume and over each solid angle.

The Discrete Transfer Method (DTM) which is categorised under hybrid methods is proven to be suitable for CFD applications. This method divides the geometry into isothermal control volumes and surfaces which have constant radiation properties. The RTE is integrated analytically and is iteratively solved along an arbitrary path. The solution of the RTE gives the local intensity of any ray in the selected direction. This method is flexible in handling complex geometries and the accuracy can be manipulated by changing the number of rays without affecting much for the computer storage capacity. This model is difficult to be implementd for the anisotropic scattering problems. Since DTM is not conservative it is difficult to couple with finite volume method-based calculations which are conservative.

2.8 Solid movement of bed

Volume decrease of wood particles during drying, pyrolysis and char reactions makes the biomass bed to shrink. Volume reduction in pyrolysis is higher than other two processes due to large quantity of mass released to the gas phase during pyrolysis. Volume reduction of fuel bed is modelled by individual particle movement in DPM approach. Aggregation and bed collapses have to be modelled to give more realistic description of the bed movement, which are limited in currently available

DPM models. Discontinuous shrinkage of packed beds in combustion was modelled in DPM approach by Mehrabian et al. [9].

Since individual particle representation is not used in Eulerian approach, different alternative methods are used to describe solid movement. One method is to model gas and solid movement by two fluids motion, which includes a convective term in the solid phase equation as was done by Yang et al [21], [43]. Hermansson and Thunman [33] used a moving coordinate system to describe solids movement in fixed beds. This method requires rescalling of computational mesh and solid movement is modelled as discrete events. Rescalling of mesh requires high computational power and introduces numerical challenges as described in [36]. Gómez et al [25] included description of solid movement explicitly to the conservation equations. Therefore, solid phase conservation equations do not include convective flux term, and the bed movement was calculated as a mass and energy exchange between cells.

Two approaches have been used in representing linkage beteen porosity field and shrinkage of the packed bed during thermal conversion. Some researchers developed bed shrinkage models based on the assumption of constant porosity field throughout the bed during entire conversion period [45], [54]. Voids created by mass loss are filled with larger particles which lie above, therefore above assumption considered to be valid. Collazo et al modelled variable porosity field throughout the bed while the bed height remained constant [55]. Some other researchers modelled variable porosity field throughout the bed with bed height change in modelling packed bed thermal conversion [8], [9], [33]. Different models were developed to describe the variable porosity field within packed beds [33], [56]. Juřena compared results of reaction front propagation speed between constant-porosity bed model and variable-porosity bed model and observed lower reaction front propagation speeds for variable-porosity model [20]. Thunman and Hermansson [33] used variable porosity models to simulate bed collapses and uneven distribution of combustion rates in packed beds.

2.9 CFD models for wood combustion in packed bed furnaces

To optimise the efficiency of a furnace, main operating variable should be controlled. To control operation of furnace, a good understanding on how these process variables affect the combustion should be studied. Conducting experiments on full scale furnaces are expensive and impossible to achieve. CFD provides feasibility of acquiring detailed description of the processes inside the packed bed than experimental studies. A CFD model with sufficient accuracy can be used to enhance the sustainability in wood fuel consumption in industries.

There have been many studies done on batch type packed bed combustion of biomass by CFD approach. Either transient or steady-state models have been used to describe conversion of biomass in packed beds. Pseudo-steady-state approach was used by Richter et al. [57] to study the spatial distribution of temperature and species in combustion and gasification zones in a fixed bed of coal char particles by two dimensional and three dimensional models. Two dimensional steady state model of moving grate furnace was developed by van der Lans et al [19]. The model was used to predict ignition propagation rate and ignition front temperature, which can be used to optimise performance of full-scale furnaces. Transient modelling of biomass combustion in packed beds have been reported in [6], [9], [60], [15], [20], [33], [43], [46], [55], [58], [59].

CFD modelling of biomass combustion in packed beds can be categorised into two main approaches according to the method used in solving biomass bed and free board. First category solves the biomass bed and the free board separately. A different solution method (other than CFD) is used for the packed bed. In this method the solutions for temperature and species that have been obtained by solving the packed bed are used as the boundary conditions for free board solver. This kind of practice was used in [45], [51], [61]. The second category solves the biomass bed and free board simultaneously by CFD approach. Three-dimensional transient modelling of batch type biomass combustion was done in [9], [55] , where biomass bed and free board were solved simultaneously.

The packed bed models are categorised according to the way of treatment of solid phase in the model. The bed of solids is considered as a continuum in Eulerian modelling framework. The Eulerian method has been used to model biomass combustion in packed beds under thermally thin assumption [25], [55], [59]. Equivalent diameter of the particles simulated is 8.8 mm, 7.6 mm and diameters less than 8.8 mm. Eulerian approach has been mainly used for modelling packed bed combustion under thermally thin assumption. Exemptions are presented in [62], [63], where thermally thick particles are modelled within the Eulerian framework. A subgrid one-dimensional model was used to describe the particles in the bed with a three-dimensional modelling of the bed. The subgrid model was recommended to use for particles from 2 mm to 20 mm size. The Eulerian approach was used by Yang et al [64] to study the combustion of wood particles of sizes from 5 -35 mm. The bed was described by three types of cells; viod cells, boundary cells of particles and inner cells of particles. He further used a double-mesh computation scheme to study burning characteristics of pine wood chips of sizes from 5 mm -50 mm by Eulerian approach in [44]. He used Eulerian approach to model combustion of 20 mm sized particles in a moving grate furnace arrangement with single mesh [21]. Thermal conversion of each individual particle is included in solid phase modelling in DPM. The DPM method was used to model thermal conversion of packed bed of thermally thick particles with the Eulerian treatment of fluid phase in [9]. The particles are modelled in one-dimensional geometry and the entire domain of the combustor is modelled as a three-dimensional geometry. The DPM was also used by Thunman et al [65] to model combustion of different sized particles. The model consists of two-dimensional particle models with one dimensional packed bed model. He compared the results of porous medium assumption with the particle model linked to the porous medium treatment of packed bed combustion. The linked model showed lower release rates compared to porous media approximation. This lower release rates were distributed over larger span of the bed height. Porous media approximation gave higher release rates which was limited to a narrow span of the bed height. A transient one dimensional particle model was incorporated into a packed bed combustion model by Peters et al [58]. He modelled particle sizes between 5 mm -25 mm.

2.10 CFD modelling of wood combustion in moving grate furnaces

Industrial packed bed wood furnaces are operated continuously, and fuel is moved along the supporting grate or resembles horizontal movement along the grate. Two methods are used to model fuel phase; Eulerian method and Lagrangian method. Fuel bed is modelled as a continuum with volume averaged properties in Eulerian approach. Discrete Particles Models (DPM) are involved in Lagrangian method of fuel bed modelling. The horizontal movement of the grate is modelled by two approaches. One category introduces the bed movement directly through boundary conditions [21], [43], [66], [67]. The effect of fuel mixing is incorporated by empirical mixing coefficient in Eulerian approach [66]. Mixing of fuel particles is accounted by the forces acting on the particles in DPM method [67]. The second category is based on the assumption that a moving grate furnace operated at steady state can be represented by transient operation of fixed beds [15], [19], [45], [68]. In this approach time passed after ignition is linked to a horizontal placement of fuel on the grate and flow of gas and movement of solid was assumed to be plug flow. Description of solids at a distance 'x' from the fuel inlet on a moving grate is related to the state of solids at time't' elapsed after ignition in a fixed bed (Figure 2.3). This approach was used in the studies presented in [15], [19], [34], [68], [69]. Van Der Lans [19] developed a homogeneous, two dimensional mathematical model to study straw combustion in grate furnaces. His model was able to produce good agreement between simulation results and measured data for ignition front temperatures and ignition front propagation speed. One dimensional model was developed by Sastamoinen [34] to describe steady state operation of moving grate biomass combustion. He used the model to study ignition front propagation and maximum bed temperature. Wurzenberger et al [15] used a particle model which was validated with experimental results to describe fuel bed processes. Kaer [68] used the above approach to study full scale straw combustion in grate furnaces. He used a two-step approach where, results obtained by solving fuel bed were applied as boundary conditions for the free board region modelling. The particle based model presented in [26] which was used for transient fixed bed combustion modelling [9] was used for moving grate combustion modelling under steady state in [69]. Since the grate bar

movement was not modelled, positions of the grate bars were chosen according to the conversion of fuel and particle velocities were predefined according to the grate bar positions. This model simultaneously solves the packed bed and free board. Similar approach with modifications was used by Juřena [20] in the model proposed in his phd thesis. A two-dimensional steady state model with flow field along the grate which is described by the momentum equation was developed. This model does not include the assumption of plug flow behavior in the model.

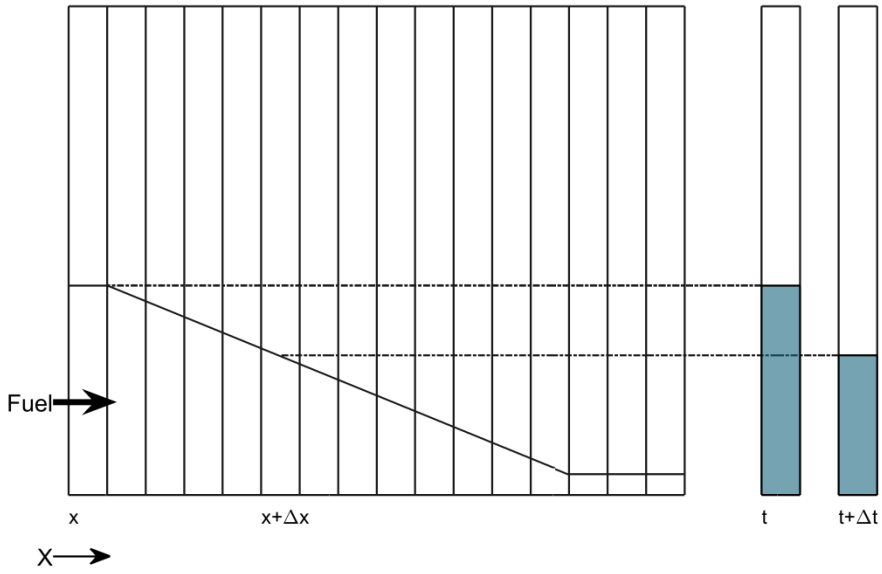

Figure 2.3 Representation of steady state operation of a moving grate furnace

The other approach of modelling combustion in moving grate furnaces tries to simulate transient operation of furnaces, therefore, imitates the grate movement through boundary conditions. This approach was used by Yang et al. [21] to model waste combustion in fixed beds. He used Eulerian representation for bed of fuel particles and used empirical diffusion coefficient for mixing of solid particles due to grate movement. Two-step approach was used for modelling of free board region where the results from biomass bed act as inlet conditions for gas phase. Discrete particle method was used to model both thermal conversion and movement of individual particle on the grate by Peters et al [70]. He simulated straw gasification on

a forward-acting grate by the above approach. His focus was on conversion of solid bed; therefore, modelling of free board region (temperature, species) was not included in the model.

In addition, empirical approaches were used in modelling biomass bed on grate furnaces [47], [48], [54] where, the predictions from the packed bed combustion of biomass acts as inlet conditions for free board region [47], [48]. The methods proposed in [48], [54] was suggested as a basis to be used for automatic process controlling.

2.11 Research justification

Wood fired furnaces used in industry are operated continuously and have behaviour closer to moving grate furnaces. Behaviour of the fuel bed is affected by the movement of fuel along the grate. Variations in combustion can be observed due to grate movement even at steady state operation in moving grate furnaces. Thermal conversion of fuel bed is closely linked with the free board processes. Therefore, to optimise and control combustion in moving grate furnaces the interaction between fuel bed and the free board should be correctly represented. The reviewed models so far have not modelled transient nature of moving grate processes which present the simultaneous interaction between fuel bed and the free board. Therefore, a comprehensive model should be developed for moving grate furnaces, which includes descriptions of solid phase conversion, gas phase reactions, turbulent flow conditions, radiation heat transfer, bed shrinkage and grate movement and which is able to model fuel bed and free board interactions simultaneously.

Chapter 3

ANALYSIS OF PYROLYSIS KINETICS

3.1 Background and objective of kinetic study

Pyrolysis is an important step in combustion which produces gas, intermediate products and char. Knowledge on pyrolysis kinetics of fuel is important for the advancements in thermal conversion technology. Pyrolysis kinetics analysis can describe the influence of devolatalisation conditions on fuel decomposition [71]. Pyrolysis kinetics has been extensively studied, and it depends on size, shape, composition, temperature and the methodology used to derive the kinetics. There have been number of studies done on evaluation of pyrolysis kinetics of Birch, Pine, Poplar and Eucalyptus [72]–[74]. Gliricidia sepium which is known as Gliricidia and Havea brasiliensis which is known as Rubber are commonly used for thermal applications in Sri Lanka, though pyrolysis kinetic data is not available. Then, a detail analysis of pyrolysis kinetics for Gliricidia and Rubber wood was conducted. Experiments can be conducted in isothermal or non-isothermal environments and kinetic parameters can be derived accordingly [75].

Two approaches; model free (iso-conversional methods) or model fitting have been applied to analyse biomass pyrolysis in isothermal or non-isothermal environments [76]. Model fitting and model free methods have their own limitations [77]. Reaction mechanism has to be pre-defined in model fitting methods. Popularity of this method is reduced due to the requirement of prior assumptions on the reaction mechanism [75]. Thermo gravimetric data obtained by single experiment is sufficient to evaluate the model-based kinetics. Model fitting methods that have been applied for analysing non isothermal pyrolysis kinetics are Differential, Freeman Carroll [78] and Coats Redfern [79] methods. Coates Redfern method was used to analyse pyrolysis kinetics of coal biomass blends by Jayaraman et al [80]. An increase in activation energy and pre-exponential constant in biomass coal blends was observed when compared to coal [80]. Higher activation energy value and pre-exponential factor of biomass caused the increase in biomass coal blends. Values they obtained agree with the

values reported in the literature. Catalytic pyrolysis kinetics of biomass was evaluated by Coats Redfern method along with Friedman model free method. According to the findings catalytic pyrolysis of biomass follows multistep reaction mechanism rather than simple first order reaction mechanism of virgin biomass [81]. A sequential method was presented by Huang et al. [82] to evaluate non-isothermal kinetic parameters. His method is based on the method presented by Kissinger [83] on the maximum reaction rate. Pyrolysis kinetics of seven kinds of biomass feed stocks was evaluated by the method presented in [82]. Obtained kinetic parameters are agreeable with the values reported in literature. Kinetics evaluated by model fitting methods has been widely used in modelling of thermal conversion. Kinetics derived according to global one step model has been extensively used in modelling studies due to the simplicity and easiness in implementation.

Distributed Activation Energy Model (DAEM) is another method which considers chemical complexity and distribution of pyrolysis products in determining pyrolysis kinetics [30]. It requires TGA data to be obtained at number of heating rates for the evaluation of pyrolysis kinetics. Reaction is assumed to proceed through infinite number of independent parallel reactions which have different activation energies. A continuous distribution function is used to present the activation energy variation. DAEM uses either distribution free or distribution fitting methods to evaluate the kinetic parameters [84]. In distribution fitting method, the distribution of activation energy is presented by Gaussian [85], Weibull [86] or Gamma distribution [28] functions. The widely used distribution function is the Gauss distribution function [85]. Distribution fitting methods were used to evaluate pyrolysis kinetics of rice husk, bamboo and pine wood [74]. A good match with experimental data was obtained by assuming Gaussian distribution for the activation energy. Gaussian distribution was used to find pyrolysis kinetics of wood by Gašparoviè et al [85]. A distribution free approach of DAEM is Miura and Maki approach [87]. Pyrolysis kinetics of different biomass types were evaluated by Miura and Maki approach of DAEM [88]–[91]. Verdugo et al. [92] used a modified version of Miura and Maki approach of DAEM to analyse pyrolysis kinetics of solid fuels under parabolic and exponential temperature increments. Wang et al. [93] coupled, non-isothermal model

fitting, iso- conversion and DAEM to manage the complexity of biomass pyrolysis kinetics. While DAEM is more accurate method for modelling pyrolysis kinetics it is more complicated to implement in CFD modelling [74].

Considering the applicability of model fitting methods for simulation of combustion systems, pyrolysis kinetics was derived according to global one step reaction mechanism of order one. The sequential approach proposed by Huang et al. [82] was used for the study of global one step pyrolysis kinetics. Miura and Maki approach [87] of DAEM was used in this study as it is more accurate method of kinetic analysis. Thermo Gravimetric Analysis (TGA), which studies mass variation as a function of temperature or time, was carried out to estimate pyrolysis kinetics of Rubber and Gliricidia fuel woods [94] .

3.2 Experimental study

Fine dust of Gliricidia and Rubber wood was used in the experiment. Gliricidia and Rubber wood properties are shown in Table 3.1. TGA instrument SDT Q600 was used for thermo gravimetric analyses which measures mass variation as a function of temperature. The accuracy of the balance of the instrument is 0.1 μg and the accuracy of differential thermal analysis is 0.001 °C. Samples of 10 mg weight were used for the experiments. Since the minimum number of experimental data sets required at different heating rates for the evaluation of pyrolysis kinetics by DAEM is three, three sets of experiments were carried out for each wood type at heating rates of 10 $^{o}Cmin^{-1}$, 20 $^{o}Cmin^{-1}$ and 30 $^{o}Cmin^{-1}$. As reported in literature different temperatures, commonly between 700 ºC and 900 ºC, were used as final target temperature of the experiments [74], [82], [92], [95]. Therefore, these samples were heated from room temperature to final temperature of 800 ^{o}C. The nitrogen gas was sent at a flow rate of 100 $mlmin^{-1}$. In order to prevent the drying reaction being interpreted from the data, weight loss data of samples in the range of 177 ^{o}C (450 K) and 800 ^{o}C (1073 K) was used for kinetic study.

Table 3.1 Gliricidia and Rubber wood properties

Wood species	Proximate analysis (wt%)				Ultimate, analysis (wt% Dry basis)			
	Moisture	Volatile Matter	Fixed Carbon	Ash	C	H	O	N
Gliricidia	11.97	67.40	14.63	6.00	50.4	5.48	23.5	0.91
Rubber	6.95	73.74	14.15	5.16	42.41	5.31	39.2	0.90

3.3 Theory

3.3.1 The sequential approach

The procedure presented by Huang et al in [82] was used in this research.

Reaction rate of pyrolysis dx/dt is expressed by Eq. (3.1).

$$\frac{dx}{dt} = kf(x) \tag{3.1}$$

x is mass conversion, t is time, k is reaction rate constant and f(x) is conversion function. Hereafter conversion is denoted by x, which is expressed by Eq. (3.2). Initial mass of the sample is m_0, final mass of the sample is m_f and mass of the sample at time t is m.

$$x = \frac{m_0 - m}{m_0 - m_f} \tag{3.2}$$

The reaction rate constant is expressed by Eq. (3.3), in which A is the pre-exponential factor, E is activation energy and T is temperature.

$$k = A\exp\left(\frac{-E}{RT}\right) \tag{3.3}$$

Assumption of n^{th} order conversion of solid leads to Eq. (3.4)

$$f(x) = (1-x)^n \tag{3.4}$$

$$\frac{dx}{dt} = A\exp\left(\frac{-E}{RT}\right)(1-x)^n \tag{3.5}$$

With the approximations given in [96] integral form of Eq. (3.5) can be written as

$$\frac{1}{(n-1)}\left[\frac{1}{(1-x)^{n-1}} - 1\right] = \frac{ART^2}{\beta E}\exp\left(\frac{-E}{RT}\right) \tag{3.6}$$

Differentiating Eq. (3.5) at the maximum reaction rate results in Eq. (3.7)

$$\frac{d}{dt}\left(\frac{dx}{dt}\right) = \left(\frac{dT}{dt}\right)\left(\frac{E}{RT^2}\right)A\exp\left(\frac{-E}{RT}\right)(1-x)^n - \left(\frac{dx}{dt}\right)nA\exp\left(\frac{-E}{RT}\right)(1-x)^{n-1} \tag{3.7}$$

Heating rate β is given by Eq. (3.8)

$$\beta = \frac{dT}{dt} \tag{3.8}$$

Substituting Eq. (3.5) and Eq. (3.8) in Eq. (3.7)

$$\frac{d}{dt}\left(\frac{dx}{dt}\right) = \left(\frac{dx}{dt}\right)\left(\frac{\beta E}{RT^2}\right) - \left(\frac{dx}{dt}\right)A\exp\left(\frac{-E}{RT}\right)(1-x)^{n-1} \tag{3.9}$$

At the maximum conversion rate $\frac{d}{dt}\left(\frac{dx_m}{dt}\right)=0$, X_m is the conversion at maximum conversion rate. Therefore,

$$\left(\frac{dx_m}{dt}\right)\left(\frac{\beta E}{RT^2}\right)-\left(\frac{dx_m}{dt}\right)A\exp\left(\frac{-E}{RT}\right)(1-x_m)^{n-1}=0 \tag{3.10}$$

By rearranging Eq. (3.6) and Eq. (3.10), the order of the reaction can be calculated by Eq. (3.11). TGA measurements can be used to calculate X_m and maximum reaction rate.

$$(1-x_m)=n^{\frac{1}{(1-n)}} \tag{3.11}$$

After obtaining reaction order, activation energy E can be calculated by Eq. (3.12) and pre-exponential factor can be calculated by Eq. (3.13).

$$E=n^{\frac{n}{(n-1)}}RT_m^2\left(\frac{dx_m}{dT}\right) \tag{3.12}$$

$$A=n^{\frac{n}{(n-1)}}\beta\left(\frac{dx_m}{dT}\right)\exp\left(n^{\frac{n}{(n-1)}}T_m\left(\frac{dx_m}{dT}\right)\right) \tag{3.13}$$

Assuming first order decomposition, integrating Eq. (3.5) results in Eq. (3.14)

$$-\ln(1-x)=\frac{ART^2}{\beta E}\exp\left(\frac{-E}{RT}\right) \tag{3.14}$$

By differentiating Eq. (3.5)

$$\frac{d^2x}{dt^2} = A\exp\left(\frac{-E}{RT}\right)\left(\frac{-dx}{dt}\right) + \frac{E}{RT^2}\left(\frac{dT}{dt}\right)A\exp\left(\frac{-E}{RT}\right)(1-x) \tag{3.15}$$

At the maximum reaction rate $d^2x_m/dt^2 = 0$

$$A\exp\left(\frac{-E}{RT_m}\right)\left(\frac{-dx}{dt}\right)_m - \frac{E}{RT_m{}^2}\left(\frac{dT_m}{dt}\right)A\exp\left(\frac{-E}{RT_m}\right)(1-x_m) = 0 \tag{3.16}$$

Since

$$\left(\frac{dx}{dt}\right)_m = k_m(1-x_m) \tag{3.17}$$

Eq. (3.16) leads to

$$k_m = \frac{\beta E}{RT_m{}^2} \tag{3.18}$$

Using Eq. (3.5) and Eq. (3.14) for a reaction of order one (n=1) at maximum reaction rate

$$E = \frac{-RT_m{}^2}{(1-x_m)\ln(1-x_m)}\left(\frac{dx}{dT}\right)_m \tag{3.19}$$

If

$$c = \frac{1}{(1-x_m)\ln(1-x_m)} \tag{3.20}$$

And

$$A = c\beta \left(\frac{dx}{dT}\right)_m \exp\left(cT_m \left(\frac{dx}{dT}\right)_m\right) \tag{3.21}$$

Above described method can be used to calculate first order or n^{th} order reaction kinetics. Eq. (3.22) was used to obtain best fitting parameters by nonlinear square fit method.

$$\text{Error} = \sum_{i=1}^{n} \left[\left(\frac{dx}{dT}\right)_{i,exp} - \left(\frac{dx}{dT}\right)_{i,sim}\right]^2 \tag{3.22}$$

It was assumed that pyrolysis kinetics obeys first order reaction. Therefore, Eq (3.19), ((3.20), and Eq. (3.21) were used to calculate activation energy and pre-exponential factor. TGA data obtained at the heating rate of 20 $^{o}Cmin^{-1}$ was used to calculate model based non isothermal pyrolysis kinetics. The numerical optimization was performed by solver fminsearch in MATLAB® software, which uses Nelder-Mead simplex algorithm to minimise the objective function given in Eq. (3.22) [97]. fminsearch is an inbuilt solver in MATLAB which has the ability to optimise multiple parameters. The calculated values of E by Eq. (3.19) and A by Eq. (3.21) were given as the initial deductions to the solver.

3.3.2 Miura and Maki approach

Fraction of fuel converted to volatiles is used to calculate pyrolysis kinetics in DAEM method (Eq. (3.23)).

$$1\text{-}x = \int_0^{\infty} \Phi(E,T) f(E) dE \tag{3.23}$$

In Eq. (3.24)

$$\Phi(E,T) = \exp\left(-\frac{k}{\beta}\int_{273.15}^{T} \exp^{-\frac{E}{RT}} dT\right) \tag{3.24}$$

Inner dT integral and the outer dE integral make it difficult to obtain exact analytical solution to DAEM. Therefore, many mathematical approximations have been proposed by different researchers. Calculation of parameters has become difficult due to complex nature of DAEM formulation. Either distribution free or distribution fitting method can be used to calculate kinetic parameters in DAEM. Miura and Maki presented a revision to DAEM which does not require prior assumptions to estimate distribution of f(E) [29], [87]. Therefore, Miura and Maki method was used in this study to estimate activation energy distribution [87].

Miura and Maki approximation of Eq. (3.23) leads to Eq. (3.25).

$$\ln\left(\frac{\beta}{T^2}\right) = \ln\left(\frac{kR}{E}\right) + 0.6075 - \frac{E}{RT} \tag{3.25}$$

Eq. (3.25) presents a linear relationship between $\ln(\beta/T^2)$ and $1/T$ where E can be calculated. The procedure described below was used to calculate E and f(E)

- $\ln(\beta/T^2)$ versus $1/T$ is calculated at heating rates of 10, 20 and 30 $^{o}C\ min^{-1}$ for same levels of conversion (1-x).
- Activation energy E is calculated from the gradient and the pre-exponential factor A is calculated from intercept using Eq. (3.25).

3.4 Results and discussion on pyrolysis kinetic analysis

3.4.1 Pyrolysis kinetics calculated by sequential approach

The method described in section 3.3.1 was used to calculate pyrolysis kinetics of Gliricidia and Rubber. The kinetic parameters obtained for Gliricidia and Rubber wood at heating rate of 20 $^{o}Cmin^{-1}$ are included in Table 3.2

Table 3.2 Pyrolysis kinetics obtained by the sequential approach

Wood species	T_m (K)	$(1-x)_m$	E ($kJmol^{-1}$)	A (s^{-1})
Gliricidia	635	0.35	107.19	$8.88x10^6$
Rubber	634	0.30	83.44	$9.5\ x10^4$

Figure 3.1 shows reaction rate calculated by the evaluate kinetic parameters (red line) and experimentally obtained reaction rate (blue line) of Gliricidia. Figure 3.2 demonstrates the reaction rate obtained by calculated kinetic parameters (red line) and experimentally obtained reaction rate of Rubber. Two separate peaks can be observed for Rubber whereas only a shoulder can be observed for Gliricidia. Pyrolysis of hemicellulose results in the low temperature peak in Rubber decomposition curve and the low temperature shoulder in Gliricidia decomposition curve [30]. Hemicellulose content in Rubber wood is around 40% while approximate cellulose content is 70% [98]. Clearly visible low temperature peak can be described by high hemicellulose to cellulose ratio in Rubber wood. The maximum decomposition rate is resulted by cellulose pyrolysis which is shown by the 1st peak in Figure 3.1 and 2nd peak in Figure 3.2. These peaks occur at 635 K for Gliricidia and 634 K for Rubber. The temperatures at which the maximum pyrolysis rate occur agree with the temperature range presented in literature for maximum rate of cellulose pyrolysis [99]. Pyrolysis of lignin spreads throughout the entire range of temperature used in the pyrolysis. Calculated kinetics does not show decomposition of individual components; hemicellulose, cellulose and lignin. Calculated kinetic parameters represent the average value of kinetics for the entire thermal conversion [77]. The activation energy of Gliricidia wood is 28% higher than that of Rubber

wood and pre-exponential factor is 92% higher than that of Rubber wood which is due differences in composition, structure etc. between two wood types.

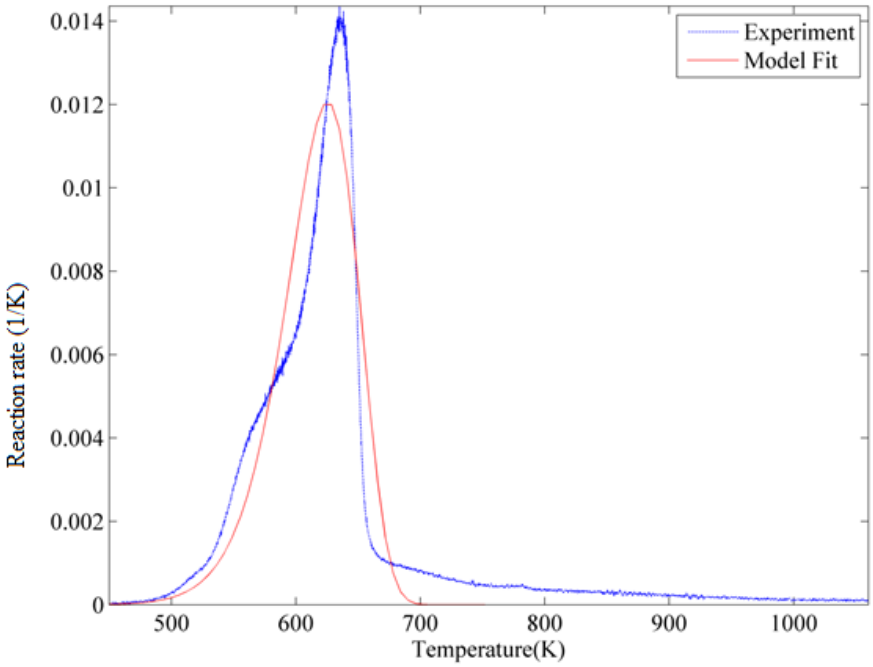

Figure 3.1 Pyrolysis rate of Gliricidia

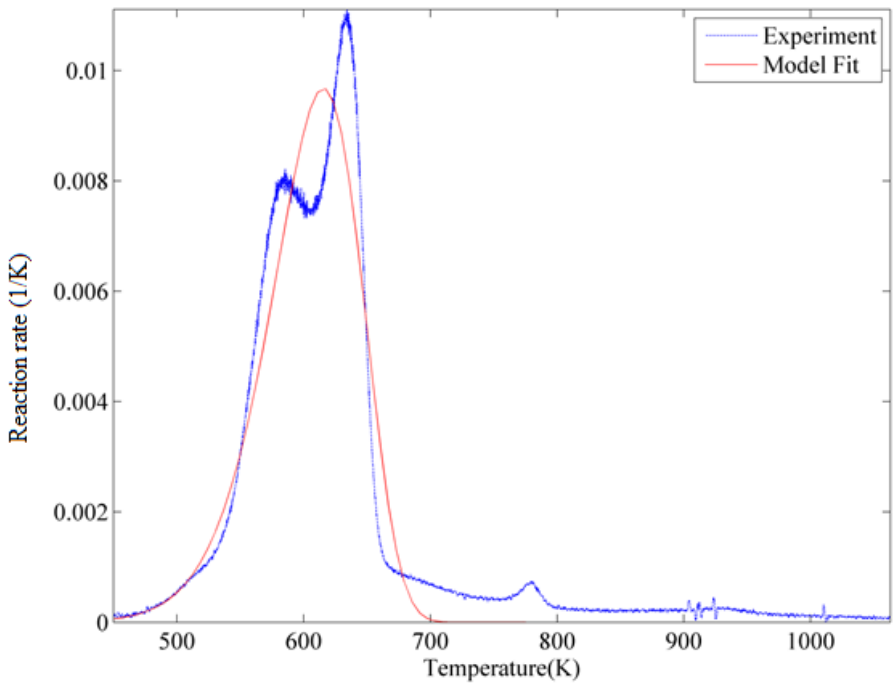

Figure 3.2 Pyrolysis rate of Rubber

3.4.2 Pyrolysis kinetics by Miura and Maki approximation

Graphs of $\ln(\beta/T^2)$ against (1/T) for Gliricidia and Rubber wood are shown in Figure 3.3 and Figure 3.4, respectively for conversion levels between 0.05 and 0.95. Gliricidia wood shows good correlation for conversions ranging from 0.15 to 0.8. High correlations factors (R^2) are observed for conversions ranging between 0.05 and 0.85 for Rubber wood (Table 3.3). Parallel and linear relationship between $\ln(\beta/T^2)$ and 1/T plots cannot be observed for conversions lower than 0.15 and for conversions higher than 0.80 for Gliricidia. For conversions higher than 0.85, Rubber wood does not show parallel and linear relationship which is shown by low correlation factors at the corresponding conversions. Therefore, activation energy values of Gliricidia wood vary from 190.58 $kJmol^{-1}$ to 230.57 $kJmol^{-1}$. Activation energy value varies from 111.52 $kJmol^{-1}$ to 179.07 $kJmol^{-1}$ for Rubber wood. Occurrence of different reactions at different stages of pyrolysis is characterized by the observed variation in activation energy and pre-exponential factor. From the results observed activation energy and pre-exponential factor of Gliricidia is higher

than that of Rubber. Gliricidia shows 6% to 100% higher value for activation energy than Rubber.

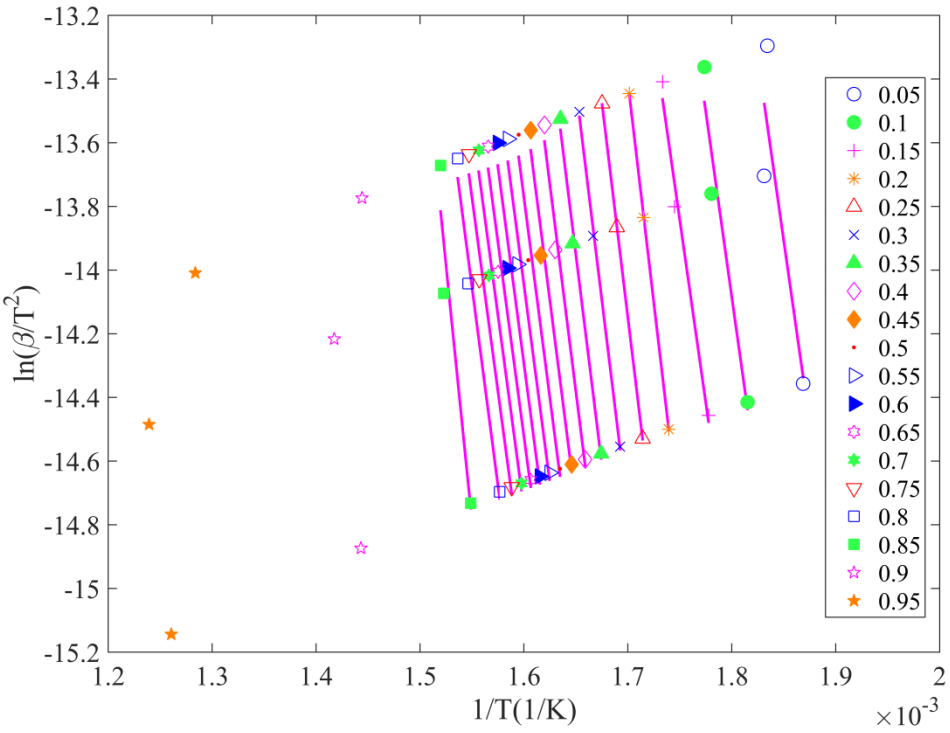

Figure 3.3 $\ln(\beta/T^2)$ versus1/T at different conversion levels for Gliricidia

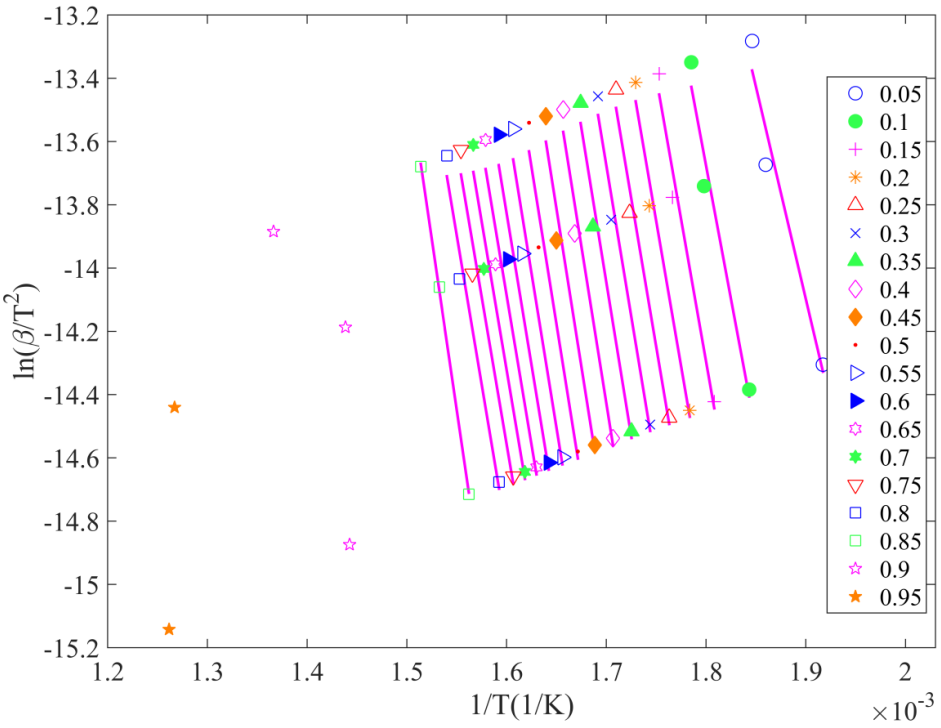

Figure 3.4 $\ln(\beta/T^2)$ versus 1/T at different conversion levels for Rubber

Table 3.3 Kinetic parameters of Gliricidia and Rubber from Miura and Maki approach

Conversion	Gliricidia			Rubber		
	A (s^{-1})	E ($kJmol^{-1}$)	R^2	A (s^{-1})	E ($kJmol^{-1}$)	R^2
0.05	$3.20x10^{16}$	190.90	0.7976	$6.45x10^{08}$	111.52	0.9578
0.10	$1.48x10^{16}$	193.40	0.9473	$1.64x10^{11}$	140.282	0.9698
0.15	$3.21x10^{15}$	190.58	0.9839	$6.75x10^{11}$	149.392	0.9777
0.20	$6.78x10^{18}$	230.57	0.9999	$9.24x10^{11}$	152.93	0.9810
0.25	$9.11x10^{17}$	224.50	0.9999	$1.16x10^{12}$	155.812	0.9821
0.30	$2.70x10^{17}$	221.61	0.9984	$1.53x10^{12}$	158.852	0.9815
0.35	$9.93x10^{16}$	219.26	0.9931	$2.09x10^{12}$	162.072	0.9788
0.40	$3.41x10^{16}$	216.11	0.9857	$2.61x10^{12}$	164.95	0.9746
0.45	$1.19x10^{16}$	212.66	0.9794	$2.30x10^{12}$	166.18	0.9682
0.50	$4.82x10^{15}$	209.69	0.9759	$1.21x10^{12}$	164.83	0.9611
0.55	$2.13x10^{15}$	206.94	0.9745	$5.24x10^{11}$	162.33	0.9568
0.60	$1.23x10^{15}$	205.42	0.9747	$2.32x10^{11}$	159.73	0.9567
0.65	$6.07x10^{14}$	202.99	0.9755	$1.13x10^{11}$	157.42	0.9597
0.70	$4.02x10^{14}$	202.05	0.9771	$6.61x10^{10}$	155.90	0.9643
0.75	$3.45x10^{14}$	202.50	0.9789	$4.33x10^{10}$	154.96	0.9697
0.80	$6.62x10^{14}$	207.37	0.9802	$4.73x10^{10}$	156.83	0.9779
0.85	$2.68x10^{19}$	266.85	0.9179	$1.97x10^{12}$	179.07	0.9995
0.90	0.0564	23.58	0.005975	$1.15x10^{03}$	75.48	0.5888
0.95	$-2.18x10^{-09}$	-93.04	0.1913	$7.13x10^{01}$	69.80	0.4565

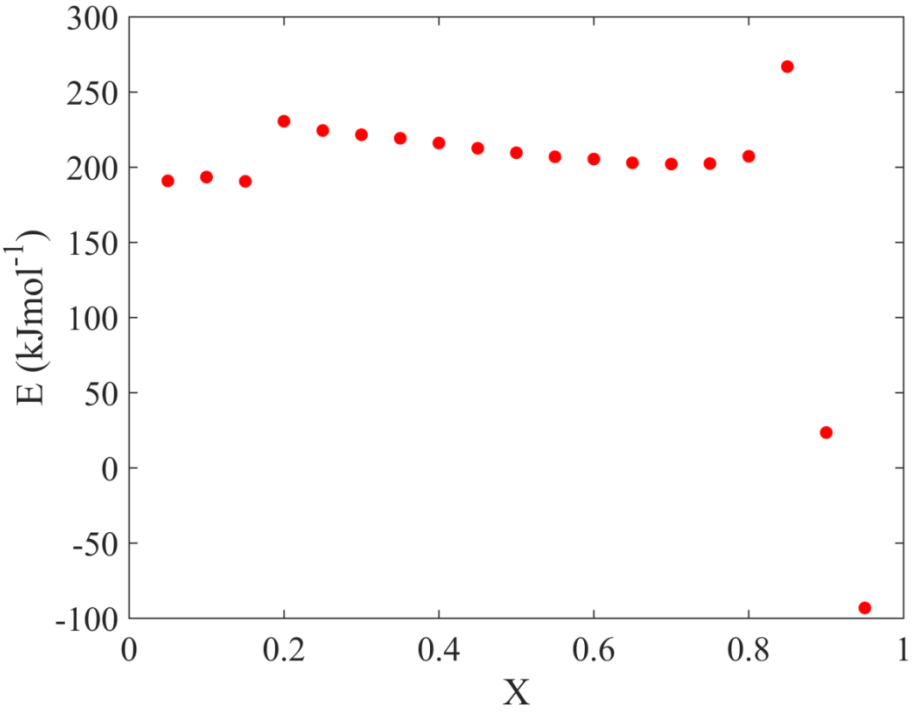

Figure 3.5 Variation of activation energy with conversion for Gliricidia

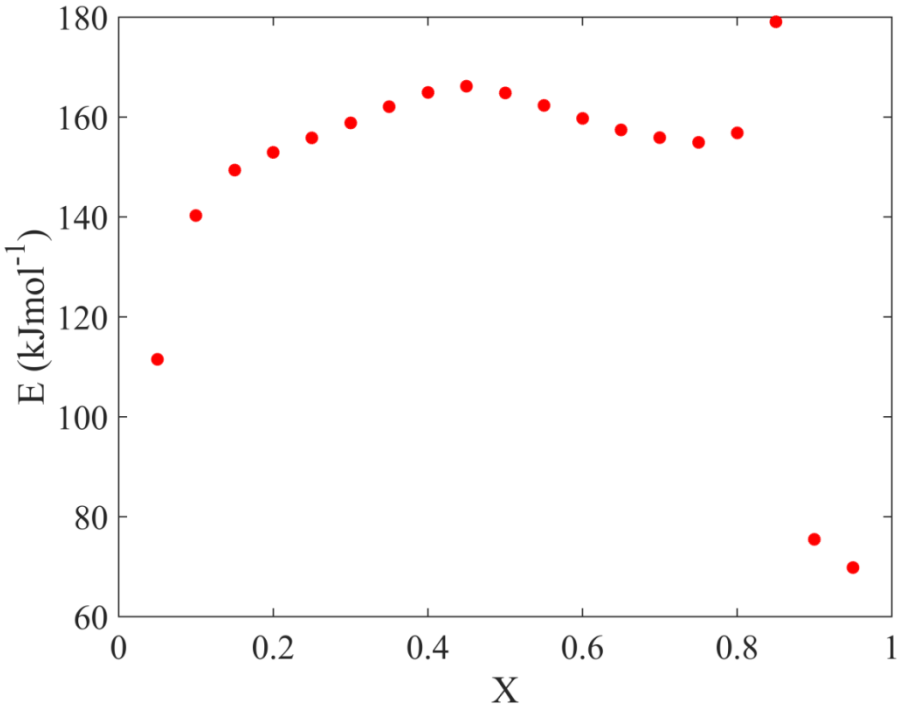

Figure 3.6 Variation of activation energy with conversion for Rubber

When the two figures, Figure 3.5 and Figure 3.6 are compared, difference in activation energy profile can be observed. Different types of wood have different compositions of hemicellulose, cellulose and lignin and different structures which are linked with the observed change in activation energy variation profile. An increase in activation energy at 0.85 conversion and a sharp decrease in the activation energy beyond conversion of 0.85 is observed for the two wood types Gliricidia and rubber (Figure 3.5 and Figure 3.6). Kinetic studies done for different wood types [88] and other biomass types [95] showed similar observation at high conversions. Decay of charcoal which has been formed during primary pyrolysis stage resulted in the observed increase in activation energy. Kinetic parameters reported in literature show wide variation even for the same variety of wood due to different experimental conditions and different procedures used in calculations even for the same method.

High correlation factor is an indication of the existence of linear and parallel relationships at conversion levels between 0.15 and 0.80 for Gliricidia and 0.05 and 0.85 for Rubber. This is an indication of the occurrence of a single or a set of parallel first order reactions in pyrolysis of Gliricidia and Rubber [87]. Therefore, Miura and Maki approach can be applied to analyse pyrolysis kinetics of Gliricidia and Rubber wood fuels.

3.5 Conclusions

Activation energy of Rubber wood calculated by the sequential approach is 83.44 $kJmol^{-1}$ and Gliricidia is 107.19 $kJmol^{-1}$. Pre-exponential factor is $8.88x10^{6}s^{-1}$and $9.5x10^{4}\ s^{-1}$for Gliricidia and Rubber respectively.

Miura and Maki, approach was used to analyse model free pyrolyisis kinetics by DAEM. Kinetic parameters obtained by Miura and Maki approach are not suitable to analyse pyrolysis kinetics of Gliricidia at conversions lower than 0.15. Variation of (β/T^2) versus $(1/T)$ is not linear for Gliricidia and Rubber at high conversions. Therefore, kinetic parameters calculated at conversions beyond 0.85 are not suitable to explain decomposition of both Gliricidia and Rubber. High correlation factors demonstrate that Miura and Maki approach can be successfully used within the

conversion range of 0.15 to 0.8 for Gliricidia and 0.05 to 0.85 for Rubber. Activation energy value analysed by Miura and Maki approach for Gliricidia wood is in the range of 190.58 $kJmol^{-1}$ to 230.57 $kJmol^{-1}$ and for Rubber wood it is in the range of 111.52 $kJmol^{-1}$ to 179.07 $kJmol^{-1}$. When the obtained kinetics for two wood types from each method is compared, a substantial difference between the values can be observed. Therefore, type of the wood can have significant effect on the burning characteristics. Thus, operating conditions should be selected to match with the wood type used in furnaces.

Chapter 4

DESCRIPTION OF MATHEMATICAL MODEL FOR PACKED BED COMBUSTION

4.1 Overview of the model

Two phase (gas and solid) model, which is incorporated with all thermochemical conversions, mass and heat transfers was developed for particulate biomass combustion. The model developed consists of a packed bed combustion model and a moving grate combustion model. These models were developed within the CFD framework. CFD method applies conservation equations to solve mass, momentum and energy change in flow fields according to conservation laws in physics. The simulated space is divided into large number of control volumes and following steps are used in solving conservation equations.

- Conservation equations are applied to each cell of the domain
- Integration of conservation equations over the cell
- Integrated equations are discretised into a set of algebraic equations
- Solving algebraic equations iteratively

Simulation results obtained from the packed bed wood combustion model were validated with the measured data taken from a laboratory scale combustor. The validated model was used to analyse the effect of particle size on ER requirement for wood combustion in packed bed arrangements.

4.2 Packed bed combustion model

A particulate biomass combustor consists of two zones, which are bed zone and free board zone. In the free board zone only gas phase presents. Bed zone can be considered as a porous media where both solid and gas phases are present.

Euler-Euler representation was used to model packed bed combustion in fixed grate type furnace. Packed bed combustion is characterized by large fuel particles, large

furnace sizes, large number of fuel particles with bulk movement of solid. Large sized particles which are in thermally thick regime are combusted in packed bed furnaces. Temperature and species gradients inside thermally thick particles are described mainly by separate DPMs. The DPMs developed so far describe the particle conversion and gradients radially in one dimension. Thermal conversion of large sized particles is three-dimensional which cannot be correctly represented by a one-dimensional model. The reviewed individual particle models so far have been limited to the size range of 5 mm - 25 mm, which limited their applicability to particles that are slightly thermally thick. Two- or three-dimensional models with sufficiently small cell sizes allow the heterogenous nature of conversion of large sized fuel particles to be represented with intra particle gradients, in Eulerian approach. Indiviual particle modelling for a packed bed which consists of large number of particles is limited by the computational power requirement. In addition, particles of different shapes can be modelled by Eulerian method by calculating surface area for different particle shapes and calculating Nusselt number and Sherwood number correlations based on different particle shapes. Therefore, within the Eulerian framework packed bed combustion can be simulated with less computational time requirement. In experimental work conducted for validation, cubed shaped particles were used. Therefore, to implement cubed shape particles in the model, particle shape was assumed to be spherical. In the present model, solid phase and gas phase are fully coupled. Therefore, biomass bed and the free board are solved simultaneously. The assumptions used in the model are as follows:

- Eulerian representation is used with volume averaged properties within the biomass bed
- Biomass particles are thermally thick
- Particles are spherical
- Heat and mass transfer of the packed bed is model by calculating the specific surface area of the biomass bed based on specific surface area of individual particle
- Porosity of the bed remains constant during entire process
- Fragmentation is neglected

- The solids movement is towards the downward direction

4.3 Selective solving of conservation equations

Simulated geometry is discretised into number of control volumes (cells) in CFD modelling procedure. The descretised furnace geometry consists of cells in the free board zone which contain only gas and cells in the bed zone which contain both gas and solid (porous media) (Figure 4.1). Conservation equations are applied separately for solid phase variables (energy, moisture, wood, char and ash) and gas phase variables (gas flow, energy, and gas species). For cells in the bed zone, both solid phase and gas phase conservation equations are solved. For cells in the free board zone, gas phase conservation equations are solved. This is done by introducing a parameter: "selection value" to select cells in the bed zone which contain solids according to the criteria given in Eq. (4.1). If solid density of a certain cell is higher than zero, it is identified as a bed zone cell that contains solid and gas, where selection value becomes 1. Then, solid and gas phase conservation equations are solved by volume averaging according to porosity value. If the solid density is equal to zero, that cell is identified as a free board cell which contains only gas phase, therefore, only gas phase conservation equations are solved.

$$\text{selection value} = \begin{cases} 1 \text{ if solid density} > 0 \\ 0 \text{ if solid density} = 0 \end{cases} \tag{4.1}$$

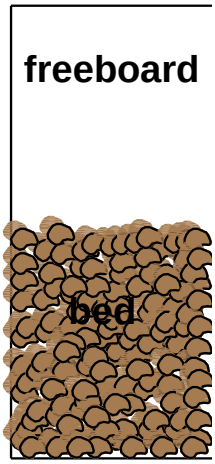

Figure 4.1 Free board zone and bed zone in the furnace

4.4 Conservation equations

Governing equations for momentum (Eq (4.2)), species (Eq (4.3)) and energy (Eq (4.4)) are applied for gas phase. Gas density is denoted by ρ_g, velocity of gas is given by u, porosity of the fuel bed is described by φ and gas phase temperature is described by T_g. The τ in Eq. (4.2) is the stress tensor due to turbulence. S_m is the momentum resistance to gas flow through the packed bed which is described in Section 4.12.1. Y_i is the gas species mass fraction. Seven gas species; CO, CO_2, CH_4, H_2O, H_2, O_2 and N_2 are modelled and $D_{eff,i}$ describes their effective diffusivities in the furnace. $S_{g,i}$ and $S_{s,i}$ are the source terms which come from gas phase and solid phase reactions. C_{pg} is the specific heat capacity of gas phase which is calculated by the relationships given in Eq (4.42). λ_g is the thermal conductivity of gas phase constitiuents. $R_{g,i}$ is the gas phase reaction rates and $H_{g,i}$ is the heat of reaction of i^{th} gas phase reaction. Radiation heat source term included in gas phase equation is described by $Q_{rad,g}$, which is calculated based on P_1 approximation [100].

Gas phase

Momentum conservation equation

$$\partial\phi\rho_g u/\partial t + \nabla.(\phi\rho_g uu) = -\phi\nabla P + \nabla.\phi\,\tau - S_m \tag{4.2}$$

Species conservation equation

$$\partial\phi\rho_g Y_i/\partial t + \nabla.(\phi\rho_g u Y_i) = +\nabla(\phi\rho_g D_{eff,i}\nabla(Y_i)) + S_{g,i} + S_{s,i} \tag{4.3}$$

Energy conservation equation

$$\begin{aligned}\partial\phi\rho_g C_{pg} T_g/\partial t + \nabla.(\phi\rho_g u C_{pg} T_g) = {} & +\nabla(\phi\lambda_g\nabla(T_g)) + hA_{spec}\left(T_s - T_g\right) \\ & + \sum S_{s,i} C_{pg}(T_s - T_g) + \sum R_{g,i} H_{g,i} + Q_{rad,g}\end{aligned} \tag{4.4}$$

Gas and solid exchange heat at the particle surface depending on surrounding fluid flow conditions. This interface heat transfer (heat transfer coefficient, h) is governed by Nusselt number (Nu), thermal conductivity of gas and the initial particle diameter ($d_{p,o}$) as described in Eq. (4.5). Nusselt number varies for different shapes and different flow conditions [26], [101]. The presented model has the capability to calculate Nusselt number according to different particle shapes. The Nusselt number correlation presented in Eq. (4.37) and Sherwood number correlation given in Eq. (4.39) was used for packed bed combustion model and it was assumed that the particles do not change their shape during conversion.

$$h = \lambda_g \frac{Nu}{d_{p,o}} \tag{4.5}$$

Species conservation (Eq (4.6)) and energy conservation (Eq (4.7)) equations are applied to solid phase. Solid phase constituents are described by $m_{s,i}$ and $R_{s,i}$ describes the solid phase reaction rates of constituents.The biomass bed reduces its volume due to mass loss in the fuel. This causes solid to move towards the grate, which is included in the solid phase conservation equations as a convective flux in Eq. (4.6) and Eq. (4.7). u_{bed} describes the velocity of fuel due to volume reduction. In solid phase energy conservation equation, T_s explains solid phase temperature, ρ_s explains fuel density, C_{ps} explains solid phase specific heat capacity, λ_s explains thermal conductivity of solids and $H_{s,i}$ heat of reaction of solid phase constituents. The last two terms in the right-hand side of the energy conservation equation describes radiation energy absorbed and emitted by solid phase. Emissivity is described by e and radiation intensity is described by G. Steffan Boltzmann constant is described by σ and a_s describes the absorption coefficient.

Solid phase

Mass conservation equation

$$\partial m_{s,i}/\partial t + \nabla.(u_{bed} m_{s,i}) = \sum R_{s,i} \tag{4.6}$$

Energy conservation equation

$$\partial((1-\phi)\rho_s C_{ps} T_s)/\partial t + \nabla.((1-\phi)\rho_s u_{bed} C_{ps} T_s) = +\nabla.(\lambda_s \nabla T_s) - hA_{spec}(T_s - T_g) + \sum R_{s,i} H_{s,i} + 4eG - A_{spec} a_s \sigma T_s^4 \tag{4.7}$$

The effective heat transfer area of an individual particle was calculated based on the ratio of particle surface area to volume. This ratio was used to calculate the specific surface area of packed bed by considering that bed volume is filled up with spherical shaped particles. To calculate heat transfer of the particle with outside flow, A_{spec} is calculated based on outer surface area of the particle. Therefore, effective packed bed surface area (A_{spec} for packed bed of spherical particles) is calculated by Eq. (4.8).

$$A_{spec} = \frac{6(1-\phi)}{d_{p,o}} \tag{4.8}$$

4.5 Drying

Combustion of thermally thick wood particles was modelled in present study. Therefore, the drying rate was assumed to be mainly controlled by heat transfer. Therefore, drying rate is described by heat sink model. Mass of water is given by $m_{s,w}$. Heat of evaporation is described by ΔH_m. Time taken for evaporation is Δt. The evaporation temperature (T_{evap}) is assumed to be 100 ^oC, which is the saturated temperature of water at atmospheric pressure.

$$R_{s,w} = \begin{cases} -\dfrac{(T_s - T_{evap}) m_{s,w} C_{p,s}}{\Delta H_m \Delta t} & \text{if } T_s \geq T_{evap} \\ 0 & \text{if } T_s < T_{evap} \end{cases} \tag{4.9}$$

Mass fraction of bound water is described by Y_b. Additional energy is required for desorption of bound water molecules from cell walls. If the moisture in wood is free water, i.e. moisture content larger than fibre saturation point, heat requirement for evaporation is calculated by Eq. (4.10). If the moisture in wood is bound water, i.e. moisture in the wood is lower than fibre saturation point heat requirement for moisture evaporation is calculated by Eq. (4.11) [11]. Fibre saturation point is considered as 30% by mass on dry basis [7].

$$\Delta H_m = 3.179 \times 10^6 - 2500 T_s \tag{4.10}$$

$$\Delta H_m = 3179 \times 10^6 - 2500 T_s + 1.1762 \times 10^6 \exp(-15 Y_b) \tag{4.11}$$

4.6 Pyrolysis

In packed bed combustion model and moving grate combustion model, global one step pyrolysis reaction R4.1 was used. Global one step model is the most widely used pyrolysis model. In addition, global one step model is the simplest model and kinetic parameters were also derived in this study according to global one step mechanism. When modelling of complex transport processes are to be done, simplication of kinetic mechanisms were adviced [102]. Kinetic parameters obtained for first order decomposition of Rubber wood which are given in Table 4.3 were used in the simulations.

Heat of pyrolysis is reported to vary from being exothermic to endothermic [22], [99], [103]–[106] . At lower temperatures (below 773 K), under inert and impurity free atmospheres heat of pyrolysis is mainly endothermic with char formation being exothermic [106]. In number of modelling studies on packed bed combustion pyrolysis was modelled as a heat-neutral process [104], [106], [107]. In addition, heat of pyrolysis, either exothermic or endothermic, reported in literature is considerably lower than heat of reaction for other heterogeneous reactions. In the present model, pyrolysis heat is assumed to be zero. Pyrolysis gas composition is tabulated in Table 4.1. The values are calculated based on the ash free fuel composition ($C_{3.98}H_{6.58}O_{2.85}$) and constraints for pyrolysis gas constituents presented in Table 4.2 [26]. Hydrocarbon gases are summed together and assumed to be equal to CH_4.

Wood $\rightarrow$ 0.145 Char + 0.85 Gas + 0.005 Ash R4.1

Table 4.1 Volatile composition

Gas component	CO_2	CO	H_2	CH_4	H_2O
Mass fraction	0.263	0.395	0.013	0.197	0.132

Table 4.2 Volatile species distribution presented in [9]

$0.1 < mCO/mCO_2 < 10$
$0.1 < mCH_4/mCO_2 < 1$
$0.05 < mH_2/mCO_2 < 0.4$
$0.5 < mH_2O/mCO_2 < 4$

4.7 Char reactions

Four char reactions (R4.2 - R4.5) were used to describe heterogeneous reactions. Char reacts with O_2 and H_2 and produces heat in the fuel phase. Reaction of char with CO_2 and H_2O is endothermic. Oxygen availability is high in combustion chambers. Therefore, in such conditions, rate of reaction of char with O_2 becomes fastest. In oxygen limited environments, gasification reactions (R4.3 - R4.5) are promoted.

$$\Omega_c\, C + O_2 \rightarrow 2(\Omega_c\text{-}1)\, CO + (2\text{-}\Omega_c)\, CO_2 \qquad \text{R4.2}$$

$$C + CO_2 \rightarrow 2\, CO \qquad \text{R4.3}$$

$$C + H_2O \rightarrow CO + H_2 \qquad \text{R4.4}$$

$$C + 2\, H_2 \rightarrow CH_4 \qquad \text{R4.5}$$

Eq. (4.12) describes apparent kinetic rate of char based on the external particle surface area (A_{spec}) and reactive gas species concentration at the particle surface (C_i). M_c is molecular weight of char and $\Omega_{c,i}$ is the stoichiometric coefficient of respective reaction

$$R_{charreactions} = A_{spec} M_c \Omega_{c,i} k_{i,eff} C_i \qquad (4.12)$$

Char reactions are limited by three mechanisms; transport of reactive gas species from the main gas flow to the particle surface, movement of reactive gas species to the pores of the particle, and kinetics of the reaction. It is assumed that density and size of the particle reduce during the thermal conversion since the particles are in thermally thick regime. Due to high porosity of biomass char, partial penetration of gases is possible. Therefore, it is assumed that the effective reaction rate $k_{i,eff}$ (Eq. (4.13)), is controlled by the three mechanisms described above . Char reaction kinetics (k_i) are given in Table 4.3. Combined effect of movement of reactant gases to the particle surface and diffusion of gas species to the pores in the char surface was included in calculating effective mass transfer coefficient ($h_{m,ieff}$) between gas flow and particle in Eq. (4.14). $h_{m,i}$ is the mass transfer coefficient of i^{th} gas component in the boundary layer and $h_{m,a,i}$ is the mass transfer coefficient of gas species through the ash film. $h_{m,i}$ is inversely proportional to particle diameter (Eq. (4.15)) and $h_{m,a,i}$ is inversely proportional to ash film thickness (Eq. (4.16)) [33]. Thickness of the ash film based on the particle diameter is calculated by Eq. (4.17).

$$k_{i,eff} = \frac{k_i h_{m,ieff}}{(k_i + h_{m,ieff})} \tag{4.13}$$

$$h_{m,ieff} = \frac{h_{m,i} h_{m,a,i}}{h_{m,i} + h_{m,a,i}} \tag{4.14}$$

$$h_{m,i} = \frac{D_{eff,i} Sh}{d_{p,o}} \tag{4.15}$$

$$h_{m,a,i} = \frac{D_{a,i} \phi}{l_a} \tag{4.16}$$

Decrease in particle volume at drying, pyrolysis and char reactions is considered in calculating ash layer thickness l_a.

$$l_a = \frac{1}{2}(d_{p,o}-d_p)\frac{X_a}{\phi_a}\frac{\rho_s}{\rho_a} \tag{4.17}$$

Particle size estimation presented in [33] was used to calculate the particle diameter (d_p) which is required in Eq. (4.17). Effective diffusion coefficient of gases through fuel bed ($D_{eff,\ i}$) is described by Eq. (4.18) [33]. Different expressions exist for Sherwood number correlation of different shapes of particles [26]. Sherwood number correlation presented in Eq. (4.39) is used to describe mass transfer of gases to the particle through boundary layer ([100]). Knudsen diffusivity ($D_{k,i}$) (Eq. (4.20)), and binary diffusivity (D_i) of gas species (Eq. (4.21)) [26] are used to calculate diffusion coefficient of i^{th} species through the ash film ($D_{a,i}$) (Eq. (4.19)). $\sigma_{i,air}$ and $\Omega_{i,air}$ in Eq. (4.21) are collision diameter and collisional integral respectively. M_i and M_{air} are molecular weight of i^{th} gas species and molecular weight of air respectively.

$$D_{eff,i} = 0.8D_i+0.5|u|d_{p,o} \tag{4.18}$$

$$D_{a,i} = \frac{D_i D_{k,i}}{D_i+D_{k,i}} \tag{4.19}$$

$$D_{k,i} = \frac{2}{3}d_{pore}\sqrt{\frac{2}{\pi}\frac{RT_g}{M_i}} \tag{4.20}$$

$$D_i = 0.0018583\sqrt{T_g^3\left(\frac{1}{M_i}+\frac{1}{M_{air}}\right)}\frac{1}{P\sigma_{i,air}^2\Omega_{i,air}} \tag{4.21}$$

Table 4.3 Kinetics of solid phase reactions

Reaction Index	Kinetics	Ref	Heat of reaction (J/kg)	Ref
R4.1	$9.5\times10^{4}\exp(-8.344\times10^{4}/RT_s)m_{s,w}$	[94]	0	[104]
R4.2	$1.715T_s \exp(-74827/RT_s)$	[26]	$(2(\Omega_c-1)9.8\times10^{6}+(2-\Omega_c)33.1\times10^{6})/\Omega_c$	[7]
R4.3	$3.42T_s \exp(-129700/RT_s)$	[108]	-14.3833×10^{6}	[7]
R4.4	$3.42T_s \exp(-1.29700/RT_s)$	[108]	-10.95×10^{6}	[7]
R4.5	$4.189T_s \exp(-19.2/RT_s)$	[109]	-6.242×10^{6}	[110]

4.8 Gas phase reactions

Availability of species and temperature affects gas phase reaction rates. Gas phase reaction rate, $R_{g,i}$ (Eq. (4.22)) is the minimum reaction rate selected from mixing and kinetic rate. Different models are available in the literature to estimate effect of mixing in gas phase reactions. Gas phase mixing rate ($R_{mix,i}$) is described by the formulae presented in Eq. 4.23 [33]. Kinetic parameters of the rate expression, $R_{k,i}$ of gas phase reactions, R4.6 to R4.10, are included in Table 4.4. Heat of reaction of gas phase reactions is calculated by formation enthalpies of participating gases. $\Omega_{g,i}$ is the stoichiometric coefficient gas species in i^{th} reaction.

$$R_{g,i} = \min(R_{mix,i}, R_{k,i}) \tag{4.22}$$

$$R_{mix,i} = 0.63\left(\frac{1.75|u|(1-\phi)}{\phi d_p}\right)\min(C_i/\Omega_{g,i}) \tag{4.23}$$

$$CO + 1/2\ O_2 \rightarrow CO_2 \qquad \text{R4.6}$$

$$H_2 + 1/2\ O_2 \rightarrow H_2O \qquad \text{R4.7}$$

$$CH_4 + 3/2\ O_2 \rightarrow CO + 2\ H_2O \qquad \text{R4.8}$$

$$CO + H_2O \rightarrow CO_2 + H_2 \qquad R4.9$$

$$CO_2 + H_2 \rightarrow CO + H_2O \qquad R4.10$$

Table 4.4 Kinetics of gas phase reactions

Reaction Index	**Kinetics**	**Ref**
R6	$1.3\times10^{11}\ \exp(-1.2554\times10^{5}/RT_g)C_{CO}C_{O2}^{0.5}C_{H2O}^{0.5}$	[7]
R7	$1\times10^{11}\ \exp(-8.3145\times10^{4}/RT_g)C_{H2}C_{O2}^{0.5}$	[7]
R8	$5.012\times10^{11}\ \exp(2\times10^{5}/RT_g)C_{CH4}^{0.5}C_{O2}$	[7]
R9	$2.78\ \exp(1.2554\times10^{4}/RT_g)C_{H2O}C_{CO}$	[7]
R10	$3.69\ \exp(4.659\times10^{4}/RT_g)C_{CO2}C_{H2}$	[7]

4.9 Turbulence

Standard k-epsilon model was used in this research due to its capability of producing accurate results with less computational power [32]. It has been the widely used turbulent model in packed bed combustion modelling applications [22], [53], [111]–[114]. Turbulent kinetic energy is presented by k and turbulent dissipation rate is described by ε. μ_t is the turbulent viscosity. σ_k, σ_ε, C_1 and C_2 are model constants applied to standard k-epsilon model.

$$\frac{\partial(\phi\rho_g k)}{\partial t}+\nabla.\left(\phi\rho_g k\vec{u}\right)=\nabla\left(\phi\left(\frac{\mu_t}{\sigma_k}\right)\nabla k\right)+2\phi\mu_t S_{ij}.S_{ij}-\phi\rho_g\varepsilon \qquad (4.24)$$

$$\frac{\partial(\phi\rho_g \varepsilon)}{\partial t}+\nabla.\left(\phi\rho_g \varepsilon\vec{u}\right)=\nabla\left(\phi\left(\frac{\mu_t}{\sigma_\varepsilon}\right)\nabla\varepsilon\right)+C_1\frac{\varepsilon}{k}2\phi\mu_t S_{ij}.S_{ij}-C_2\phi\rho_g\frac{\varepsilon^2}{k} \qquad (4.25)$$

4.10 Radiation

DOM is applicable to both optically thin and optically thick problems and is able to produce accurate results. Although DOM is available as an inbuilt model in OpenFOAM, in the development of in-house solvers as in present work, including DOM through solver codes is a complicated task. Therefore, P1 approximation is used in the present work. In addition, P1 model is simple and computer resource requirement is less [100]. Therefore, radiation intensity was modelled by Eq. (4.26).

$$\nabla.\frac{1}{3\left(a_g+a_s+\sigma_s\right)}\nabla G-4\pi\left(a_g n^2\frac{\sigma T_g^4}{\pi}+E_p\right)-(a_g+a_s)G=0 \tag{4.26}$$

Refractive index (n) of gas is assumed to be 1. The scattering coefficient is defined by σ_s. The radiation energy emitted from the particles is included by Eq. (4.27). The surface area of the particle participating in radiation is expressed by A_p. The emmisivity of solid (e), is assumed to be constant throughout the simulations and emmisivity of wood was used for e in the presented model.

$$E_p=eA_p\sigma T_s^4 \tag{4.27}$$

4.11 Bed shrinkage

In the present model, it is assumed that biomass bed shrinks while porosity remains constant during the entire thermal conversion. The assumption of constant porosity helps to maintain the stability of the solver. The effect of bed shrinkage is included as a convective flux in solid phase conservation equations. Only the movement of fuel towards the mesh due to shrinkage is assumed in this fixed grate combustion model. The model assumes bulk movement of the bed and does not include estimation on the irregularities present in bed shrinkage. The difference in solid bed volume at two consecutive time steps is used to calculate volume reduction. If the total mass of a cell is higher than a predefined value, its volume is added to the fuel bed volume. The cells with lower total mass than the predefined value, are taken as

cells with reduced volume and are subtracted from the solid bed volume. The predefined value was obtained as 95 kgm^{-3} by trial simulations of the system. Variable β is used to identify the cells in the fuel bed according to the Eq. (4.28) and Eq. (4.29).

$$\beta = 1 \text{ total mass of the cell} \geq 95 \text{ kgm}^3 \tag{4.28}$$

$$\beta = 0 \text{ total mass of the cell} < 95 \text{ kgm}^3 \tag{4.29}$$

Summation of the volume of cells that contains solids according to Eq. (4.30) results in the fuel bed volume.

$$\text{current bed volume} = \int \beta V_{cell} \tag{4.30}$$

The difference in bed volume at two consecutive time steps is manipulated according to Eq. (4.31) to calculate bed velocity due to shrinkage.

$$u_{bed} = \frac{(\text{bed volume at previous time step-current bed volume})}{\Delta t}\gamma \tag{4.31}$$

In order to maintain the stability of the solver, bed velocity, u_{bed} has to be maintained below 0.1 ms^{-1} in the packed bed model and 0.0001 ms^{-1} in the moving grate furnace model, respectively.

4.12 Thermophysical properties

4.12.1 Momentum resistance source term (S_m)

A drop-in pressure inside the fuel bed is resulted by the resistance of the particles. Relationship for calculation this resistance term is by the Ergun equation (Eq. (4.32)) [9].

$$S_m = \frac{\mu 150(1-\phi)^2}{{d_{p,o}}^2 \phi^3} u + \frac{3.5(1-\phi)}{d_{p,o}\phi^3} \rho_g |u| u \tag{4.32}$$

4.12.2 Dimensionless numbers

Nusselt number

Heat transfer calculation given in Eq. (4.5), is based on Nusselt number relationship. Numerous formulations have been derived for different shapes under different flow conditions are presented in [101], [115]. Nusselt number is represented as a relationship between Reynolds number (Re) and Prandtle number (Pr). Nusselt number for a sphere in a stationary fluid is 2. Nusselt number for a sphere which has constant surface temperature in a flowing fluid is described by Eq. (4.33) [115].

$$Nu = 2 + 0.6 Re^{0.5} Pr^{0.33} \tag{4.33}$$

Nusselt number for a cylinder with constant temperature in a flowing fluid at low velocities under steady state conditions is described by Eq. (4.34) [101].

$$Nu = W_o(Re) Pr^{0.33} + W_1(Re) \tag{4.34}$$

Another correlation for the Nusselt number for cylinder is given by Eq. (4.35)

$$Nu = 2 + \left(0.4 Re^{0.5} + 0.06 Re^{0.66}\right) Pr^{0.4} \left(\frac{\mu_\infty}{\mu_o}\right)^{0.25} \tag{4.35}$$

Nusselt number for a particle that is in a bed of particles is different from that of an individual particle. For a packed bed of spheres Nusselt number is expressed by Eq. (4.36)

$$Nu = 2+0.1Re^{0.5}Pr^{0.33} \quad (4.36)$$

and another correlation given in Eq. (4.37) [116].

$$Nu = (7-10\phi+5\phi^2)(1+0.7Re^{0.2}Pr^{0.33})+(1.33-2.4\phi+1.2\phi^2)Re^{0.7}Pr^{0.33} \quad (4.37)$$

Sherwood number

Sherwood number correlations present in an analogous manner to the Nusselt number. Sherwood number for different shapes depends on Reynolds number and Schmidt number. Sherwood number for spheres, cylinders and flat plates is presented in [115]. Sherwood number for sphere is described by Eq. (4.38).

$$Sh = 2+0.6Re^{0.5}Sc^{0.33} \quad (4.38)$$

Sherwood number for a packed bed of spheres is presented by Eq. (4.39).

$$Sh = 2+0.1Re^{0.5}Sc^{0.33} \quad (4.39)$$

4.12.3 Thermal conductivity

Thermal conductivity of both gas and solid affects the heat transfer in solid fuel combustion. A number of formulations exist for thermal conductivity of gas and solid phases as well as for packed bed of particles.

Thermal conductivity of gases is expressed by correlations presented in [117], [118]. Thermal conductivity of wood depends on temperature, density, composition, structure and grain orientation in the direction of heat transfer. Different relationships have been proposed to describe thermal conductivity of solids in packed beds. Effective thermal conductivity of wood has been used in the solid phase energy conservation equation [118]. This value is calculated based on thermal conductivity

of solid in a non-moving fluid. A modification to this representation was used in [119].

Effective thermal conductivity of fuel was calculated by combining, thermal conductivity of fuel phase constituents and the radiation contribution within the pores [8], [44]. In [120] contribution from radiative factor in the thermal conductivity was not included. Modelling radiative heat transport within the solid phase by conductivity term is valid for conversion of thermally thin particles in a thermally thick bed during entire conversion. In order to estimate solid phase conductivity, heat electrical analogy was used in [25]. They considered thermal conduction of solid as equivalent to that through and contact point of spheres which are in series connection. Nield and Bejan presented formulations for thermal conductivity where heat conduction occurs in parallel and series. This parallel thermal conduction model was used in [121] ,where one temperature model was used for evaluation of heat transfer in packed bed gasification. In the present work thermal conductivity of gas is calculated by Eq. (4.40) [118]. Thermal conductivity of solid was calculated by mass weighted average of moist wood, char and ash as given in Eq. (4.41) [14]. Table 4.5 presents the thermal conductivities of solid phase constituents.

$$\lambda_g = 4.8\times10^{4} T_g^{0.717} \tag{4.40}$$

$$\lambda_s = Y_{wood}\lambda_{wood} + Y_{char}\lambda_{char} + Y_{ash}\lambda_{ash} \tag{4.41}$$

Table 4.5 Thermal conductivities of solid constituents

Constituent	Thermal conductivity ($Wm^{-1}K^{-1}$)	Ref
Wood	$(0.129\text{-}4.9\times10^{-2}\ Y_w)(1+(2.05+4\ Y_w)\times10^{-3}(T_s\ \text{-}273.15))(0.986+2.695\ Y_w)$	[14]
Char	0.071	[14]
Ash	1.2	[26]

4.12.4 Specific heat capacity

Specific heat capacity of a gas mixture is calculated by the individual specific heat capacities of constituent gases. Therefore, mass weighted specific heat capacity can be used to calculate the average specific heat capacity of a gas mixture. A simplified approach for calculation of gas phase heat capacity was used by Jurena [20] which is used in the present model (Eq. (4.42)).

$$Cp_g = 990 + 0.122T_g - 5680 \times 10^3 T_g^{-2} \quad (4.42)$$

Specific heat capacity of solid depends on its constituents. Therefore, specific heat capacity was calculated based on the constituents as given below in Eq. (4.43). Specific heat capacities of solid phase species were obtained by [16] (Table 4.6).

$$Cp_s = Cp_{moisture} Y_{moisture} + Cp_{wood} Y_{wood} + Cp_{char} Y_{char} + Cp_{ash} Y_{ash} \quad (4.43)$$

Table 4.6 Specific heat capacities of solid constituents

Constituent	Specific heat capacity ($Jkg^{-1}K^{-1}$)	Ref
Moisture	4200	[16]
Wood	$1500+T_s$	[16]
Char	$420+2.09T_s-6.85\times10^{-4}T_s^2$	[16]

4.12.5 Viscosity

Laminar viscosity of gas (μ) was calculated by the relationship described in Zhou et al. [118] (Eq. (4.44)).

$$\mu = 1.98 \times 10^{-5} \left(\frac{T_g}{300} \right)^{0.66} \tag{4.44}$$

The turbulent viscosity was calculated by Eq. (4.45) which describes turbulent viscosity term related to standard k-epsilon model. C_μ is a constant which has the value of 0.09 as applicable to standard k-epsilon model which was obtained by comprehensive data fitting for turbulent flows.

$$\mu_t = \rho_g C_\mu \frac{k^2}{\varepsilon} \tag{4.45}$$

4.13 Equivalence Ratio calculations

The developed packed bed combustion model was used to calculate Equivalence Ratio (ER) requirement for different sizes of wood particles. Model described in Chapter 4 was used to simulate wood combustion and ER was calculated by Eq. (4.46). Moles of air available, and moles of air required under stoichiometric conditions were used in calculations.

$$(ER) = \text{Actual air supplied} / \text{Stoichiometric air required} \tag{4.46}$$

Eq. (4.47) was used to calculate the stoichiometric air required for combustion. Y_i is the mass fraction of reactive gas species emitted in pyrolysis. M_i is the molecular weight of i^{th} constituent and $\Omega_{g,i,o,}$ $\Omega_{c,o}$ are stoichiometric factors of oxygen participating in each gas phase and solid phase combustion reaction.

$$\text{Stoichiometric air required} = 4.76 \left(\begin{array}{c} \text{mWood} \times 0.85 \times \sum \left(\frac{Y_i \Omega_{g,i,o}}{M_i} \right) \\ + \text{mChar} \left(\frac{\Omega_{c,o}}{M_c} \right) \end{array} \right) \tag{4.47}$$

4.14 Numerical procedures

The open source software OpenFOAM was used to carry out CFD simulations. OpenFOAM is a free software and provides the opportunity to access and modify the source code. The computational mesh has to be developed in the first step of CFD modelling. The blockMesh utility in OpenFOAM was used for mesh development. Two different meshes were developed for packed bed combustion model and moving grate combustion model. The mesh consists of hexahedron cells for the two models. The setFields utility in OpenFOAM was used to set initial field values of packed bed to the mesh. In-built PISO algorithm in openFOAM was used to solve the conservation equations. PISO algorithm gives more stable results with less computational time compared to other algorithms like SIMPLE and SIMPLEC. The OpenFOAM programme developed for packed bed combustion model is included in Appendix A. Discretisation schemes illustrated in Table 4.7 were applied to discretise convective flux at cell faces.

Table 4.7 Discretisation schemes for packed bed furnace

Term	Discretisation schemes
$\nabla.(\phi\rho_g uu)$	upwind
$\nabla.(\phi\rho_g uY_i)$	upwind
$\nabla.(\phi\rho_g uC_{pg}T_g)$	upwind
$\nabla.(u_{bed}m_{s,i})$	MUSCL
$\nabla.((1-\phi)\rho_s u_{bed}C_{ps}T_s)$	limited linear 1
$\nabla.\left(\phi\rho_g k\vec{u}\right)$	upwind
$\nabla.\left(\phi\rho_g \varepsilon\vec{u}\right)$	upwind
$\nabla.(u_{grate}m_{s,i})$	upwind

.

Chapter 5

MODEL VALIDATION AND ER ANALYSIS OF PACKED BED COMBUSTION

5.1 Experimental setup and boundary conditions

Mathematical model described in Chapter 4 was solved by CFD solving method in OpenFOAM platform. The packed bed combustion model was validated with the laboratory experiments. Then the model was used to analyse the excess air requirement for combustion of different sized wood particles in packed beds.

Combustor illustrated in Figure 5.1 was used for experimental validation of packed bed combustion CFD model. Combustor was fabricated by mild steel and has a square cross section with side length of 300 mm and height of 600 mm. Fuel is packed on a mesh fixed at the bottom of the combustor. Air for combustion is supplied beneath the mesh. Air flow was manually controlled by an air flow valve to maintain a constant level in a water column by an orifice meter. A weighing scale (W) was used to measure the weight variation of the combustor with time. Three k-type thermocouples were used to measure temperature at different heights. Thermocouple 1 (Th1) is placed at the bottom of the fuel bed. Second one (Th2) is placed at 220 mm above the mesh and the third one (Th3) is placed at 40 mm below the outlet. Bed height variation was measured by the vertical movement of the pointer (H) shown in Figure 5.1

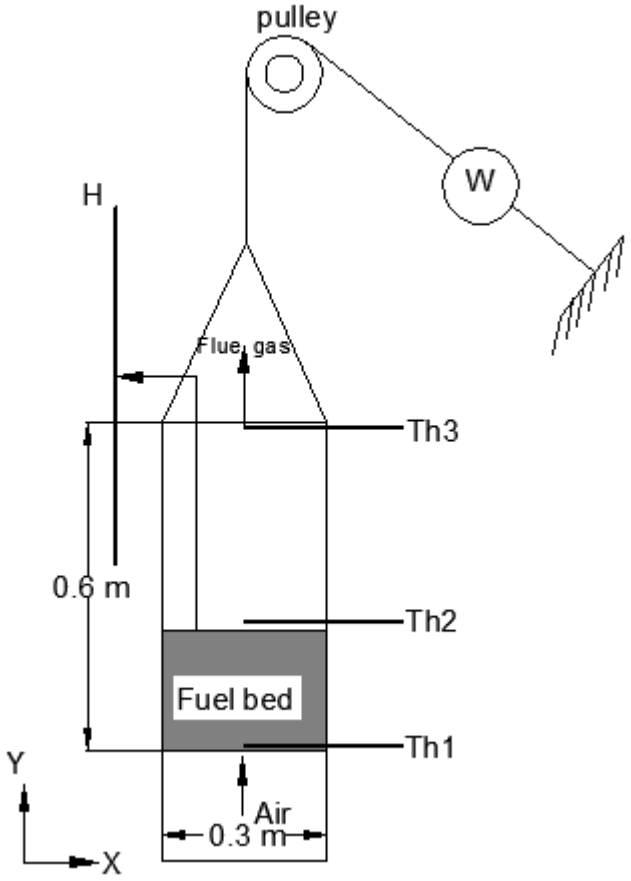

Figure 5.1 Laboratory scale batch type packed bed combustor

Inbuilt PISO algorithm in OpenFOAM was used to solve the gas flow inside the combustor under transient conditions. Two-dimensional computational domain of combustor geometry illustrated in Figure 5.1 Laboratory scale batch type packed bed combustor was simulated by CFD method. Boundary conditions used in the simulations are described in Table 5.1 Boundary conditions. Inlet air properties were assumed to be that of atmospheric air. Inlet air flow velocity was measured for each batch of fuel which gave the value of 0.18 ms^{-1} for 25 mm (1 inch) sized particles. Measured value of inlet air flow velocity was 0.12 ms^{-1} for 38 mm (1.5 inch) and 63 mm (2.5 inch) sized particles. Inlet boundary conditions for variables in the turbulence model were calculated by the estimations presented by Malalasekara [32]. No slip velocity condition is applied for walls of the reactor. For the temperature at the wall, zero gradient boundary condition is applied. Since the walls of the

laboratory scale combustor were not insulated a radiation heat loss term was applied to the radiation intensity of combustor walls. Thermo physical properties used in the simulations are included in Table 5.2.

Table 5.1 Boundary conditions for packed bed furnace

Variable	Inlet	Outlet	Walls
u	0.18 ms^{-1} for 25 mm sized particles 0.12 $ms^{-1}$for 38 mm,63 mm sized particles	$\partial T_g/\partial y=0$	0 ms^{-1}
P	$\partial P/\partial y=0$	1atm	$\partial P/\partial x=0$
T_g	300 K	$\partial T_g/\partial y=0$	$\partial T_g/\partial x =0$
T_s	300 K	$\partial T_s/\partial y=0$	$\partial T_s/\partial x=0$
Y_i	Atmospheric air properties	$\partial Y_i/\partial y=0$	$\partial Y_i/\partial x=0$
k	$2/3(U_{ref}T_i)^2$ T_i= 1%	$\partial k/\partial y=0$	$\partial k/\partial x=0$
ε	$k^{3/2}C_\mu^{0.75}/0.07l$ l= 0.3 m	$\partial \varepsilon/\partial y =0$	$\partial \varepsilon/\partial x=0$
G	- $4e\sigma T_s^4$ (T_s=solid temperature immediately above the grate)	- $4e\sigma T_g^4$	- $4e\sigma(T_{mean}^4-300^4)$, $T_{mean}=T_s+T_g$

Table 5.2 Fuel Specifications used in packed bed model

Property	Value
Moisture	0.05 (Wet basis mass fraction)
Volatiles	0.85 (Dry basis mass fraction)
Char	0.145 (Dry basis mass fraction)
Ash	0.005 (Dry basis mass fraction)
Wood density	499 kgm^{-3}, (bulk density of 159.8 kgm-3)
Weight per batch	3.32 kg
Porosity	0.68
Wood Emissivity	0.85

Mesh refinement was carried out for three different mesh resolutions to evaluate the accuracy and the time required for simulations. Mesh sizes are 800cells (20 cells in 'X' direction, 40 cells in 'Y' direction - mesh 1), 1800 cells (30 cells in 'X' direction, 60 cells in 'Y' direction mesh 2) and 7200 cells (60 cells in 'X' direction, 120 cells in 'Y' direction mesh 3). Time step sizes used for the simulations are 0.02 s for mesh 1 and mesh 2. Time step size is 0.005 s for mesh 3. The results from the simulations are compared to find the effect of mesh size for total mass of the batch for three particle sizes. The results are presented in Figure 5.2, Figure 5.3 and Figure 5.4. Average percentage change in the results between mesh 1 and mesh 2 for 25 mm sized particles is 58%. Percentage change between mesh 2 and mesh 3 is 5.8% for 25 mm sized particles. Average percentage change in the results between mesh 1 and mesh 2 for 38 mm sized particles is 16.9%. Average percentage change in the total mass of the batch between mesh 2 and mesh 3 is 2.9% for 38 mm sized particles. Average percentage change in the results between mesh 1 and mesh 2 for 63 mm sized particles is 5.2%. Average percentage change between mesh 2 and mesh 3 is 2.6% for 63 mm sized particles. Change in the results is insignificant between mesh 2 and mesh 3. Therefore, mesh 2 has been selected for this study considering the less computational time required. Tolerance for each variable was set to 10^{-6}.

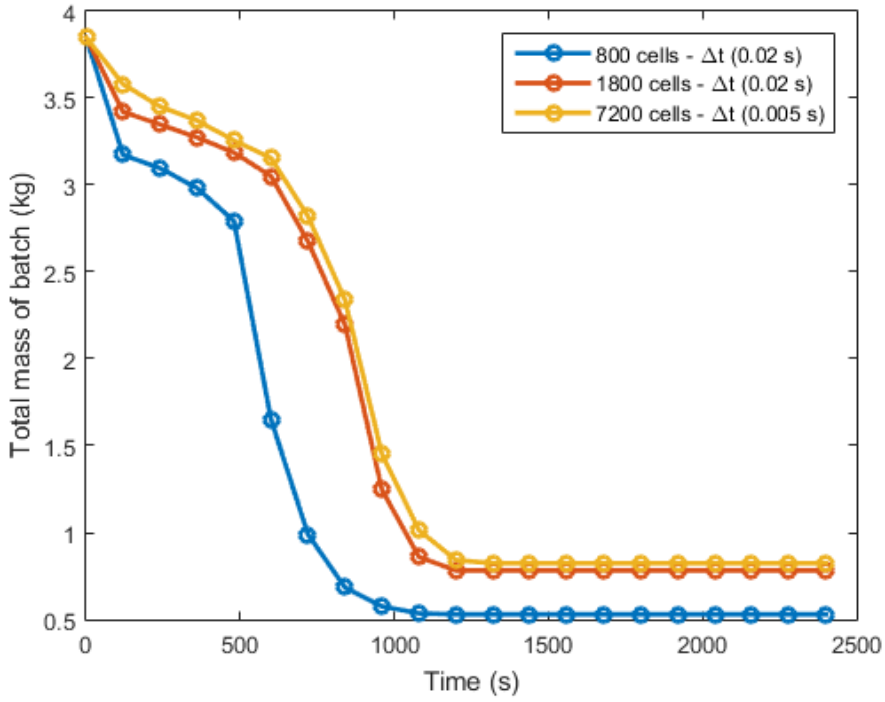

Figure 5.2 Mesh refinement for 25 mm sized particles

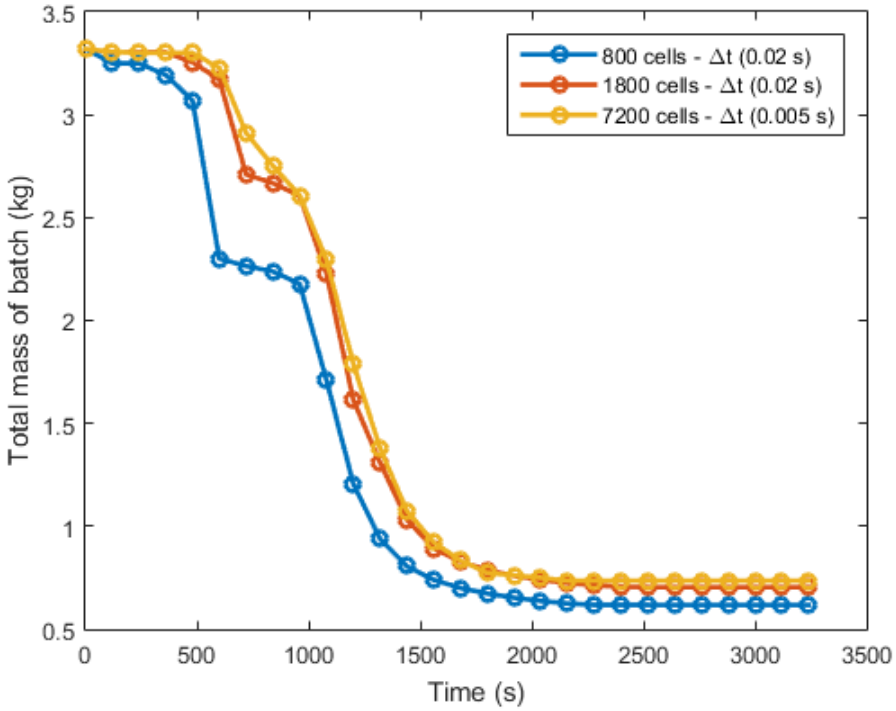

Figure 5.3 Mesh refinement for 38 mm sized particles

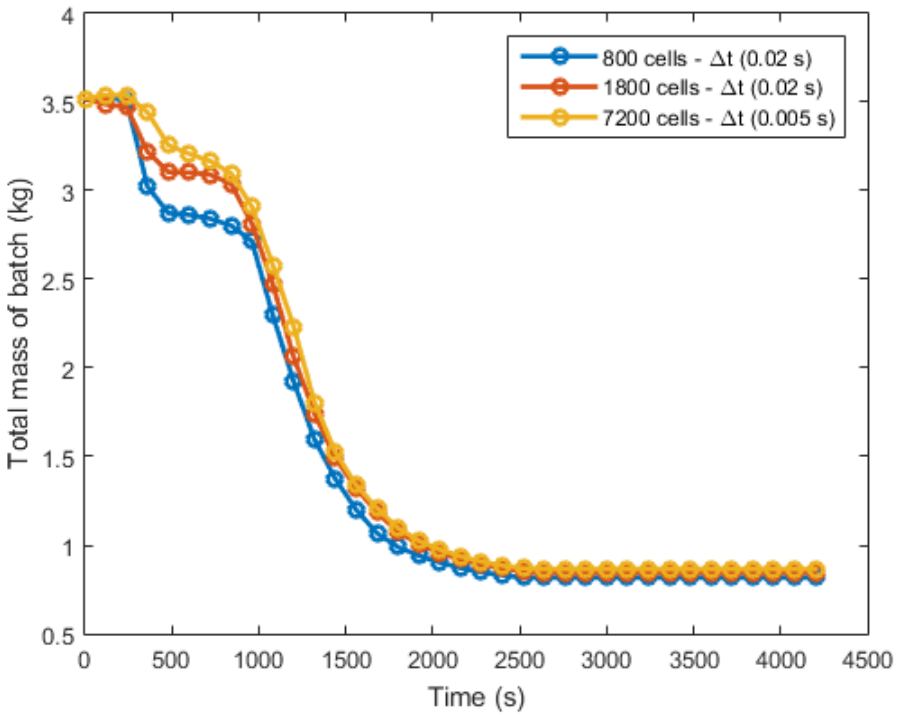

Figure 5.4 Mesh refinement for 63 mm sized particles

5.2 Model validation

Mass fraction variation was used to validate the packed bed combustion model. Validation results are shown for particle sizes of 25 mm (Figure 5.5), 38 mm (Figure 5.6) and 63 mm (Figure 5.7). Cubed shaped Rubber particles were used in the three experiments. Inlet air flow velocity was maintained at 0.18 ms^{-1} for 25 mm particle size. Inlet air flow velocity was maintained at 0.12 ms^{-1} for 38 mm and 63 mm particle sizes. Fuel particles were packed up to an approximate height of 220 m. A heat source placed on the mesh is used to ignite the bed. Figure 5.5 and Figure 5.6 show that there is good agreement between simulation results and experimental data. The root mean square error is 0.06, 0.05 and 0.07 for 25 mm, 38 mm and 63 mm particle sizes respectively. The air flow was manually adjusted during the experiments to maintain a constant air flow which was the reason for the higher deviation observed for 63 mm particle size.

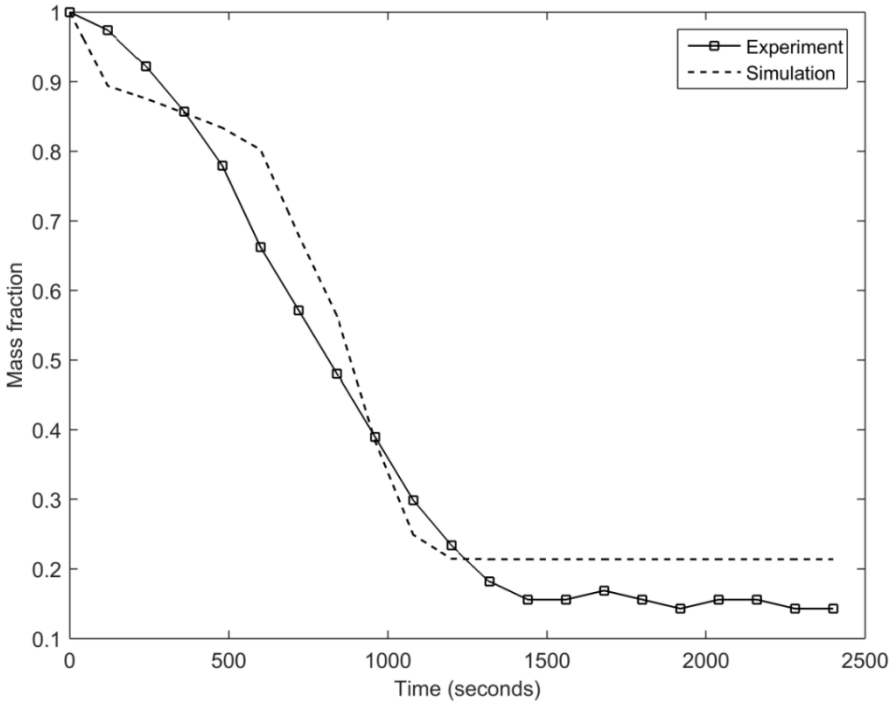

Figure 5.5 Model validation for 25 mm sized wood particles

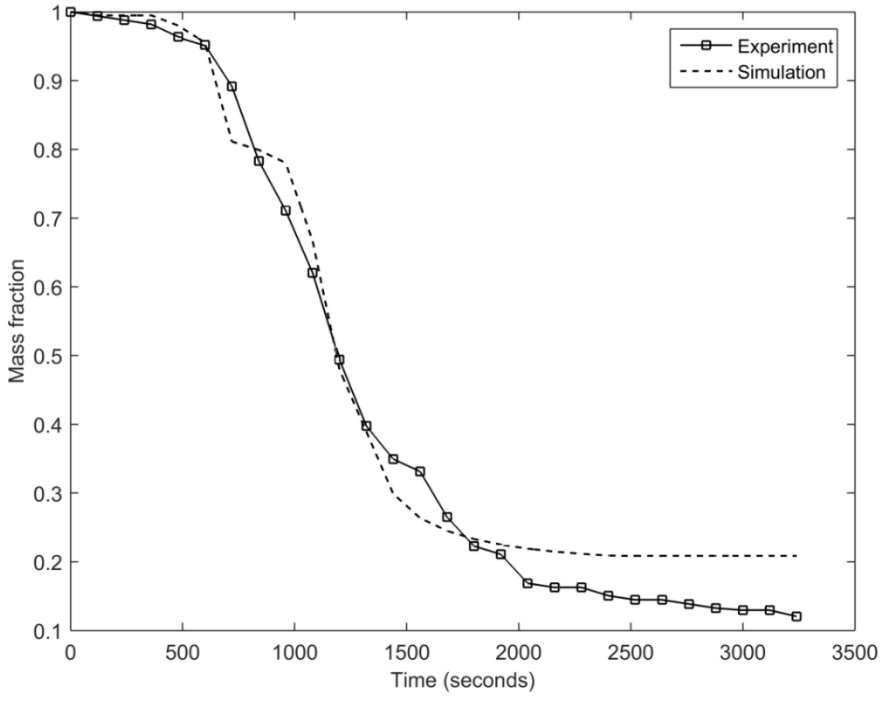

Figure 5.6 Model validation for 38 mm sized wood particles

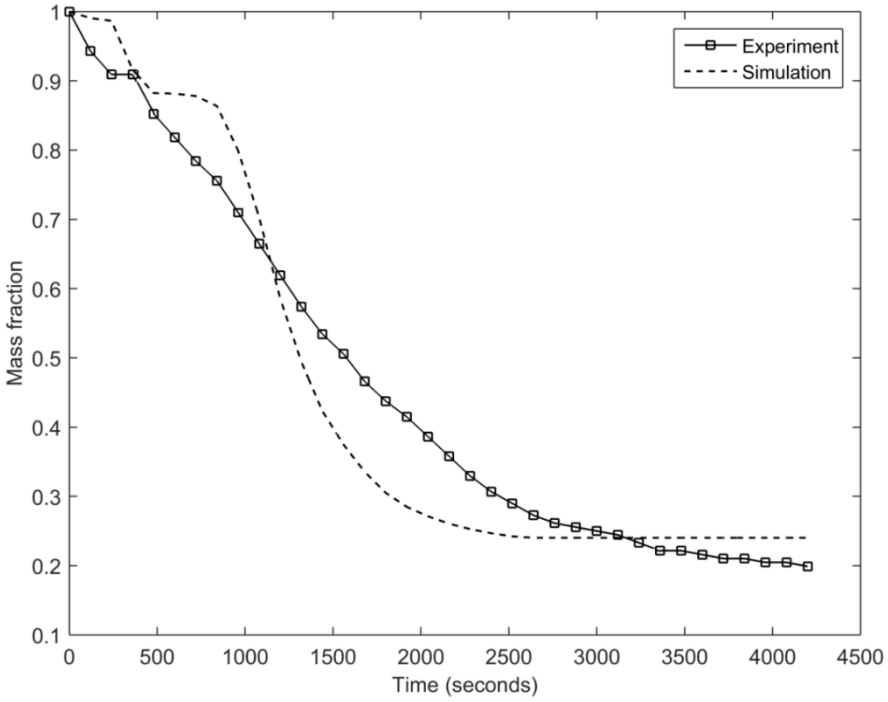

Figure 5.7 Model validation for 63 mm sized wood particles.

5.3 Thermal analysis of wood combustion in packed bed furnaces

5.3.1 Analysis of particle size effect for ER requirement for wood combustion in packed bed furnaces

Furnace geometry, quality of the fuel used, and the air supply affect the performance of furnace. Optimum combustion of wood is decided by adequate supply of air. Insufficient amount of air causes pollutants to generate while high excess air quantities will carry away the heat [122]. Quantity of excess air required for complete combustion of wood in different furnaces has been stated in literature. For wood fired boilers, Kubler stated that excess air requirement is 25% -50% [122]. As stated by Hughes excess air requirement is 50% - 100% for burning moist wood in boilers [123]. Recommended excess air ratio for biomass burning in a grate firied furnace is 25% or above [124]. Combustion behavior of wood makes it difficult to decide optimum amount of excess air required. Increase in burning rate with smaller sized particles and variation of ER with particle size was observed by some researchers [35], [44], [125], [126]. Spatial variation of temperature and wood

particle size in a fixed bed furnace makes the reaction rate to change spatially within the combustor. The effect of particle size on ER ratio was observed in [35], [125], [126]. Recommendation of common ER for different sized particles results in inefficient combustion in furnaces.

Many researchers have done experimental and model-based studies on wood combustion in fixed bed furnaces. The main areas of studies were the effect of particle size variation, shape, inlet air flow rate and moisture content in fixed bed combustions. Effect of particle size, air flow rate and bulk density on the ignition front speed, burning rate, percentage of mass loss, ER and temperature gradient was researched by experimental studies done by Yang et al for biomass combustion in packed beds [125]. When the air flow rate is increased, they observed increased ignition propagation speed and increased mass loss rate. Lower ignition front speed and burning rate was observed for larger particle sizes [125]. Above mentioned variations in packed bed combustion was described by a mathematical model developed for thermally thin particles [35]. They witnessed low values of ER for small particle sizes.

Consequences of variation of quantity of excess air and particle size on CO_2 and CO concentration profiles, combustion efficiency and temperature profile for fluidized bed combustion of biomass were studied by Suranani et al [127]. For fixed excess air amounts, lower temperature inside the reactor was observed for large particle sizes, while higher temperature inside the reactor was observed for small particle sizes. Pérez et al studied influence of particle size and superficial velocity on temperature, maximum temperature inside the bed, flame front velocity, biomass consumption rate, and composition and calorific value of the producer gas in a fixed bed down draft biomass gasification [126]. Increase in particle size causes the maximum temperature to decrease while increase in ER causes maximum temperature to increase. One-dimensional, steady state numerical model was used to analyse a top feed, updraft, and fixed bed furnace by Bryden and Ragland [128]. The model was used to study influence of bed height, under fire air flow rate, wood particle size and under fire air pre heat temperature to obtain a required heat generation rate in the

furnace. Model predicted a low heat release rate for larger wood particle sizes. Existence of a relationship between particle size and equivalence ratio was observed by these researchers. Apart from the general recommendations presented in some literature [122] optimum ERs for wood combustion in packed beds have not been studied hitherto.

Efficient combustion with less pollutant can be achieved by assuring suitable amount of air supply. Relationship of ER with other operating variables can be used to control the air supply to achieve efficient combustion with less pollutant. Particle size affects the reaction rates of solids and heat and mass transfer between gas and solids, as described by Eq. (4.4), Eq. (4.5), Eq. (4.7), Eq. (4.15), Eq. (4.16) and Eq. (4.18), in the presented model. Therefore, effect of particle size, an important factor which influences the ER ratio is studied by packed bed wood combustion model presented in Chapter 4, and optimum ER values for different particle sizes of wood were also evaluated and presented.

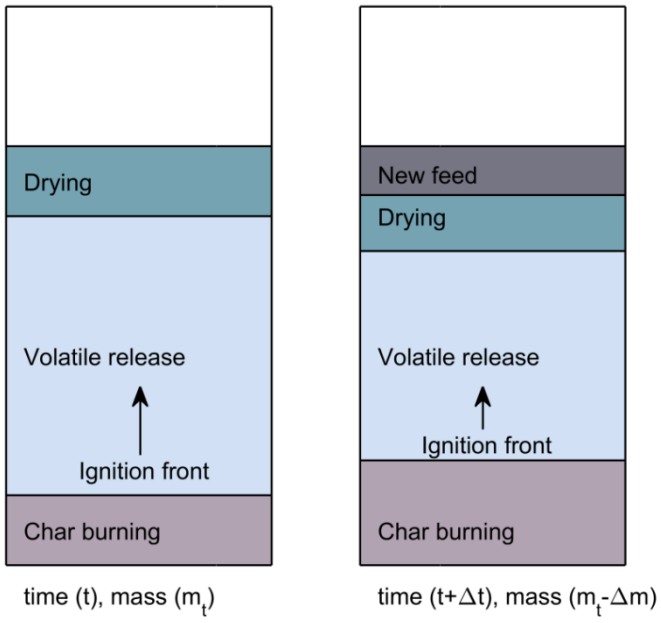

Figure 5.8 Ignition front propagation in continuous feeding arrangement

In the initial stage of combustion fuel gets heated and moisture starts to evaporate. At the next stage, fuel is ignited and ignition front starts to travel through the bed. This

occurs at a constant speed according to properties and flow conditions that exist within the bed. This constant speed of ignition front propagation results in mass loss rate to proceed at a constant speed. Once the ignition front comes to final fuel layers char burning becomes significant. Constant mass decrease rate can be maintained for a longer time if the existing fuel is adequate for the ignition front to travel through. By supplying quantity of fuel which is equal to the mass reduction (Δm) within time step (Δt), amount of fuel available for combustion will be positioned to a state at time (t) (Figure 5.8). Hence ignition front continues to travel in the same speed as in the batch reactor as long as the mass reduction rate is refilled by an equivalent feeding rate to the furnace when all the operating conditions remained unaltered. Therefore, steady state burning characteristics of such continuously operated furnace can be predicted by combustion behaviour within the period in which decrease in mass occurs at a constant rate in a batch type furnace. Therefore, optimum ER values deduced within the constant mass reduction rate period for a batch type furnace can be used as optimum ER values for continuously operated furnace where same operating conditions like fuel properties, air flow, and furnace geometry are maintained as in a batch type reactor. Optimum ER ratios in this study were calculated by decrease in mass within the so observed constant mass loss rate period.

5.3.2 Discussion on simulation results

Effect of particle size for ER was studied through simulations for batches of wood cubes of three particle sizes; 25 mm, 38 mm, 63 mm. Furnace geometry and other conditions were similar to that of the validation described in Section 5.1 and Section 5.2. For the three particle sizes similar fuel properties were used for moisture content, volatile content etc. Simulated and measured mass variation results illustrated in Figure 5.5, Figure 5.6 and Figure 5.7, show a constant mass loss rate between initial and final burning periods. Figure 5.9 shows a similar pattern for the three particle sizes at flow rate of 0.12 ms^{-1}. Within the initial heating up period, it can be observed that large sized particles (63 mm, 38 mm) heat up rapidly than the smaller sized particles. In the model, heat is supplied to the solid phase by an ignition heat source. The air at 300 K is supplied under the fuel bed. Heat supplied to fuel phase will be readily transferred to the gas when the particle sizes are smaller due to

larger specific surface area available for heat transfer. Heat transfer to the gas phase is reduced for larger sized particles which have smaller specific surface area. This proceeds until the ignition occurs. Once the ignition starts ignition front propagates through the bed at a constant speed. Constant mass loss rate period similar to present study was observed in the researches described in [9], [64]. Drying, pyrolysis and char burning reactions proceed at a constant rate throughout the bed until there is sufficient quantity of fuel. The rate of decrease in mass observed within this period can be used as the feeding rate for a furnace which is operated continuously, and the burning characteristics observed within the period become the steady state characteristics of the continuously operated combustor. Therefore, ER was calculated based on decrease in mass observed within the constant mass loss rate period by Eq. (4.46) and Eq. (4.47) for each particle size separately. This ER can be used as ER ratio for a continuously operated furnace. The ER results are shown in Table 5.3.

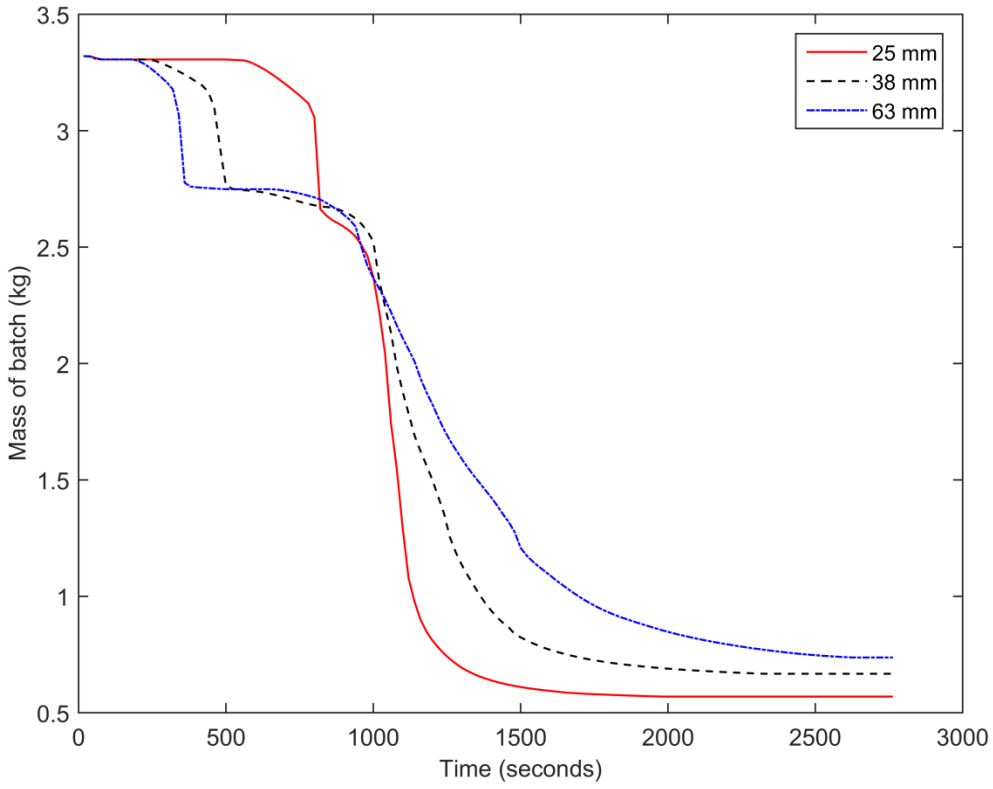

Figure 5.9 Simulated mass variation of biomass bed for three different particle sizes at the same air flow rate

Table 5.3 ER for packed bed combustion of different sized wood particles at inlet air flow velocity of 0.12 ms^{-1}

Particle size (mm)	ER
25	0.28
38	0.44
63	0.76

An increase in ER can be observed with the increase in particle size (Table 5.3). Highest ER is observed for the largest sized particles of 63 mm. Lowest ER is observed for the smallest sized particles of 25 mm. Small sized particles offer larger surface area per unit volume (specific surface area) for the heterogeneous reactions as well as for the heat and mass transport. According to Eq. (4.14) and (4.15), diffusion of reactive gas species to the particle is high due to smaller particle diameter. Therefore, when the particle size is small, both pyrolysis and char reaction rates are high. This explains the reason for high rate of reduction of mass observed in Figure 5.9 for small sized particles. Elevated reaction rates will release more volatile gases and heat. Oxygen that is consumed by increased solid phase reaction rates and gas phase reaction rates results in low ERs. Low specific surface area available for heat and mass transfer and heterogeneous reactions for large sized particles, reduces heat transport and diffusion rate of reactive gaseous agents. Therefore, pyrolysis and char reaction rates are reduced. Thus, Figure 5.9 shows a lower mass reduction rate for larger particle sizes. Release of pyrolysis gases and heat will be slowed down which in turn reduces the gas phase reactions.

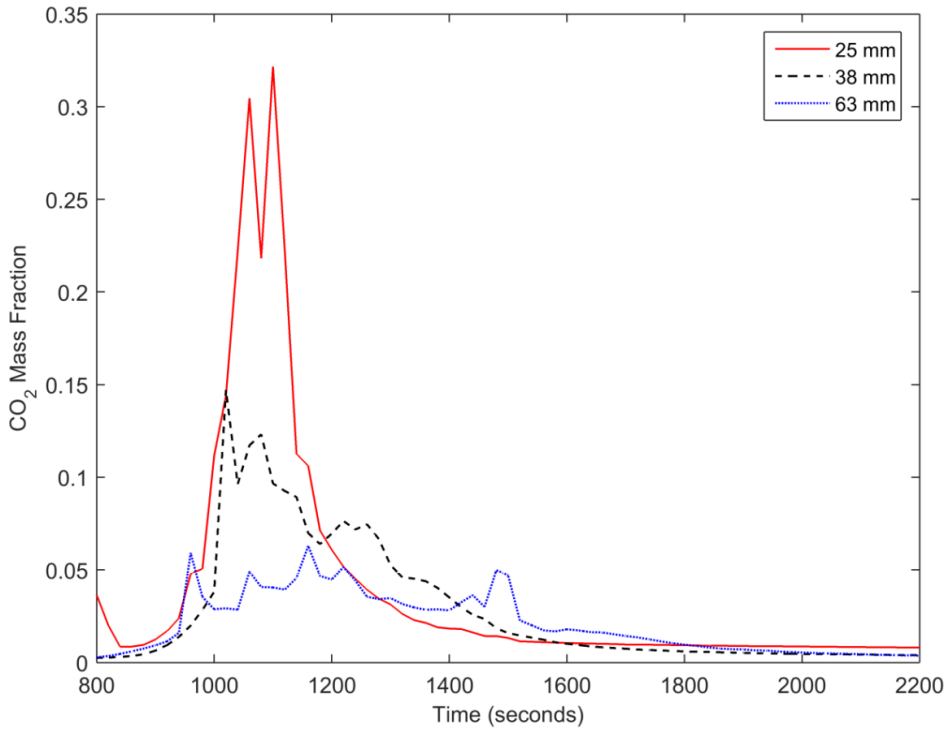

Figure 5.10 Simulated outlet CO_2 mass fraction

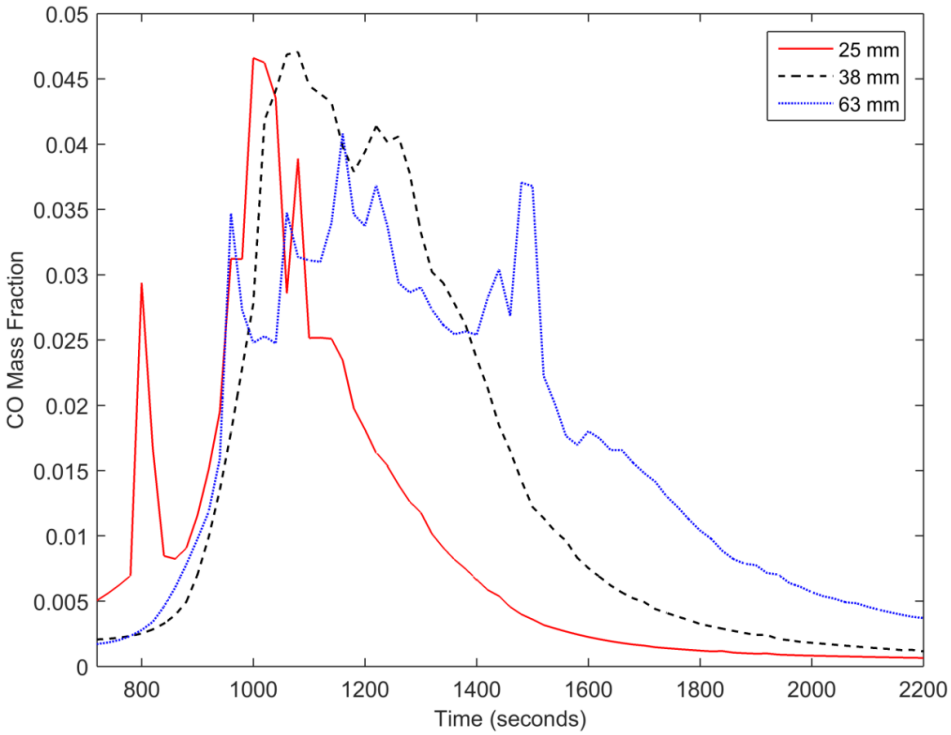

Figure 5.11 Simulated outlet CO mass fraction

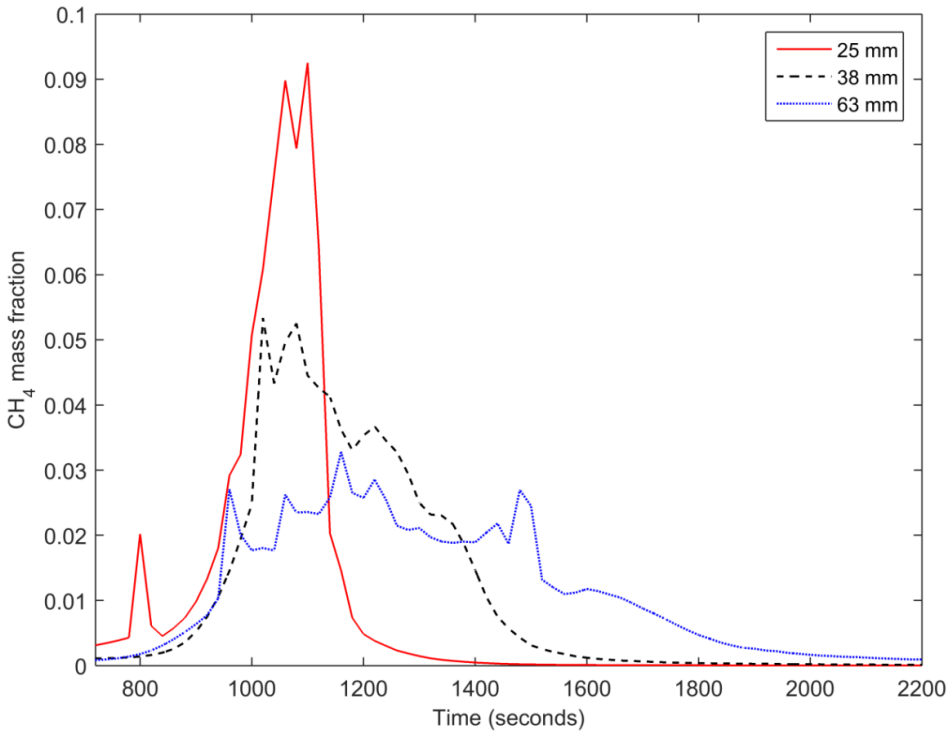

Figure 5.12 Simulated outlet CH_4 mass fraction

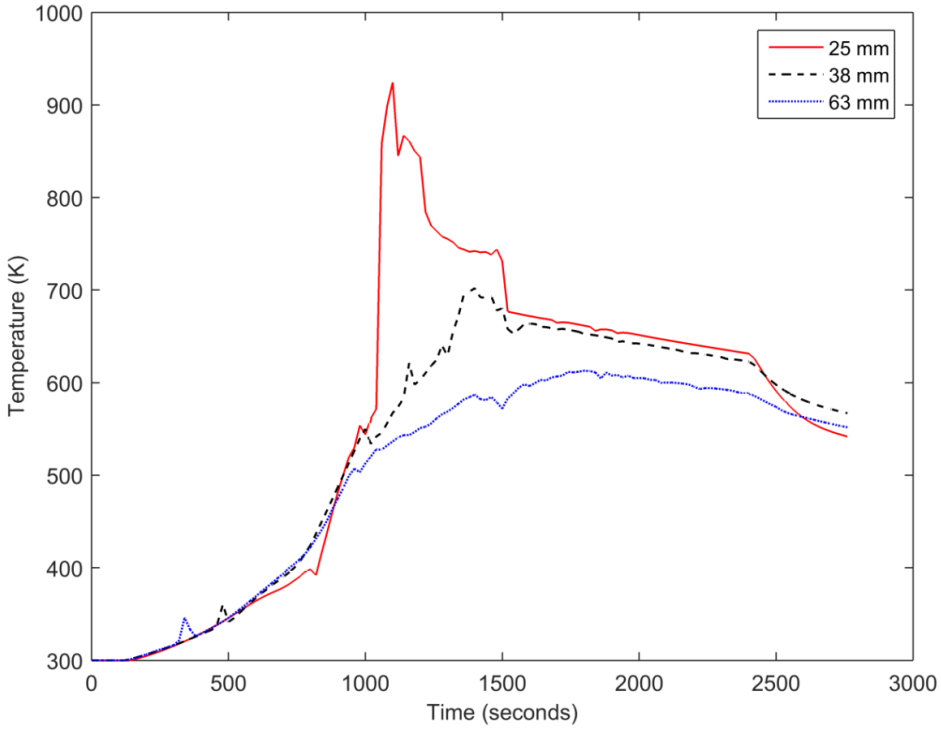

Figure 5.13 Simulated outlet gas temperature

When the four figures, Figure 5.10 to Figure 5.13 are compared, the respective time window at which the maximum CO_2 fraction, maximum CO fraction, maximum CH_4 fraction and highest temperature occur coincides with each other for each particle size. It can be further observed that this is within the constant mass reduction rate period for each particle size. Hence the above parameters illustrate the characteristics of a continuously operated combustor which has a feeding rate equal to mass reduction rate within the constant mass reduction rate period for a batch type reactor for each particle size.

Small particle sizes offer large specific surface area for heat and mass transfer as well as for the heterogeneous reactions. Penetration of heat and diffusion of reactive gases to the centre of the particle is high. Therefore, solid phase reactions proceed at a rapid pace. High volatile release rate from the solid phase increases the gas phase CO_2, CO and CH_4 fractions for small particles (Figure 5.10, Figure 5.11 and Figure 5.12). Increased diffusion of oxygen to the particles results in efficient combustion. This will increase heat generation in the solid phase. Heat is transferred to the gas phase and provides required temperature for the gas phase reactions which increases the gas phase temperature. Although distinct difference in maximum CO fraction cannot be observed among three particle sizes, the average CO fraction and the total mass of CO emitted is lowest for 25 mm particle size (see Figure 5.11). The higher released rates of volatiles to the gas phase increase CO fraction in the gas phase while high temperatures promote the reaction of CO with oxygen to generate more CO_2 as in Figure 5.10. Although the high mass reduction rates with high reaction rates at 25 mm produces more CO, high temperature promotes the combustion of CO, which reduces CO fraction in gas phase. In addition, more oxygen is available for the solid phase combustion reactions which contribute to high CO_2 fraction in the outlet gas stream. Simulated profiles of CH_4, CO, CO_2 and gas phase temperature agree with the above description (see Figure 5.14). Observed concentration of CH_4, CO, CO_2 and gas phase temperature are higher at the centre compared to the sides of the furnace for the three cases observed. Heat loss terms were added to the walls of the reactor as boundary conditions. Therefore, generated heat gets lost from the

walls, which intern reduces the reaction rates near the walls, which is associated with the observed difference in species and gas phase temperature profiles.

High reaction rates for smaller particle sizes consume more oxygen. Therefore, smaller particles can combust with high efficiency and give higher temperature which results in less excess air amounts. When the particles are larger, surface area available for heat and mass transfer reduces and resistance to diffusion of reactant gases increases. The area available for solid phase reactions also decreases. The reaction rates in the solid phase are low. Limited amount of oxygen is available for combustion reactions, which consequently reduces heat generated in the solid phase. Therefore, reactions will not propagate through the bed as fast as smaller particles. The heat generated in the solid phase will not be able to increase the gas phase temperatures as for smaller particle sizes. Gas phase reaction rates will be slowed according to the existing temperature in the gas phase. Reaction of CO with oxygen does not progress due to low temperature in the gas phase. In addition, once the oxygen is depleted by solid phase combustion, gasification reactions are promoted. This results in higher average CO fraction (Figure 5.11) with lower CO_2 fractions (Figure 5.10). Therefore, larger particles combust with less efficiency and lower temperatures and results in high excess air amounts.

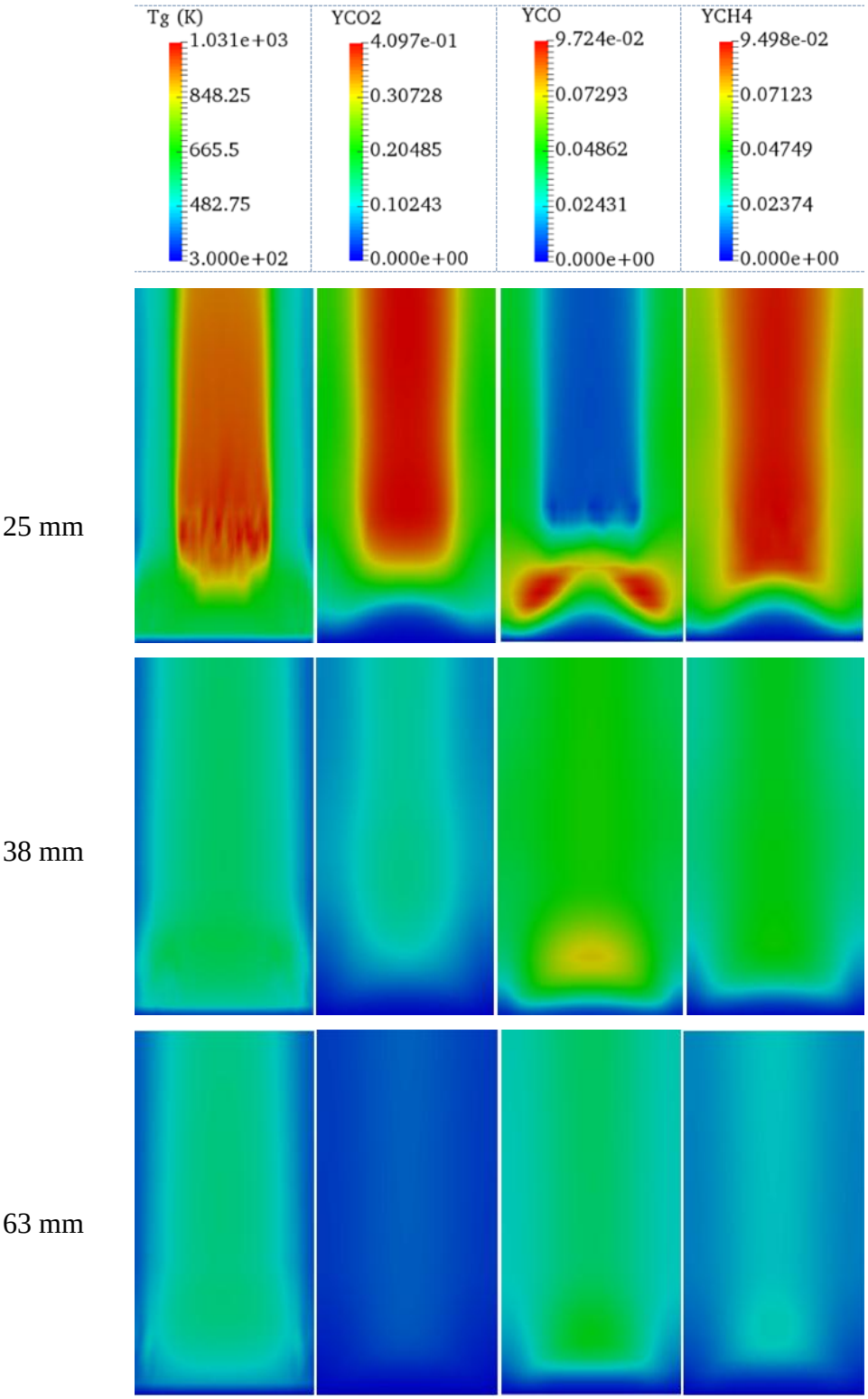

Figure 5.14 Simulated gas phase temperature and species profiles at 1100 s

Simulations were run at air flow velocities of 0.18 ms^{-1}, 0.12 ms^{-1} and 0.05 ms^{-1} to study the ER variation for particle sizes of 25 mm, 38 mm and 63mm. Figure 5.15 shows the variation of ER with air flow velocities for three particle sizes for fixed bed combustion in the lab scale furnace used in the present study (Figure 5.1). ER was calculated within the constant mass reduction rate period. ER increases with the size of the particle for the same flow velocity and also increases with the increased air flow velocity.

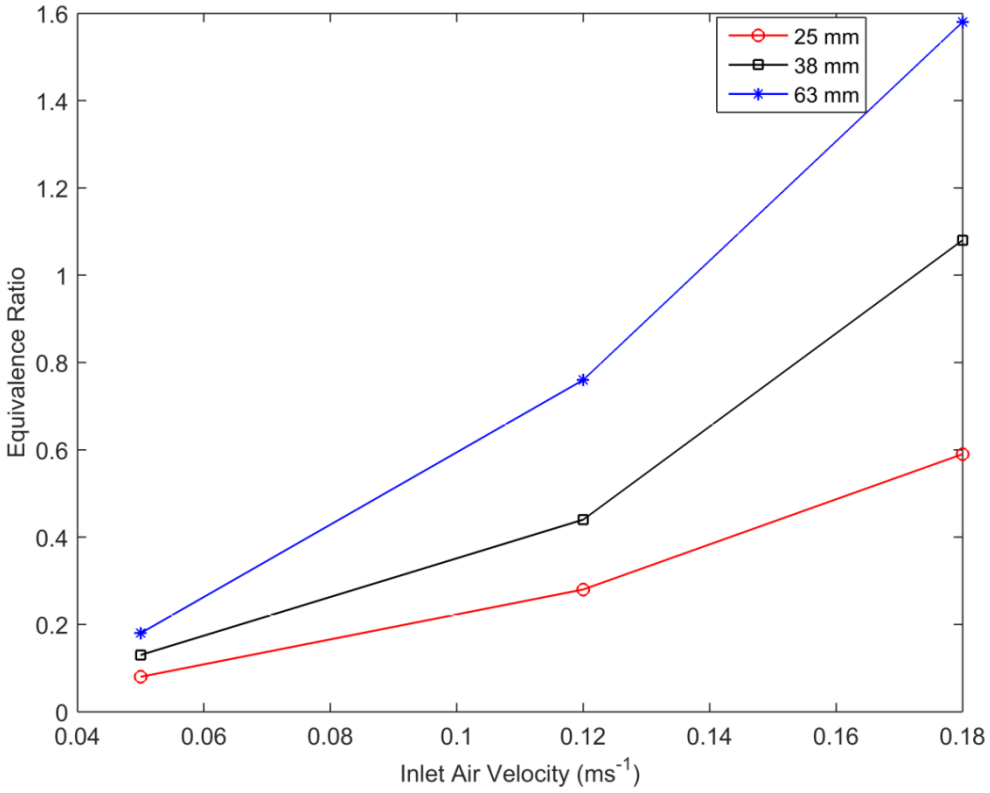

Figure 5.15 ER variation with inlet air flow velocity for 25 mm, 38 mm and 63 mm sized particles

The most suitable ER which gives maximum outlet gas temperature with minimum CO fraction (average) inside the reactor was identified for each particle size through simulations. Table 5.4 shows the maximum outlet gas temperature variation for the calculated ERs for the three particle sizes. The maximum temperature of 924 K is illustrated for ER of 0.28 for 25 mm particle. Although the observed CO fraction at

0.28 ER is slightly higher than the CO fraction observed at 0.59 ER, the outlet gas temperature is comparatively higher at 0.28 ER. The maximum temperature of 883 K was reported at ER of 0.13 for 38 mm particles. The lowest CO fraction of 0.006 is observed at the same ER which resulted in the maximum temperature. 63 mm sized particles resulted in maximum temperature of 877 K at ER of 0.18. At the ER ratio of 0.18, the CO fraction is the second lowest with the value of 0.009. This value is higher than the CO fraction of 0.006 reported at ER of 1.58 due to less oxygen present. ER of 1.58 presented a maximum outlet gas temperature of 532 K, which is considerably lower than the temperature of 877 K at ER of 0.18. The optimum ER value for 38 mm particle is lower than that for 63 mm particle size. From the selected inlet air velocities, optimum ER for both 38 mm particle and 63 mm particle are observed at 0.05 ms^{-1}. At same air flow rates, larger particles burn with lower mass loss rates than the smaller particles. Therefore, ER is high for the large sized particles. Further reduction in air flow velocity causes the combustion to extinct.

The maximum bed temperature decreases when the particle size increases for inlet air flow velocity of 0.05 ms^{-1}. Oxygen availability controls the reaction rates at low air flow rates [45]. Therefore, high diffusion rate of oxygen for small sized particles increases the bed temperature at low flow rates. The reported bed temperature increases when the particle size increases for flow rate of 0.18 ms^{-1}. This is due to the fact that lower specific surface area available for larger particle sizes which reduces the convective cooling at higher air flow rates while high oxygen availability increases the solid phase reactions. Deviation occurs for 38 mm particle at 0.12 ms^{-1} velocity, may be due to the bed movement which affects the solid phase temperature. For the particles of same size, optimum ER ensures the availability of sufficient oxygen for the reactions to occur and to achieve good temperatures and low CO fraction. When the ER is increased more than a certain limit, generated heat is carried away and diluted by the gas flow and the gas phase temperature is decreased which in turn increases the CO fraction. Further increase in ER, reduces bed temperature which results in low volatile release, therefore low CO fractions. When ER is reduced for the combustion of same sized particles, lack of oxygen reduces the combustion reaction rates where the gasification reactions are promoted, which

results in a decrease in gas phase temperature and increase in CO fraction. Consequently, optimum ERs calculated for the furnace illustrated in Figure 5.1, under the above-mentioned operating conditions are 0.28, 0.13 and 0.18 for the particle sizes of 25 mm, 38 mm and 63 mm respectively. According to simulation results, combustion performance highly depends on furnace configuration. Developed CFD model in the study can be used to analyse and optimise particulate biomass combustion in a given furnace configuration. The relevant codes are shown in the Appendix A.

Table 5.4 Simulation results for 25 mm, 38 mm and 63 mm sized particles at different ERs

Particle size (mm)	Parameter	Inlet air velocity (ms^{-1})		
		0.05	0.12	0.18
25	ER	0.08	0.28	0.59
	Maximum bed temperature (K)	1178	789	612
	Maximum outlet gas temperature (K)	886	924	631
	Average CO fraction inside the reactor	0.007	0.006	0.006
38	ER	0.13	0.44	1.08
	Maximum bed temperature (K)	1026	773	665
	Maximum outlet gas temperature (K)	883	702	575
	Average CO fraction inside the reactor	0.006	0.009	0.007
63	ER	0.18	0.76	1.58
	Maximum bed temperature (K)	1019	864	822
	Maximum outlet gas temperature (K)	877	615	532
	Average CO fraction inside the reactor	0.009	0.010	0.006

5.4 Sensitivity analysis for ER

An additional set of simulations were carried out for the packed be geometry described in Figure 5.1 with inlet air flow velocity (u) of 0.12 ms^{-1}, to evaluate the degree of importance of particle size and initial moisture content of wood on ER of packed bed combustion. For each parameter ±10% deviation from the reference value was evaluated and only one parameter was changed at a time. The reference value for moisture content was 30% (wet basis) selected considering common value

of moisture content in wood used in packed bed furnaces [3]. The particle size was selected as 38 mm (1.5 inch). Table 5.5 shows the values of each parameter used in the analysis. Table 5.6 shows the calculated sensitivity of moisture content and particle size. Sensitivity is defned as the ratio between percentage change in outputs to percentage change in input variables.

Table 5.5 Sensitivity factors for particle size and moisture content

Parameter	Reference value	-10%	+10%
Particle size (mm)	38	34.2	41.8
Moisture content (%)	30	27	33

Table 5.6 Sensitivity of ER to particle size and moisture content

Parameter	Sensitivity of ER
Particle size (-)	0.9298
Particle size (+)	0.6029
Moisture content (-)	1.0710
Moisture content (+)	0.8375

Highest sensitivity can be observed for moisture content in the wood. Therefore, moisture content of wood is the most significant variable which affects the ER in packed bed combustion. For optimum ERs moisture content should be controlled.

5.5 Conclusions

Particle size effect for ER in packed bed combustion of wood was investigated by CFD modelling. A constant mass reduction rate period was observed for a batch type furnace. Ignition front travels throughout the bed at a constant speed during the constant mass reduction rate period. Constant mass reduction rate period can be continued for a longer time if it is assured that adequate quantity of fuel is available.

Performance of the batch type combustor within constant mass reduction rate period can be used to illustrate the performance of a continuously operated furnace which is at steady state and in which the feeding rate is assumed to be equal to the rate of mass reduction where same operating conditions are maintained. Therefore, ER ratio analysed for a batch reactor within the constant mass reduction rate period can be used to represent the ER for a continuously operated reactor under same conditions. Increase in particle size shows decrease in flue gas temperature with increased CO concentration. Thus, specifying common ER for different sized wood or biomass fuel combustion is not suitable. Therefore, ER must be recommended corresponding to the particle size to achieve optimum efficiency and optimum heat in industrial wood furnaces. Furnace shown in Figure 5.1 was numerically simulated and optimum ER for combustion of three particle sizes of wood was studied. For 25 mm sized particles optimum ER was identified as 0.28, which gives maximum gas temperature with second lowest CO fraction. Maximum gas temperature and minimum CO fraction was observed at ER of 0.13 for 38 mm sized particles. The largest sized particles of 63 mm require ER of 0.18 to have the maximum gas temperature and second lowest CO fraction. Although, the obtained optimum results cannot be generalised for other furnace geometries and particle sizes, constant mass loss rate obtained by developed model can be used to evaluate the optimum ER for furnaces with different operating conditions. Sensitivity analysis was carried out to evaluate the relative significant of the two parameters, particle size and moisture content on ER. Moisture content was identified as the most significant factor for determining ER, therefore, which has to be controlled to optimise ER.

Chapter 6

WOOD COMBUSTION IN MOVING GRATE FURNACES

6.1 Packed bed combustion in moving grate furnaces

Moving grate combustion provides the opportunity to fire biomass fuels with different properties. Fuels with large particle sizes and high moisture contents can be burnt in moving grate furnaces [124]. Description of moving grate combustion process is required for optimum operation of moving grate furnaces. Numerical modelling of moving grate processes has attracted the attention of researchers due to difficulties and costs associated with experimental work on full scale moving grate furnaces.

In the present research a heterogeneous mathematical model was developed for combustion of biomass in a travelling grate furnace (Figure 6.1). The packed bed combustion model presented in Chapter 4 was further developed and used to simulate the moving grate combustion process. Movement of solid along the grate is included into the model through boundary conditions similar to the approaches used in [21], [43], [66]. Full coupling between fuel phase and gaseous phase solves both solid phase and gas phase variables simultaneously. Full coupling between packed bed and free board with the movement of grate through boundary conditions does not characterize the models reviewed so far.

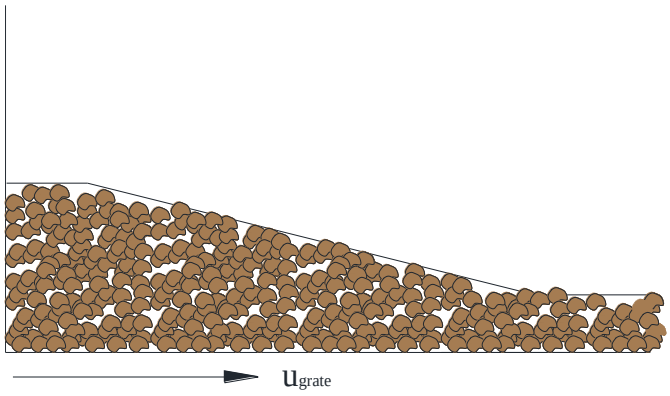

Figure 6.1 Wood combustion on moving grate furnace

The presented model for moving grate combustion is an extention of the developed fixed grate, packed bed combustion model presented in Chapter 4. Therefore, conservation equations for gas phase variables, models for turbulence and radiation and description of other physical and chemical phenomenae which were included in the packed bed combustion model are included unaltered in the moving grate combustion model. To charcterise the solid movements due to grate movement, additional convective flux terms were included in the solid phase conservation equations. The grate velocity u_{grate} is used to describe the convective flux of solids. The solid phase species and energy conservation equations for moving grate furnace are modified as in Eq. (6.1) and Eq. (6.2).

Solid phase

Species conservation equation

$$\partial m_{s,i}/\partial t + \nabla.\left(\left(u_{bed}+u_{grate}\right)m_{s,i}\right) = \sum R_{s,i} \tag{6.1}$$

Energy conservation equation

$$\begin{aligned}\partial((1-\phi)\rho_s C_{ps} T_s)/\partial t + \nabla.((1-\phi)\rho_s\left(u_{bed}+u_{grate}\right)C_{ps}T_s) &= +\nabla.(\lambda_s \nabla T_s) \\ &\quad -hA_{specific}(T_s-T_g) \\ &\quad + \sum R_{s,i}H_{s,i} \\ &\quad + 4eG - A_{specific}a_s\sigma T_s^{\,4}\end{aligned} \tag{6.2}$$

6.2 Numerical procedures

PISO algorithm in OpenFOAM was used to carry out CFD simulations as for the packed bed combustion model. The solver codes developed in OpenFOAM for moving grate furnace is shown in Appendix B. The blockMesh utility in OpenFOAM was used for mesh generation. The geometry of the moving grate furnace was devided into hexahedron cells using blockMesh utility. The descretizisation schemes used in the simulations are tabulated in Table 6.1.

Table 6.1 Discretisation schemes for moving grate furnace

Term	Discretisation schemes
$\nabla.(\phi\rho_g uu)$	upwind
$\nabla.(\phi\rho_g uY_i)$	upwind
$\nabla.(\phi\rho_g uC_{pg}T_g)$	upwind
$\nabla.(u_{bed}m_{s,i})$	MUSCL
$\nabla.((1-\phi)\rho_s u_{bed}C_{ps}T_s)$	MUSCL
$\nabla.\left(\phi\rho_g k\vec{u}\right)$	bounded upwind
$\nabla.\left(\phi\rho_g \varepsilon\vec{u}\right)$	bounded upwind
$\nabla.(u_{grate}m_{s,i})$	upwind
$\nabla.((1-\phi)\rho_s u_{grate}C_{ps}T_s)$	limited linear 1

6.3 Wood combustion on moving grates

The moving grate model described in Section 6.1 was used to analyse wood combustion in moving grate furnaces. Graphical illustration of the moving grate furnace is shown in Figure 6.2. Boundary conditions used in the simulations are shown in Table 6.2. Simulations were run for particle size of 38 mm. Wood is filled up to a height of 0.2 m at the fuel inlet. The grate is moved at a velocity of 0.002 ms^{-1} in 'X' direction. The described domain is divided into 120 cells in 'X' direction 60 cells in 'Y' direction. The time step for the simulation is set to be 0.01 seconds.

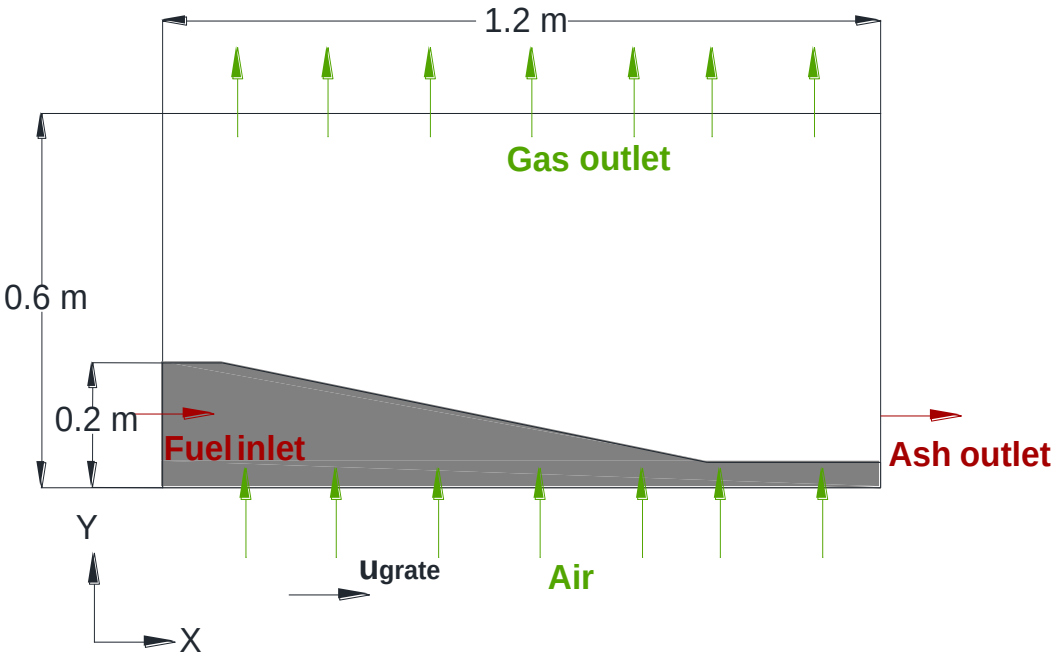

Figure 6.2 Moving bed furnace geometry

Table 6.2 Boundary conditions for moving grate furnace

	Boundary			
	Fuel Inlet	Fuel Outlet	Grate	Gas Outlet
Fuel phase				
ρ_s	499 kgm^{-3}	$\partial m/\partial x = 0$	$\partial m/\partial y = 0$	-
T_s	300 K	$\partial T_g/\partial x = 0$	800 K	-
Gas phase				
u	0 ms^{-1}	0 ms^{-1}	0.12 ms^{-1}	$\partial U/\partial y = 0$
T_g	$\partial T_g/\partial x = 0$	$\partial T_g/\partial x = 0$	300 K	$\partial T_g/\partial y = 0$
Y_i	$\partial Y_i/\partial x = 0$	$\partial Y_i/\partial x = 0$	Atmospheric air properties	$\partial Y_i/\partial y = 0$
P	$\partial P/\partial x = 0$	$\partial P/\partial x = 0$	$\partial P/\partial y = 0$	1.013×10^5 Pa
G	$-4e\sigma(T_{mean}^4-300^4)$, $T_{mean} = T_s+T_g$	$-4e\sigma(T_{mean}^4-300^4)$, $T_{mean}=T_s+T_g$	$4e\sigma T_s^4$	$-4e\sigma T_g^4$
k	$2/3(U_{ref}T_i)^2$ $T_i = 1\%$	$\partial k/\partial x = 0$	$\partial k/\partial y = 0$	$\partial k/\partial y = 0$
ε	$k^{3/2}C_\mu^{0.75}/0.07l$ l= 0.3 m	$\partial \varepsilon/\partial x = 0$	$\partial \varepsilon/\partial y = 0$	$\partial \varepsilon/\partial y = 0$

The simulations were performed to study variation of gas phase temperature, solid phase temperature, gas species and solid phase species variations along the grate length.

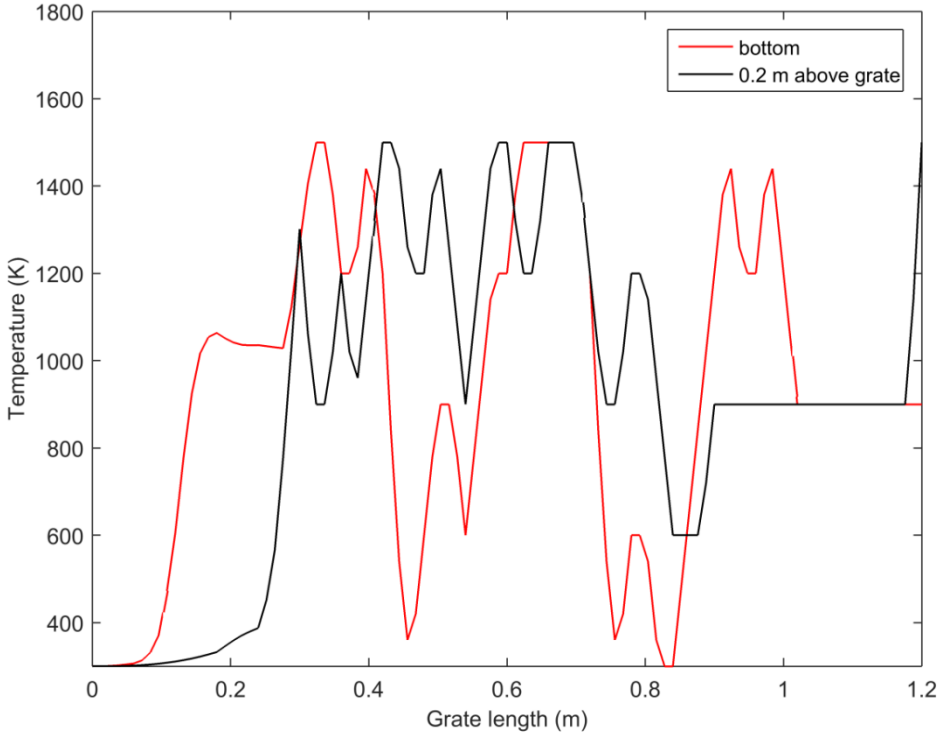

Figure 6.3 Bed temperature variation along the grate

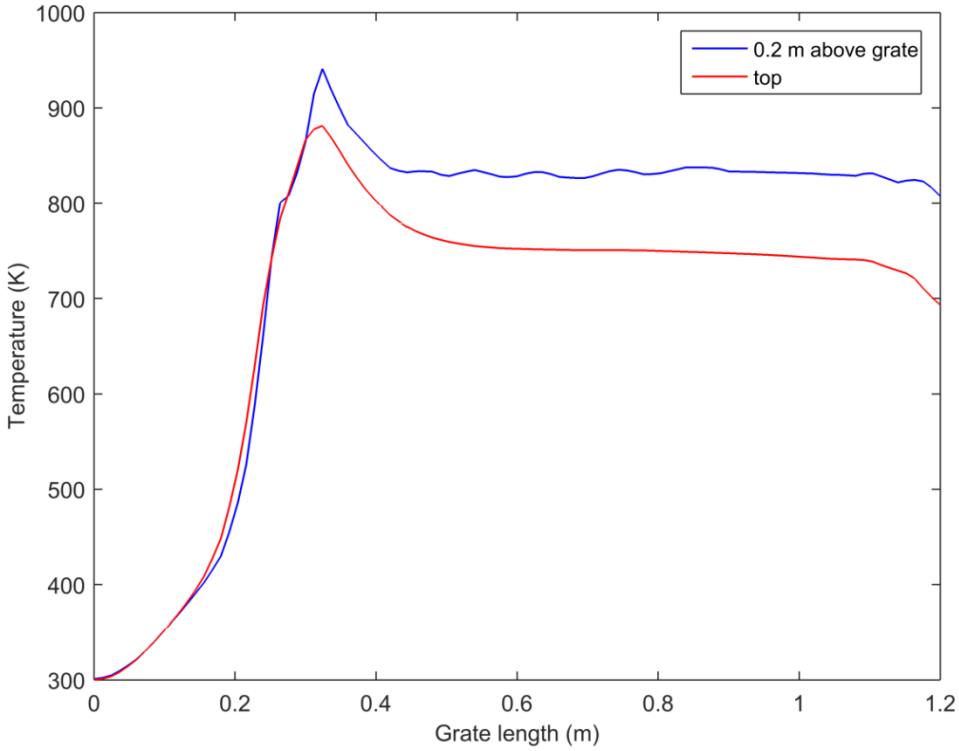

Figure 6.4 Gas temperature variation along the grate

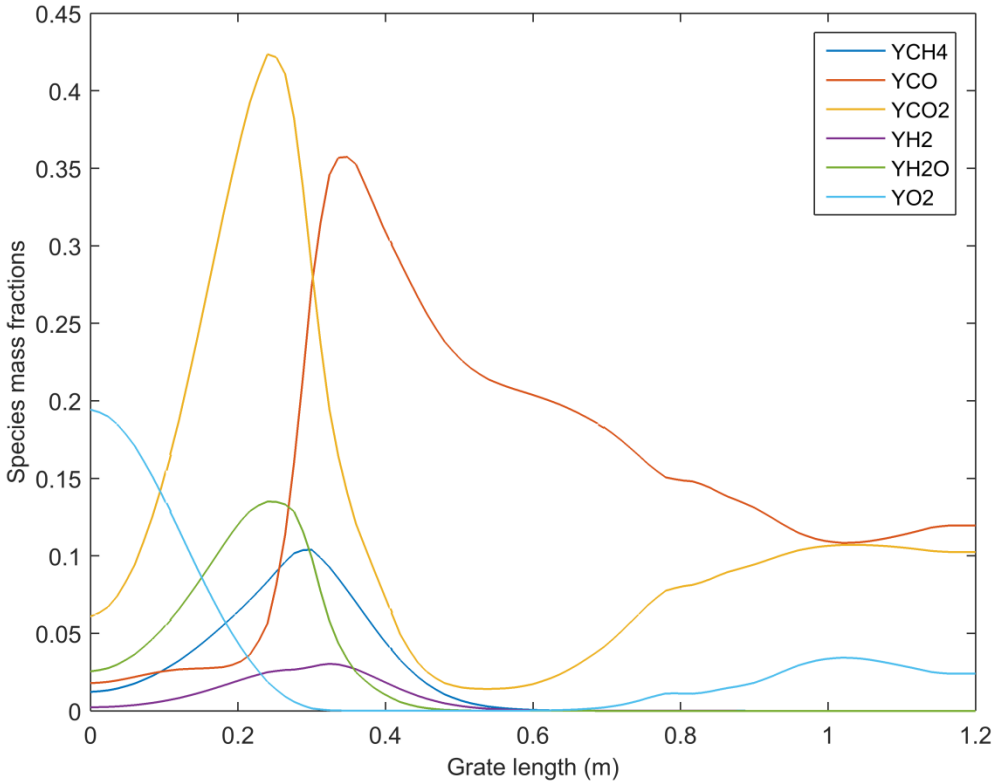

Figure 6.5 Gas compositions along the grate

The simulated results after achieving steady state conditions in moving grate furnace are discussed below. Figure 6.3 shows temperature variation of the bed along the grate at the bottom of the bed and 0.2 m above the grate. A sharp increase in bed temperature can be observed near the fuel inlet at the bottom of the bed. At the surface of the bed this sharp increase in bed temperature is observed around 0.2 m away from the fuel inlet. A heap of fuel is placed near the inlet at the beginning of the simulation which spreads up to a length of 0.3 m along the grate. When the fuel is ignited from the bottom it starts to burn from the edge of the heap and temperature at this edge increases sharply. After reaching steady state, peak temperature occurs near the same position where the above described burning occurs. Therefore, highest temperature occurs at some distance away from the fuel inlet. Similar observation was made by Yang in experimental measurements conducted in a full scale moving grate furnace, where the length of the grate is 10 m [21]. A sharp increase in

temperature was observed at 2 m length from the fuel inlet. Fluctuations in temperature can be observed through out the grate length which is due to the movement of the fuel. After 0.4 m from fuel inlet, major fraction of fuel is consumed. Therefore, heat generation in the solid is decreased and the solid phase mass is also decreased. With the incoming air from the bottom of the grate which is at 300 K, the bed cools down to a temperature as 300 K. The bed temperature fluctuates between 300 K and 1500 K after reaching steady state in the present simulations. Similar fluctuations were observed in the measured data reported in [21] with temperature fluctuations between 1273 K and 350 K.

Similar to solid temperature, gas temperature shown in Figure 6.4, shows sharp increase at 0.2 m from fuel inlet. The peak gas temperature at 0.2 m above the grate is above 900 K. Peak temperature at the top of the furnace (0.6 m above the grate) is below 900 K. The gas phase temperature is high near the bed surface due to convective heat transfer from the bed surface. After initial increase in temperature gas phase temperature decreases considerably and lies around 750 K to 800 K. This is due to consumption of volatile fraction of fuel within the first 0.4 m of the grate length.

When the simulation results are compared with measured data for a furnace of 1.4 m in length and 0.7 m in height reported in [129], highest temperature of the gas phase observed at the free board at the fuel exit is in the same temperature range (around 700 K - 800 K). According to [129] the highest temperature (around 825 K) was observed 0.5 m away from the packed bed surface, whereas the temperature at the packed bed – free board interface was low (around 675 K). According to the present model the maximum temperature observed at the packed bed-free board interface near the fuel outlet is around 800 K.

According to gas composition shown in Figure 6.5, O_2 concentration decreased after 0.2 m from the fuel inlet. Oxygen is consumed by volatile reactions and char reactions. Increase in CO_2 concentration is observed at 0.2 m from fuel inlet due to volatile combustion. A decrease in CO_2 concentration is observed afterwards with an increase in CO concentration which, can be described by the char gasification

reaction with CO_2. Further to that low temperature in gas phase is not favourable for CO conversion process, which increases the CO fraction in the gas phase.

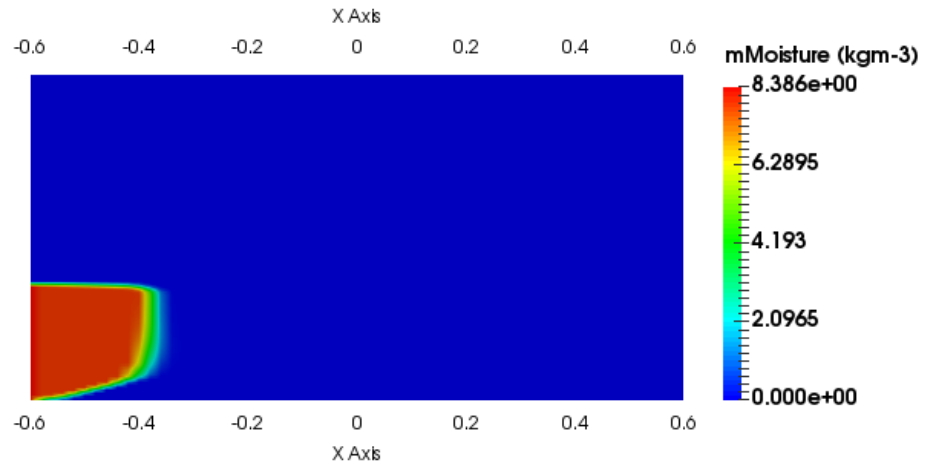

Figure 6.6 Moisture variation along the grate after reaching steady state

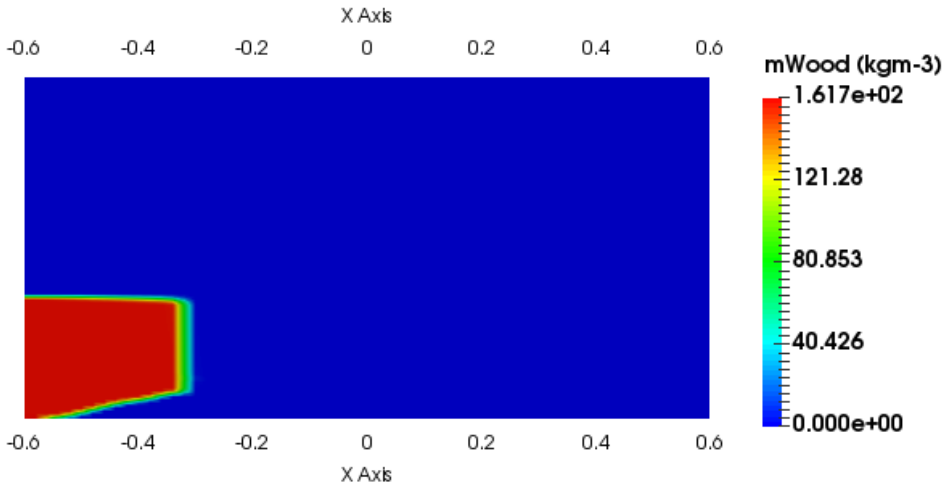

Figure 6.7 Wood mass variation along the grate after reaching steady state

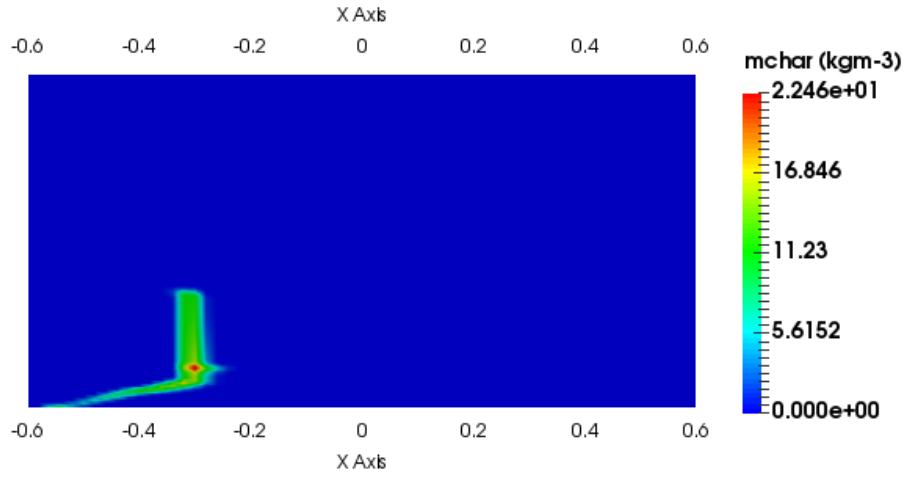

Figure 6.8 Char variation along the grate after reaching steady state

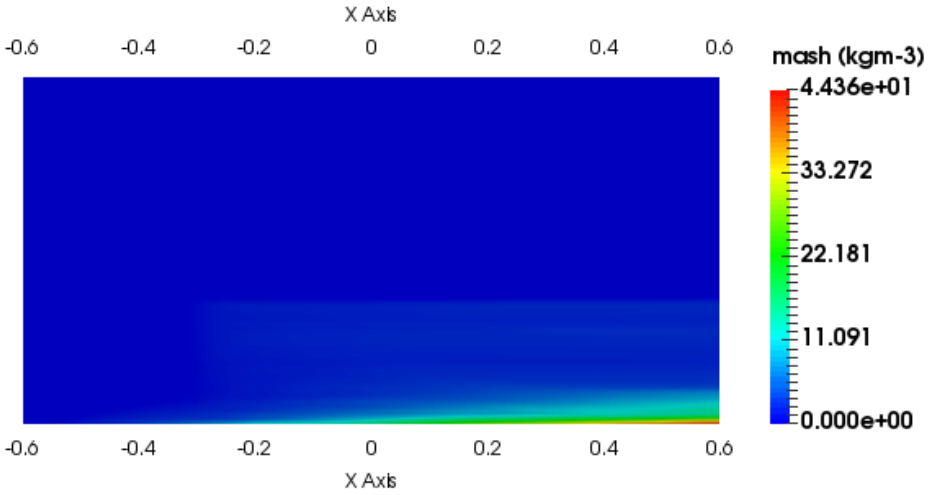

Figure 6.9 Ash variation along the grate after reaching steady state

Figure 6.6, Figure 6.7, Figure 6.8 and Figure 6.9, show moisture, wood, char and ash variation along the grate respectively. The shrinkage effect is not clearly visible in the simulated solid phase constituents as the velocity due to shrinkage has to be maintained below $0.0001 ms^{-1}$ to maintain the solver stability.

6.4 Conclusions

A comprehensive CFD model was developed which includes the progression of fuel along the grate by boundary conditions and which can simulate the bed and free

board simultaneously. Therefore, the model is an advanced model over the models that have been presented so far in the literature. Simulated results are qualitatively in similar range with the measured data obtained in industrial scale moving grate furnaces. The validity of the model has to be checked quantitatively with the measured data. The bed velocity due to shrinkage has to be limited to maintain the stability of the solver and the methods to improve the stability have to be used. Since the model predicts the transient operation of moving grate furnace it can be used for predictive model control applications.

Chapter 7

CONCLUSIONS AND RECOMMENDATIONS

A comprehensive mathematical model was developed and solved by CFD method for wood combustion in packed beds. Analysis of pyrolysis kinetics of Rubber and Gliricidia wood types was done in the research. This research consists of a fixed grate combustion model and a wood combustion model for moving grate furnaces. Two models are heterogeneous models developed within Eulerian framework. The fixed bed combustion model was validated with experimental results for mass variation of different sized particles and was used to study the particle size effect for ER requirement for packed bed combustion of wood.

7.1 Kinetic study of local wood types

Rubber and Gliricidia are popular fuel wood types in thermal applications in Sri Lanka. Therefore, kinetic analysis of these woody biomass types was conducted. The pyrolysis kinetics found out in this study is useful in designing and optimisation of performance of thermal conversion equipment, where these local fuel wood varieties are used.

7.2 CFD simulation of wood combustion in packed bed furnaces

Gas and solid two-phase transient model developed in this study was validated by laboratory scale packed bed combustor. The CFD model solves both free board and packed bed zone simultaneously. In addition, model solves solid phase reactions, gas phase reactions, bed movement, turbulence and radiation heat transfer. Therefore, the model is comprehensive and variation of system parameters like flow velocity, ignition heat should be limited for a given furnace configuration.

7.3 CFD simulation of wood combustion in moving grate furnaces

Fully coupled wood combustion model was developed which represents continuous progression of fuel on the grate due to grate movement. The presented model is able to predict gas and solid phase temperature and species variations. The CFD

simulations help to understand the packed bed combustion in moving grate configuration, which is commonly used in industries. The developed solver in this study is useful in designing and optimising continuously operated moving grate biomass furnaces. Relevant CFD codes are presented in Appendix B.

7.4 Recommendations and future works

7.4.1 Kinetic study

Gaseous emissions of pyrolysis affect the combustion process. In the present evaluation emission profiles were not studied due to experimental limitations. Therefore, more insight of the pyrolysis characteristics can be drawn from such analysis.

7.4.2 Packed bed wood combustion model

In the present model radiation was modelled by P1 modelling approach. DOM model which is more accurate and appropriate modelling method was not used due to complications in angular descretizisation and defining boundary conditions in OpenFOAM. The method of implementing DOM model for in-house solver codes should be studied. Since the present simulations were carried out for two-dimensions, in future analysis it can be extended for three-dimensional analysis according to the requirement. In the presented model global one step kinetics was used to simulate the pyrolysis process. Evaluated DAEM kinetics can incorporated in the model to describe pyrolysis.

7.4.3 Moving grate combustion model

The moving grate combustion combustion model was an extension of the previously developed fixed grate type packed bed combustion model. The packed bed model was validated with experiments conducted in a laboratory scale combuster due to difficulties in finding experimental facilities to validate moving grate furnace model. The validity of the moving grate model must be evaluated by the experimental data presented in literature for moving grate furnaces. The presented model can be used to study time and space varying nature of combustion in moving grate type furnaces by

applying time dependent boundary conditions and variable boundary conditions according to grate position. Since this moving grate model is a transient model which solves both the gas and solid phases simultaneously, this model can be used for predictive model controlling to optimise combustion.

REFERENCES

[1] S. S. Punchihewa, C. Chandrakumar, and A. K. Kulatunga, “Adaptation of Biomass Based Thermal Energy Generation of Sri Lankan Manufacturing Sector: Paragon for Policy Development,” *Procedia CIRP*, vol. 40, pp. 56–61, 2016.

[2] H. and G. S. (Pvt.)Limited, “Final Report, Fuelwood Resource Survey of Sri Lanka, 2016,” 2016.

[3] T. H. Jayah, “Evaluation of a Downdraft Wood Gasifier for Tea Manufacturing in Sri Lanka,” no. March, 2002.

[4] T. Nussbaumer, “OVERVIEW OF BIOMASS COMBUSTION,” in *Developments in Thermochemical Biomass Conversion*, 1997, pp. 1229–1243.

[5] P. Basu, *Biomass gasification and pyrolysis*, vol. 5. 2012.

[6] T. Klason, “Modelling of Biomass Combustion in Furnaces,” Ph.D. dissertation, Division of Fluid Mechanics, Department of Energy Science, Lund Institute of Technology, Media Tryck AB, 2006.

[7] N. Duffy, “Investigation of Biomass Combustion in Grate Furnaces using CFD,” Ph.D.dissertation,Department of Mechanical and Biomedical Engineering, National University of Ireland, Galway, 2012.

[8] N. T. M. Duffy and J. a. Eaton, “Investigation of factors affecting channelling in fixed-bed solid fuel combustion using CFD,” *Combust. Flame*, vol. 160, no. 10, pp. 2204–2220, Oct. 2013.

[9] R. Mehrabian, A. Shiehnejadhesar, R. Scharler, and I. Obernberger, “Multi-physics modelling of packed bed biomass combustion,” *Fuel*, vol. 122, no. April, pp. 164–178, 2014.

[10] B. Peters, E. Schröder, C. Bruch, and T. Nussbaumer, “Measurements and

particle resolved modelling of heat-up and drying of a packed bed," *Biomass and Bioenergy*, vol. 23, no. 4, pp. 291–306, 2002.

[11] U. Sand, J. Sandberg, J. Larfeldt, and R. Bel Fdhila, "Numerical prediction of the transport and pyrolysis in the interior and surrounding of dry and wet wood log," *Appl. Energy*, vol. 85, no. 12, pp. 1208–1224, 2008.

[12] B. Peters and C. Bruch, "Drying and pyrolysis of wood particles: experiments and simulation," *J. Anal. Appl. Pyrolysis*, vol. 70, no. 2, pp. 233–250, Dec. 2003.

[13] W. C. R. Chan, M. Kelbon, and B. B. Krieger, "Modelling and experimental verification of physical and chemical processes during pyrolysis of a large biomass particle," *Fuel*, vol. 64, no. 11, pp. 1505–1513, 1985.

[14] H. Lu, W. Robert, G. Peirce, B. Ripa, and L. L. Baxter, "Comprehensive study of biomass particle combustion," *Energy and Fuels*, vol. 22, no. 4, pp. 2826–2839, 2008.

[15] J. C. Wurzenberger, S. Wallner, H. Raupenstrauch, A.- Graz, and J. G. Khinast, "Thermal Conversion of Biomass : Comprehensive Reactor and Particle Modeling," vol. 48, no. 10, 2002.

[16] M. G. Grønli, "A theoretical and experimental study of the thermal degradation of biomass," The Norwegian University of Science and Technology, 1996.

[17] J. E. White, W. J. Catallo, and B. L. Legendre, "Biomass pyrolysis kinetics: A comparative critical review with relevant agricultural residue case studies," *J. Anal. Appl. Pyrolysis*, vol. 91, no. 1, pp. 1–33, May 2011.

[18] Y. B. Yang, J. Goodfellow, V. N. Sharifi, and J. Swithenbank, "Investigation of biomass combustion systems using CFD techniques: a parametric study of packed-bed burning characteristics," *Prog. Comput. Fluid Dyn.*, vol. 6, pp. 262–271, 2006.

[19] R. P. Van Der Lans, L. T. Pedersen, A. Jensen, and P. Glarborg, “Modelling and experiments of straw combustion in a grate furnace,” vol. 19, pp. 199–208, 2000.

[20] T. Juřena, “Numerical Modelling of Grate Combustion,” *Vutium.Vutbr.Cz*, 2012.

[21] Y. B. Yang, C. Ryu, J. Goodfellow, V. N. Sharifi, and J. Swithenbank, “Modelling Waste Combustion in Grate Furnaces,” *Process Saf. Environ. Prot.*, vol. 82, no. 3, pp. 208–222, May 2004.

[22] D. Kurz, U. Schnell, and G. Scheffknecht, “CFD simulation of wood chip combustion on a grate using an Euler–Euler approach,” *Combust. Theory Model.*, vol. 16, no. 2, pp. 251–273, 2012.

[23] S. Frigerio, H. Thunman, B. Leckner, and S. Hermansson, “Estimation of gas phase mixing in packed beds,” *Combust. Flame*, vol. 153, no. 1–2, pp. 137–148, Apr. 2008.

[24] C. Di Blasi, “Multi-phase moisture transfer in the high-temperature drying of wood particles,” *Chem. Eng. Sci.*, vol. 53, no. 2, pp. 353–366, 1998.

[25] M. a. Gómez, J. Porteiro, D. Patiño, and J. L. Míguez, “CFD modelling of thermal conversion and packed bed compaction in biomass combustion,” *Fuel*, vol. 117, pp. 716–732, Jan. 2014.

[26] R. Mehrabian *et al.*, “A CFD model for thermal conversion of thermally thick biomass particles,” *Fuel Process. Technol.*, vol. 95, pp. 96–108, 2012.

[27] L. A. W. Joseph H. Flynn, “A Quick Direct Method for The Determination of Activation neergy from Thermogravimetric Data,” *Polym. Sci. Part - B,Polymer Phys.*, vol. 4, pp. 323–328, 1966.

[28] A. K. Burnham and R. L. Braun, “Global Kinetic Analysis of Complex Materials,” *Energy & Fuels*, vol. 13, no. 1, pp. 1–22, 1999.

[29] K. Miura, “A New and Simple Method to Estimate f(E) and k0(E) in the Distributed Activation Energy Model from Three Sets of Experimental Data,” *Energy & Fuels*, vol. 9, no. 2, pp. 302–307, 1995.

[30] C. Diblasi, “Modeling chemical and physical processes of wood and biomass pyrolysis,” *Prog. Energy Combust. Sci.*, vol. 34, no. 1, pp. 47–90, Feb. 2008.

[31] R. A. Yetter, “Combustion of Nonvolatile Fuels,” in *Combustion*, Fifth Edit., Elsevier, 1996, pp. 435–481.

[32] H. K. Versteeg and W. Malalasekera, *An Introduction to Computational Fluid Dynamics THE FINITE VOLUME METHOD*, Second Edi. Pearson Education Limited, 2007.

[33] S. Hermansson and H. Thunman, “CFD modelling of bed shrinkage and channelling in fixed-bed combustion,” *Combust. Flame*, vol. 158, no. 5, pp. 988–999, May 2011.

[34] J. J. . Sastamoinen, R. Taipale, M. Horttanainen, and P. Sarkomaa, “Propagation of the ignition front in beds of wood particles,” *Combust. Flame*, vol. 123, no. 1–2, pp. 214–226, 2000.

[35] Y. Yang, C. Ryu, a Khor, N. Yates, V. Sharifi, and J. Swithenbank, “Effect of fuel properties on biomass combustion. Part II. Modelling approach—identification of the controlling factors,” *Fuel*, vol. 84, no. 16, pp. 2116–2130, Nov. 2005.

[36] H. Ström, S. Sasic, and H. Thunman, “Challenges and opportunities in the Eulerian approach to numerical simulations of fixed-bed combustion of biomass,” *Procedia Eng.*, vol. 102, pp. 1573–1582, 2015.

[37] F. El-Mahallawy and S. E.-D. Habik, “Chapter 5 - Combustion, Heat Transfer, and Emission in Boilers and Furnaces,” *Fundam. Technol. Combust.*, pp. 499–746, 2002.

[38] A. Shiehnejadhesar, R. Mehrabian, R. Scharler, G. M. Goldin, and I. Obernberger, “Development of a gas phase combustion model suitable for low and high turbulence conditions,” *Fuel*, vol. 126, pp. 177–187, 2014.

[39] S. Chapela, J. Porteiro, and M. Costa, “Effect of the Turbulence-Chemistry Interaction in Packed-Bed Biomass Combustion,” *Energy and Fuels*, vol. 31, no. 9, pp. 9967–9982, 2017.

[40] W. B. Age *et al.*, “Combustion 14.1,” 1950.

[41] M. G. Carvalho and T. L. Farias, “MODELLING OF HEAT TRANSFER IN RADIATING and Combusting Systems,” *Mech. Eng.*, vol. 76, no. February, 1998.

[42] R. Viskanta, “Computation of radiative transfer in combustion systems,” *Int. J. Numer. Methods Heat Fluid Flow*, vol. 18, pp. 415–442, 2008.

[43] Y. B. Yang, Y. R. Goh, R. Zakaria, V. Nasserzadeh, and J. Swithenbank, “Mathematical modelling of MSW incineration on a travelling bed,” *Waste Manag.*, vol. 22, pp. 369–380, 2002.

[44] Y. B. Yang, V. N. Sharifi, and J. Swithenbank, “Numerical Simulation of the Burning Characteristics of Thermally-Thick Biomass Fuels in Packed-Beds,” *Process Saf. Environ. Prot.*, vol. 83, no. 6, pp. 549–558, Nov. 2005.

[45] D. Shin and S. Choi, “The combustion of simulated waste particles in a fixed bed,” *Combust. Flame*, vol. 121, pp. 167–180, 2000.

[46] H. Thunman and B. Leckner, “Co-current and counter-current fixed bed combustion of biofuel—a comparison☆,” *Fuel*, vol. 82, no. 3, pp. 275–283, Feb. 2003.

[47] Robert Scharler, Ingwald Obernberger, “Numerical Modelling of Biomass Grate Furnaces,” in *European Conference on Industrial Furnaces and Boilers*, 2000, vol. 1, no. 3, pp. 550–556.

[48] A. Shiehnejadhesar, K. Schulze, R. Scharler, and I. Obernberger, “A new innovative CFD-based optimisation method for biomass combustion plants,” *Biomass and Bioenergy*, vol. 53, pp. 48–53, Jun. 2013.

[49] M. Miltner, A. Makaruk, M. Harasek, and A. Friedl, “CFD-modelling for the combustion of solid baled biomass,” *5th Int. Conf. CFD Process Ind.*, no. December, pp. 1–6, 2006.

[50] P. in C. F. Dynamics, “CFD simulation of ash deposit formation in fixed bed biomass furnaces and boilers,” vol. 6, no. 4/5, pp. 248–261, 2006.

[51] R. Scharler and I. Obernberger, “Deriving guidelines for the design of biomass grate furnaces with CFD analysis - a new multifuel-Low-NOx furnace as example,” *6th Int. Conf. Ind. Furn. Boil.*, no. x, p. 15, 2001.

[52] C. Jordan and M. Harasek, “Improvement of a combustion unit based on a grate furnace for granular dry solid biofuels using CFD methods,” *Heat Transf. Eng.*, vol. 31, no. 9, pp. 774–781, 2010.

[53] J. Chaney, H. Liu, and J. Li, “An overview of CFD modelling of small-scale fixed-bed biomass pellet boilers with preliminary results from a simplified approach,” *Energy Convers. Manag.*, vol. 63, pp. 149–156, Nov. 2012.

[54] R. Bauer, M. Gölles, T. Brunner, N. Dourdoumas, and I. Obernberger, “Modelling of grate combustion in a medium scale biomass furnace for control purposes,” *Biomass and Bioenergy*, vol. 34, no. 4, pp. 417–427, Apr. 2010.

[55] J. Collazo, J. Porteiro, D. Patiño, and E. Granada, “Numerical modeling of the combustion of densified wood under fixed-bed conditions,” *Fuel*, vol. 93, pp. 149–159, Mar. 2012.

[56] Y. B. Yang, J. Goodfellow, Y. R. Goh, V. Nasserzadeh, and J. Swithenbank, “Investigation of Channel Formation Due to Random Packing in a Burning Waste Bed,” *Process Saf. Environ. Prot.*, vol. 79, no. September, pp. 267–277,

2001.

[57] S. Schulze, P. Nikrityuk, F. Compart, A. Richter, and B. Meyer, “Particle-resolved numerical study of char conversion processes in packed beds,” *Fuel*, vol. 207, pp. 655–662, 2017.

[58] C. Bruch, B. Peters, and T. Nussbaumer, “Modelling wood combustion under fixed bed conditions,” *Fuel*, vol. 82, pp. 729–738, 2003.

[59] M. R. Karim and J. Naser, “Numerical study of the ignition front propagation of different pelletised biomass in a packed bed furnace,” *Appl. Therm. Eng.*, vol. 128, pp. 772–784, 2018.

[60] K. Goerner and T. Klasen, “Modelling, simulation and validation of the solid biomass combustion in different plants,” *Prog. Comput. Fluid Dyn. An Int. J.*, vol. 6, no. 4/5, p. 225, 2006.

[61] J. Porteiro, J. Collazo, D. Patiño, E. Granada, J. C. M. Gonzalez, and J. L. Míguez, “Numerical modeling of a biomass pellet domestic boiler,” *Energy and Fuels*, vol. 23, no. 2, pp. 1067–1075, 2009.

[62] M. A. Gómez, J. Porteiro, D. Patiño, and J. L. Míguez, “Fast-solving thermally thick model of biomass particles embedded in a CFD code for the simulation of fixed-bed burners,” *Energy Convers. Manag.*, vol. 105, pp. 30–44, 2015.

[63] M. A. Gï¿½mez, J. Porteiro, D. De la Cuesta, D. Patiï¿½o, and J. L. Mï¿½guez, “Dynamic simulation of a biomass domestic boiler under thermally thick considerations,” *Energy Convers. Manag.*, vol. 140, pp. 260–272, 2017.

[64] Y. Bin Yang, C. Ryu, A. Khor, V. N. Sharifi, and J. Swithenbank, “Fuel size effect on pinewood combustion in a packed bed,” *Fuel*, vol. 84, no. 16, pp. 2026–2038, 2005.

[65] R. Johansson, H. Thunman, and B. Leckner, “Influence of intraparticle gradients in modeling of fixed bed combustion,” *Combust. Flame*, vol. 149, no. 1–2, pp. 49–62, Apr. 2007.

[66] Y. B. Yang, C. N. Lim, J. Goodfellow, V. N. Sharifi, and J. Swithenbank, “A diffusion model for particle mixing in a packed bed of burning solids,” *Fuel*, vol. 84, no. 2–3, pp. 213–225, 2005.

[67] B. J. Peters, “Heat Transfer in Fixed and Moving Packed Beds Predicted by the Extended Discrete Element Method,” pp. 295–338.

[68] S. K. Kær, “Numerical modelling of a straw-fired grate boiler,” *Fuel*, vol. 83, no. 9, pp. 1183–1190, Jun. 2004.

[69] R. Mehrabian and A. Shiehnejadhesar, “Numerical modelling of biomass grate furnaces with a particle based model,” *10th Eur. Conf. Ind. Furn. Boil. – Porto, Port.*, no. April, pp. 1–14, 2015.

[70] B. J. Peters, A. D?iugys, L. Raslavicius, and L. Narbutas, “Prediction of straw gasification on a forward acting grate,” *CHISA 2012 - 20th Int. Congr. Chem. Process Eng. PRES 2012 - 15th Conf. PRES*, no. January, 2012.

[71] X. Zhang, M. Xu, R. Sun, and L. Sun, “Study on Biomass Pyrolysis Kinetics,” *J. Eng. Gas Turbines Power*, vol. 128, p. 493, 2006.

[72] M. Van de Velden, J. Baeyens, A. Brems, B. Janssens, and R. Dewil, “Fundamentals, kinetics and endothermicity of the biomass pyrolysis reaction,” *Renew. Energy*, vol. 35, no. 1, pp. 232–242, Jan. 2010.

[73] D. Tapasvi, R. Khalil, G. Várhegyi, K. Q. Tran, M. Grønli, and Ø. Skreiberg, “Thermal decomposition kinetics of woods with an emphasis on torrefaction,” *Energy and Fuels*, vol. 27, no. 10, pp. 6134–6145, 2013.

[74] M. Hu *et al.*, “Thermogravimetric kinetics of lignocellulosic biomass slow pyrolysis using distributed activation energy model , Fraser – Suzuki

deconvolution , and iso-conversional method," *ENERGY Convers. Manag.*, vol. 118, pp. 1–11, 2016.

[75] A. Khawam and D. R. Flanagan, "Complementary use of model-free and modelistic methods in the analysis of solid-state kinetics," *J. Phys. Chem. B*, vol. 109, no. 20, pp. 10073–10080, 2005.

[76] T. Martí-rosselló, J. Li, and L. Lue, "Kinetic models for biomass pyrolysis .," pp. 4–7, 2016.

[77] S. Vyazovkin and C. A. Wight, "Model-free and model-fitting approaches to kinetic analysis of isothermal and nonisothermal data," *Thermochim. Acta*, vol. 340–341, pp. 53–68, Dec. 1999.

[78] E. S. Freeman and B. Carroll, "The application of thermoanalytical techniques to reaction kinetics: the thermogravimetric evaluation of the kinetics of the decomposition of calcium oxalate monohydrate," *J. Phys. Chem.*, vol. 62, no. 4, pp. 394–397, 1958.

[79] A. W. A. Coats and J. P. J. P. Redfern, "Kinetic parameters from thermogravimetric data," *Nature*, vol. 201, no. 4914, pp. 68–69, 1964.

[80] K. Jayaraman, M. V. Kok, and I. Gokalp, "Thermogravimetric and mass spectrometric (TG-MS) analysis and kinetics of coal-biomass blends," *Renew. Energy*, vol. 101, pp. 293–300, 2017.

[81] C. Lu, W. Song, and W. Lin, "Kinetics of biomass catalytic pyrolysis," *Biotechnol. Adv.*, vol. 27, no. 5, pp. 583–587, 2009.

[82] Y. F. Huang, W. H. Kuan, P. T. Chiueh, and S. L. Lo, "A sequential method to analyze the kinetics of biomass pyrolysis.," *Bioresour. Technol.*, vol. 102, no. 19, pp. 9241–6, Oct. 2011.

[83] H. E. Kissinger, "Reaction Kinetics in Differential Thermal Analysis," *Anal. Chem.*, vol. 29, no. 11, pp. 1702–1706, 1957.

[84] J. Cai, W. Wu, and R. Liu, “An overview of distributed activation energy model and its application in the pyrolysis of lignocellulosic biomass,” *Renew. Sustain. Energy Rev.*, vol. 36, pp. 236–246, 2014.

[85] L. Gašparoviè, J. Labovský, and J. Markoš, “Calculation of Kinetic Parameters of the Thermal Decomposition of Wood by Distributed Activation Energy Model (DAEM),” vol. 26, no. 1, pp. 45–53, 2012.

[86] L. Kuo-Chao, W. Keng-Tung, C. Chien-Song, and T. Wei-The, “A New Study on Combustion Behavior of Pine Sawdust Characterized by the Weibull Distribution,” *Chinese J. Chem. Eng.*, vol. 17, no. 5, pp. 860–868, 2009.

[87] K. Miura and T. Maki, “A Simple Method for Estimating f(E) and k0(E) in the Distributed Activation Energy Model,” *Energy & Fuels*, vol. 12, no. 5, pp. 864–869, 1998.

[88] D. K. Shen, S. Gu, B. Jin, and M. X. Fang, “Thermal degradation mechanisms of wood under inert and oxidative environments using DAEM methods,” *Bioresour. Technol.*, vol. 102, no. 2, pp. 2047–2052, 2011.

[89] L. Li, X. Wang, J. Sun, Y. Zhang, and S. Qin, “Pyrolytic and kinetic analysis of two coastal plant species: Artemisia annua and Chenopodium glaucum,” *Biomed Res. Int.*, vol. 2013, pp. 1–7, 2013.

[90] J. L. Goldfarb and S. Ceylan, “Second-generation sustainability: Application of the distributed activation energy model to the pyrolysis of locally sourced biomass-coal blends for use in co-firing scenarios,” *Fuel*, vol. 160, pp. 297–308, 2015.

[91] B. B. Nyakuma, “Thermogravimetric and kinetic analysis of Melon (Citrullus colocynthis L.) seed husk using the distributed activation energy model,” *Environ. Clim. Technol.*, vol. 15, no. 1, pp. 77–89, 2015.

[92] A. Soria-Verdugo, E. Goos, J. Arrieta-Sanagustín, and N. García-Hernando, “Modeling of the pyrolysis of biomass under parabolic and exponential

temperature increases using the Distributed Activation Energy Model," *Energy Convers. Manag.*, vol. 118, no. June, pp. 223–230, 2016.

[93] S. Wang *et al.*, "Kinetic modeling of biomass components pyrolysis using a sequential and coupling method," *Fuel*, vol. 185, pp. 763–771, 2016.

[94] K.U.C.Perera and M Narayana, "Kissinger method: The sequential approach and DAEM forkinetic study of Rubber and Gliricidia," *J. Natl. Sci. Found. Sri Lanka*, vol. 46, no. 2, pp. 187–196, 2018.

[95] D. Chen, Y. Zheng, and X. Zhu, "In-depth investigation on the pyrolysis kinetics of raw biomass. Part I: kinetic analysis for the drying and devolatilization stages.," *Bioresour. Technol.*, vol. 131, pp. 40–6, Mar. 2013.

[96] M. Otero, L. F. Calvo, M. V Gil, A. I. García, and A. Morán, "Co-combustion of different sewage sludge and coal: a non-isothermal thermogravimetric kinetic analysis.," *Bioresour. Technol.*, vol. 99, no. 14, pp. 6311–9, Sep. 2008.

[97] J. A. Nelder and R. Mead, "A Simplex Method for Function Minimization," *Comput. J.*, vol. 7, no. 4, pp. 308–313, 1965.

[98] J. Riyaphan *et al.*, "Variability in chemical and mechanical properties of Pará rubber (Hevea brasiliensis) trees," *ScienceAsia*, vol. 41, no. 4, pp. 251–258, 2015.

[99] H. Yang, R. Yan, H. Chen, D. H. Lee, and C. Zheng, "Characteristics of hemicellulose, cellulose and lignin pyrolysis," *Fuel*, vol. 86, no. 12–13, pp. 1781–1788, 2007.

[100] A. Inc., *ANSYS Fluent Theory Guide*, no. November. Southpointe 275, Technology Drive, Canonsburg, PA 15317, 2013.

[101] V. Kurdyumov and E. Fernandez, "Heat transfer from a circular cylinder at low Reynolds numbers," *J. Heat Transfer*, vol. 120, no. 1, pp. 72–75, 1998.

[102] I. Marsi, "Numerical Simulation of the Thermal Degradation of Biomass –

Approaches," *Transform. Biomass Theory to Pract.*, pp. 285–303, 2014.

[103] R. W. Nachenius, F. Ronsse, R. H. Venderbosch, and W. Prins, "Biomass Pyrolysis," in *Chemical Engineering for Renewables Conversion*, 1st ed., vol. 42, Elsevier, 2013, pp. 83–89.

[104] H. Ström and H. Thunman, "A computationally efficient particle submodel for CFD-simulations of fixed-bed conversion," *Appl. Energy*, vol. 112, pp. 808–817, Dec. 2013.

[105] B. . Babu and a. . Chaurasia, "Modeling for pyrolysis of solid particle: kinetics and heat transfer effects," *Energy Convers. Manag.*, vol. 44, no. 14, pp. 2251–2275, Aug. 2003.

[106] H. Ström and H. Thunman, "CFD simulations of biofuel bed conversion: A submodel for the drying and devolatilization of thermally thick wood particles," *Combust. Flame*, vol. 160, no. 2, pp. 417–431, Feb. 2013.

[107] M. Bellais, *Modelling of the pyrolysis of large wood particles*, vol. 79. 2007.

[108] N. Fernando and M. Narayana, "A comprehensive two dimensional Computational Fluid Dynamics model for an updraft biomass gasifier," *Renew. Energy*, vol. 99, pp. 698–710, 2016.

[109] A. K. Sharma, "Equilibrium and kinetic modeling of char reduction reactions in a downdraft biomass gasifier: A comparison," *Sol. Energy*, vol. 82, no. 10, pp. 918–928, Oct. 2008.

[110] P. Energy, C. Sci, M. L. Hobbs, and P. T. Radulovic, "Pergamon COMBUSTION AND GASIFICATION OF COALS IN FIXED-BEDS Up d ," *Prog. Energy Combust. Sci.*, vol. 19, pp. 505–586, 1994.

[111] T. M. Ismail and M. A. El-Salam, "Parametric studies on biomass gasification process on updraft gasifier high temperature air gasification," *Appl. Therm. Eng.*, vol. 112, pp. 1460–1473, 2017.

[112] M. R. Karim and J. Naser, “Numerical Modelling of Solid Biomass Combustion: Difficulties in Initiating the Fixed Bed Combustion,” *Energy Procedia*, vol. 110, no. December 2016, pp. 390–395, 2017.

[113] C. A. Forero-Núñez, S. Ramirez-Rubio, and F. E. Sierra-Vargas, “Analysis of charcoal gasification on a downdraft fixed bed gasifier by CFD modeling,” *Int. Rev. Mech. Eng.*, vol. 9, no. 4, pp. 382–390, 2015.

[114] R. Gupta, P. Jain, and S. Vyas, “CFD Modeling and Simulation of 10KWE Biomass Downdraft Gasifier,” vol. 7, no. 4, pp. 0–2, 2017.

[115] R. B. Bird, W. E. Stewart, and E. N. Lightfoot, *Transport Phenomena*. 2002.

[116] D. J. Gunn, “Transfer of heat or mass to particles in fixed and fluidised beds,” *Int. J. Heat Mass Transf.*, vol. 21, no. 4, pp. 467–476, 1978.

[117] S. R.K, *Chemical Engineering Design*, vol. 70, no. 3. 2004.

[118] H. Zhou, A. D. Jensen, P. Glarborg, P. A. Jensen, and A. Kavaliauskas, “Numerical modeling of straw combustion in a fixed bed,” *Fuel*, vol. 84, no. 4, pp. 389–403, 2005.

[119] J. S. Ryan and W. L. H. Hallett, “Packed bed combustion of char particles: Experiments and an ash model,” *Chem. Eng. Sci.*, vol. 57, no. 18, pp. 3873–3882, 2002.

[120] Q. Xiong and S. C. Kong, “High-Resolution Particle-Scale Simulation of Biomass Pyrolysis,” *ACS Sustain. Chem. Eng.*, vol. 4, no. 10, pp. 5456–5461, 2016.

[121] K. Kwiatkowski, K. Bajer, A. Celińska, M. Dudyński, J. Korotko, and M. Sosnowska, “Pyrolysis and gasification of a thermally thick wood particle - Effect of fragmentation,” *Fuel*, vol. 132, no. November, pp. 125–134, 2014.

[122] H. Kubler, “Indicators and significance of air supply in the combustion of wood for heat,” *Wood Fiber Sci.*, vol. 23, no. 2, pp. 153–164, 1991.

[123] A. D. Hughes, “Fuelling around the boiler room,” *For. Prod. J.*, vol. 26, pp. 33–38, 1976.

[124] C. Yin, L. a. Rosendahl, and S. K. Kær, “Grate-firing of biomass for heat and power production,” *Prog. Energy Combust. Sci.*, vol. 34, no. 6, pp. 725–754, Dec. 2008.

[125] C. Ryu, Y. Bin Yang, A. Khor, N. E. Yates, V. N. Sharifi, and J. Swithenbank, “Effect of fuel properties on biomass combustion: Part I. Experiments - Fuel type, equivalence ratio and particle size,” *Fuel*, vol. 85, no. 7–8, pp. 1039–1046, 2006.

[126] J. F. Pérez, A. Melgar, and F. V Tinaut, “Modeling of fi xed bed downdraft biomass gasi fi cation : Application on lab-scale and industrial reactors,” no. April 2013, pp. 319–338, 2014.

[127] S. Suranani and V. R. Goli, “Fuel Particle Size Effect on Performance of Fluidized Bed Combustor Firing Ground Nutshells,” *Int. J. Chem. Eng. Appl. Vol. 3, No. 2, April 2012 Fuel*, vol. 3, no. 2, pp. 147–151, 2012.

[128] K. M. Bryden and K. W. Ragland, “Numerical Modeling of a Deep, Fixed Bed Combustor,” *Energy & Fuels*, vol. 10, no. 2, pp. 269–275, 1996.

[129] J. K. A. T. Rajika and M. Narayana, “Modelling and simulation of wood chip combustion in a hot air generator system,” *Springerplus*, vol. 5, no. 1, 2016.

APPENDIX A- OpenFoam Programme for Packed Bed Combustion

```
/*---------------------------------------------------------------------------*\
  =========                 |
  \\      /  F ield         | OpenFOAM: The Open Source CFD Toolbox
   \\    /   O peration     |
    \\  /    A nd           | Copyright (C) 2011-2013 OpenFOAM Foundation
     \\/     Manipulation  |
-------------------------------------------------------------------------------
License
    This file is part of OpenFOAM.

    OpenFOAM is free software: you can redistribute it and/or modify it
    under the terms of the GNU General Public License as published by
    the Free Software Foundation, either version 3 of the License, or
    (at your option) any later version.

    OpenFOAM is distributed in the hope that it will be useful, but WITHOUT
    ANY WARRANTY; without even the implied warranty of MERCHANTABILITY or
    FITNESS FOR A PARTICULAR PURPOSE.  See the GNU General Public License
    for more details.

    You should have received a copy of the GNU General Public License
    along with OpenFOAM.  If not, see <http://www.gnu.org/licenses/>.

Application
    PackedbedFoam

Description
    Transient solver for incompressible, laminar flow of Newtonian fluids.

\*---------------------------------------------------------------------------*/

#include "fvCFD.H"
#include "fvcVolumeIntegrate.H"
#include "pisoControl.H"
#include "OFstream.H"
#include "wallDist.H"

// * * * * * * * * * * * * * * * * * * * * * * * * * * * * * * * * * * * * * //

int main(int argc, char *argv[])
{
    #include "setRootCase.H"
    #include "createTime.H"
    #include "createMesh.H"

    pisoControl piso(mesh);

    #include "createFields.H"
    #include "nut.H"
    #include "initContinuityErrs.H"


    // * * * * * * * * * * * * * * * * * * * * * * * * * * * * * * * * * * * * //

    Info<< "\nStarting time loop\n" << endl;

    while (runTime.loop())
    {
        Info<< "Time = " << runTime.timeName() << nl << endl;


   volScalarField nu
     (
      "nu",
       (1.98e-5)*nu_c*(Tg/(300*Tc))/(rhog/rhoc)
     );

   volScalarField nuporosity
```

```
      (
       "nuporosity",
        nu*bedporosity
      );

   volScalarField nutporosity
      (
       "nutporosity",
        nut*bedporosity
      );

    volTensorField velocityGradient
      (
       "velocityGradient",
        fvc::grad(U)
      );

    volTensorField S
      (
       "S",
        0.5*(velocityGradient+T(velocityGradient))
      );

   volScalarField SintoS
      (
       "SintoS",
        S && S
      );

   volTensorField turbulance
      (
       "turbulance",
        2*nut*S-2/3*(k+ksmall)*I
      );

volVectorField momentumresistance
      (
       "momentumresistance",
 ( selectionvalue*150*(1-0.5)*(1-0.5)*nu/((dp_o)*(dp_o)*0.5*0.5)*mag(U)*(-
shrinkagevector)+1.75*(1-0.5)/((dp_o)*0.5)*mag(U)*mag(U)*(-
shrinkagevector))*(Time/unitlength)
      );

#include "particlesize.H"
#include "variables.H"
#include "Gasdiffusioninsideparticle.H"
#include "shrinkage.H"
#include "phibed.H"
#include "Reactionrates.H"

// Solve Gas Phase Velocity and Pressure Equations:

  fvVectorMatrix UEqn
        (
            fvm::ddt(bedporosity, U)
          + fvm::div(phis, U)
          - fvm::laplacian(nuporosity, U)
        );
       solve(UEqn == -fvc::grad(p)*bedporosity-fvc::div(turbulance)-
momentumresistance);

        // --- PISO loop

        while (piso.correct())
        {
            volScalarField rAU(1.0/UEqn.A());
            volVectorField HbyA(constrainHbyA(rAU*UEqn.H(), U, p));
            surfaceScalarField phisHbyA
            (
                "phisHbyA",
                fvc::flux(HbyA)
              + fvc::interpolate(rAU)*fvc::ddtCorr(U, phis)
```

```
            );

            adjustPhi(phisHbyA, U, p);

            // Update the pressure BCs to ensure flux consistency
            constrainPressure(p, U, phisHbyA, rAU);

            // Non-orthogonal pressure corrector loop
            while (piso.correctNonOrthogonal())
            {
                // Pressure corrector

                fvScalarMatrix pEqn
                (
                    fvm::laplacian(rAU, p) ==
(1/bedporosity)*fvc::div(phisHbyA)+gasgeneration/rhog
                );

                pEqn.setReference(pRefCell, pRefValue);
                pEqn.solve(mesh.solver(p.select(piso.finalInnerIter())));

                if (piso.finalNonOrthogonalIter())
                {
                    phis = phisHbyA - pEqn.flux();
                }
            }

            #include "continuityErrs.H"

            U = HbyA - rAU*fvc::grad(p);
            U.correctBoundaryConditions();
        }
// --End Piso loop

#include "kepsilon.H"
#include "heatrelease.H"
#include "radiation.H"
#include "TgEqn.H"
#include "TsEqn.H"
#include "gasspeciesconservationEqn.H"
#include "solidmassconservationEqn.H"

     runTime.write();

        Info<< "ExecutionTime = " << runTime.elapsedCpuTime() << " s"
            << "  ClockTime = " << runTime.elapsedClockTime() << " s"
            << nl << endl;
    }
    Info<< "End\n" << endl;
    return 0;
}
// ************************************************************************* //




// ************************************************************************* //
```

createfields.H

```
/*****************************************************************************
*********************************/

//Read Physical Properties from physicalProperties Dictionary:


Info<< "Reading physicalProperties\n" << endl;

IOdictionary physicalProperties
    (
        IOobject
```

```
    (
        "physicalProperties",
        runTime.constant(),
        mesh,
        IOobject::MUST_READ_IF_MODIFIED,
        IOobject::NO_WRITE
    )
);

dimensionedScalar rhowater
(
    physicalProperties.lookup("Water_density")
);
dimensionedScalar rhoabsWood
(
    physicalProperties.lookup("Absolute_Wood_density")
);
dimensionedScalar rhoabschar
(
    physicalProperties.lookup("Absolute_Char_density")
);
dimensionedScalar rhoabsash
(
    physicalProperties.lookup("Absolute_Ash_density")
);

dimensionedScalar Cr
(
    physicalProperties.lookup("Cr")
);
dimensionedScalar Crp
(
    physicalProperties.lookup("Crp")
);
dimensionedScalar mn
(
    physicalProperties.lookup("mn")
);

dimensionedScalar dp_o
(
    physicalProperties.lookup("Initial_particle_diameter")
);
dimensionedScalar Lp_o
(
    physicalProperties.lookup("Initial_particle_length")
);
dimensionedScalar dpore
(
    physicalProperties.lookup("Pore_diameter")
);

dimensionedScalar Achamber
(
    physicalProperties.lookup("surface_area_combustion_chamber")
);

dimensionedScalar Ap_init
(
    physicalProperties.lookup("Initial_Ap")
);
dimensionedScalar Vptot_init
(
    physicalProperties.lookup("Initial_Vptot")
);
dimensionedScalar AcharO2
(
    physicalProperties.lookup("AcharO2")
);
dimensionedScalar AcharCO2
(
    physicalProperties.lookup("AcharCO2")
```

```
 );
dimensionedScalar AcharH2O
 (
     physicalProperties.lookup("AcharH2O")
 );
dimensionedScalar AcharH2
 (
     physicalProperties.lookup("AcharH2")
 );
dimensionedScalar ACO2_H2
 (
     physicalProperties.lookup("ACO2_H2")
 );
dimensionedScalar ACO_O2
 (
     physicalProperties.lookup("ACO_O2")
 );
dimensionedScalar ACO_H2O
 (
     physicalProperties.lookup("ACO_H2O")
 );
dimensionedScalar AH2_O2
 (
     physicalProperties.lookup("AH2_O2")
 );
dimensionedScalar ACH4_O2
 (
     physicalProperties.lookup("ACH4_O2")
 );
dimensionedScalar EcharCO2
 (
     physicalProperties.lookup("EcharCO2")
 );
dimensionedScalar EcharH2O
 (
     physicalProperties.lookup("EcharH2O")
 );
dimensionedScalar EcharH2
 (
     physicalProperties.lookup("EcharH2")
 );
dimensionedScalar EcharO2
 (
     physicalProperties.lookup("EcharO2")
 );
dimensionedScalar ECO2_H2
 (
     physicalProperties.lookup("ECO2_H2")
 );
dimensionedScalar ECO_O2
 (
     physicalProperties.lookup("ECO_O2")
 );
dimensionedScalar ECO_H2O
 (
     physicalProperties.lookup("ECO_H2O")
 );
dimensionedScalar EH2_O2
 (
     physicalProperties.lookup("EH2_O2")
 );
dimensionedScalar ECH4_O2
 (
     physicalProperties.lookup("ECH4_O2")
 );
dimensionedScalar Mchar
 (
     physicalProperties.lookup("MolarweightChar")
 );
dimensionedScalar MCO
 (
     physicalProperties.lookup("MolarweightCO")
```

```
    );
    dimensionedScalar MCO2
    (
        physicalProperties.lookup("MolarweightCO2")
    );
    dimensionedScalar MCH4
    (
        physicalProperties.lookup("MolarweightCH4")
    );
    dimensionedScalar MH2
    (
        physicalProperties.lookup("MolarweightH2")
    );
    dimensionedScalar MH2O
    (
        physicalProperties.lookup("MolarweightH2O")
    );
    dimensionedScalar MN2
    (
        physicalProperties.lookup("MolarweightN2")
    );
   dimensionedScalar MO2
    (
        physicalProperties.lookup("MolarweightO2")
    );
    dimensionedScalar woodporosity
    (
        physicalProperties.lookup("Wood_porosity")
    );
    dimensionedScalar charporosity
    (
        physicalProperties.lookup("Char_porosity")
    );
    dimensionedScalar ashporosity
    (
        physicalProperties.lookup("Ash_porosity")
    );
    dimensionedScalar Wooddensity
    (
        physicalProperties.lookup("Wood_density")
    );
    dimensionedScalar Chardensity
    (
        physicalProperties.lookup("Char_density")
    );
    dimensionedScalar Ashdensity
    (
        physicalProperties.lookup("Ash_density")
    );
    dimensionedScalar DCOref
    (
        physicalProperties.lookup("DCOref")
    );
    dimensionedScalar DCO2ref
    (
        physicalProperties.lookup("DCO2ref")
    );
    dimensionedScalar DCH4ref
    (
        physicalProperties.lookup("DCH4ref")
    );
    dimensionedScalar DH2ref
    (
        physicalProperties.lookup("DH2ref")
    );
    dimensionedScalar DH2Oref
    (
        physicalProperties.lookup("DH2Oref")
    );
    dimensionedScalar DO2ref
    (
        physicalProperties.lookup("DO2ref")
```

```
    );

   dimensionedScalar DN2ref
    (
        physicalProperties.lookup("DN2ref")
    );
//Moisture diffusion parameters

   dimensionedScalar Do
    (
        physicalProperties.lookup("Do")
    );
   dimensionedScalar a1bw
    (
        physicalProperties.lookup("a1bw")
    );
   dimensionedScalar a2bw
    (
        physicalProperties.lookup("a2bw")
    );

   dimensionedScalar CpsMoisture
    (
        physicalProperties.lookup("CpsMoisture")
    );
   dimensionedScalar Cpschar
    (
        physicalProperties.lookup("Cpschar")
    );
   dimensionedScalar Cpsash
    (
        physicalProperties.lookup("Cpsash")
    );
   dimensionedScalar Cpfactor
    (
        physicalProperties.lookup("Cpfactor")
    );
  dimensionedScalar kmoisture
    (
        physicalProperties.lookup("moisture_thermalconductivity")
    );
  dimensionedScalar kWood
    (
        physicalProperties.lookup("Wood_thermalconductivity")
    );
  dimensionedScalar khemicellulose
    (
        physicalProperties.lookup("hemicellulose_thermalconductivity")
    );
  dimensionedScalar klignin
    (
        physicalProperties.lookup("lignin_thermalconductivity")
    );
 dimensionedScalar kchar
    (
        physicalProperties.lookup("char_thermalconductivity")
    );
  dimensionedScalar kash
    (
        physicalProperties.lookup("ash_thermalconductivity")
    );
   dimensionedScalar Hwater
    (
        physicalProperties.lookup("Enthalpy_Water_Evaporation")
    );
   dimensionedScalar deltaHC_O2A
    (
        physicalProperties.lookup("Enthalpy_char_combustion_A")
    );
   dimensionedScalar deltaHC_O2B
    (
        physicalProperties.lookup("Enthalpy_char_combustion_B")
```

```
    );
    dimensionedScalar deltaHC_CO2
    (
        physicalProperties.lookup("Enthalpy_char_CO2")
    );
    dimensionedScalar deltaHC_H2O
    (
        physicalProperties.lookup("Enthalpy_char_H2O")
    );
    dimensionedScalar deltaHC_H2
    (
        physicalProperties.lookup("Enthalpy_char_H2")
    );
    dimensionedScalar deltaHCO_O2
    (
        physicalProperties.lookup("Enthalpy_CO_O2")
    );
    dimensionedScalar deltaHH2_O2
    (
        physicalProperties.lookup("Enthalpy_H2_O2")
    );
    dimensionedScalar deltaHCH4_O2
    (
        physicalProperties.lookup("Enthalpy_CH4_O2")
    );
    dimensionedScalar deltaHCO_H2O
    (
        physicalProperties.lookup("Enthalpy_CO_H2O")
    );
    dimensionedScalar deltaHCO2_H2
    (
        physicalProperties.lookup("Enthalpy_CO2_H2")
    );
    dimensionedScalar universalgasconstant
    (
        physicalProperties.lookup("universalgasconstant")
    );
dimensionedScalar abscoeffsolid
    (
        physicalProperties.lookup("solid_absorption_coefficient")
    );
    dimensionedScalar abscoeff
    (
        physicalProperties.lookup("gas_absorption_coefficient")
    );
    dimensionedScalar sigma
    (
        physicalProperties.lookup("SteffanBoltzmann_constant")
    );
    dimensionedScalar C
    (
        physicalProperties.lookup("C_radiationconstant")
    );
    dimensionedScalar econt
    (
        physicalProperties.lookup("emissioncoefficient_continuousphase")
    );
    dimensionedScalar esolid
    (
        physicalProperties.lookup("emissioncoefficient_solid")
    );
    dimensionedScalar Econt
    (
        physicalProperties.lookup("E_continuousphase")
    );
    dimensionedScalar Esolid
    (
        physicalProperties.lookup("E_solid")
    );
    dimensionedScalar sigmarad
    (
        physicalProperties.lookup("sigma_rad")
```

```
    );
    dimensionedScalar Tomega
    (
         physicalProperties.lookup("Tomega")
    );
    dimensionedScalar Twall
    (
         physicalProperties.lookup("Twall")
    );

//turbulence properties
    dimensionedScalar Cmu
    (
         physicalProperties.lookup("Cmu")
    );
    dimensionedScalar C1
    (
         physicalProperties.lookup("C1")
    );

    dimensionedScalar C2
    (
         physicalProperties.lookup("C2")
    );
    dimensionedScalar C3
    (
         physicalProperties.lookup("C3")
    );

    dimensionedScalar sigmak
    (
         physicalProperties.lookup("sigmak")
    );
    dimensionedScalar sigmaEps
    (
         physicalProperties.lookup("sigmaEps")
    );
    dimensionedScalar Prt
    (
         physicalProperties.lookup("Prt")
    );
    dimensionedScalar unitvolume
    (
         physicalProperties.lookup("unitvolume")
    );
    dimensionedScalar unitlength
    (
         physicalProperties.lookup("unitlength")
    );
    dimensionedScalar verysmallvaluevolume
    (
         physicalProperties.lookup("verysmallvaluevolume")
    );
    dimensionedScalar verysmallvaluemass
    (
         physicalProperties.lookup("verysmallvaluemass")
    );
dimensionedScalar ksmall
  (
   physicalProperties.lookup("ksmall")
);
dimensionedScalar epsilonsmall
  (
   physicalProperties.lookup("epsilonsmall")
);
dimensionedScalar smallmu
  (
   physicalProperties.lookup("smallmu")
);
dimensionedScalar smallkg
  (
   physicalProperties.lookup("smallkg")
```

```
);
dimensionedScalar Prsmall
 (
  physicalProperties.lookup("Prsmall")
);
dimensionedScalar g
 (
  physicalProperties.lookup("g")
);
dimensionedScalar smalltime
 (
  physicalProperties.lookup("smalltime")
);
dimensionedScalar smallmolarweight
 (
  physicalProperties.lookup("smallmolarweight")
);
dimensionedScalar smallphi
 (
  physicalProperties.lookup("smallphi")
);
dimensionedScalar smallheat
 (
  physicalProperties.lookup("smallheat")
);
dimensionedScalar ksolid
 (
  physicalProperties.lookup("ksolid")
);
   dimensionedScalar Cpsolid
   (
        physicalProperties.lookup("Cpsolid")
   );
   dimensionedScalar Tflame
   (
        physicalProperties.lookup("Tflame")
   );
   dimensionedScalar Tig
   (
        physicalProperties.lookup("Tig")
   );
   dimensionedScalar Tinitial
   (
        physicalProperties.lookup("Tinitial")
   );
   dimensionedScalar Time
   (
        physicalProperties.lookup("Time")
   );
   dimensionedScalar Temp
   (
        physicalProperties.lookup("Temp")
   );
   dimensionedScalar rhos
   (
        physicalProperties.lookup("rhos")
   );
   dimensionedScalar x
   (
        physicalProperties.lookup("x")
   );
//from niranjan
    dimensionedScalar sigmaH2O
    (
        physicalProperties.lookup("sigmaH2O")
    );
    dimensionedScalar sigmaH2
    (
        physicalProperties.lookup("sigmaH2")
    );
    dimensionedScalar sigmaCH4
    (
```

```
    physicalProperties.lookup("sigmaCH4")
);
dimensionedScalar sigmaCO
(
    physicalProperties.lookup("sigmaCO")
);
dimensionedScalar sigmaCO2
(
    physicalProperties.lookup("sigmaCO2")
);

dimensionedScalar sigmaO2
(
    physicalProperties.lookup("sigmaO2")
);
dimensionedScalar sigmaN2
(
    physicalProperties.lookup("sigmaN2")
);
dimensionedScalar D
(
    physicalProperties.lookup("D")
);
   dimensionedScalar kH2O
(
    physicalProperties.lookup("kH2O")
);
dimensionedScalar kH2
(
    physicalProperties.lookup("kH2")
);
dimensionedScalar kCH4
(
    physicalProperties.lookup("kCH4")
);
dimensionedScalar kCO
(
    physicalProperties.lookup("kCO")
);
dimensionedScalar kCO2
(
    physicalProperties.lookup("kCO2")
);
dimensionedScalar kO2
(
    physicalProperties.lookup("kO2")
);
dimensionedScalar kN2
(
    physicalProperties.lookup("kN2")
);
dimensionedScalar nu_c
(
     physicalProperties.lookup("nu_c")
);
dimensionedScalar rhoc
(
     physicalProperties.lookup("rhoc")
);
dimensionedScalar Tc
(
    physicalProperties.lookup("Tc")
);
dimensionedScalar Ac
(
     physicalProperties.lookup("Ac")
);

dimensionedScalar Tcinv
(
    physicalProperties.lookup("Tcinv")
);
```

```
    dimensionedScalar kc
    (
         physicalProperties.lookup("kc")
    );
    dimensionedScalar sigmac
    (
        physicalProperties.lookup("sigmac")
    );
    dimensionedScalar Dc
    (
         physicalProperties.lookup("Dc")
    );
    dimensionedScalar Cc
    (
         physicalProperties.lookup("Cc")
    );
    dimensionedScalar muc
    (
         physicalProperties.lookup("muc")
    );
    dimensionedScalar Pc
    (
         physicalProperties.lookup("Pc")
    );
    dimensionedScalar Hc
    (
         physicalProperties.lookup("Hc")
    );

/*****************************************************************************
*************************************/


// Read Initial Fields:

     Info<< "Reading field Xposition\n" << endl;
    volScalarField Xposition
    (
        IOobject
        (
            "Xposition",
            runTime.timeName(),
            mesh,
            IOobject::MUST_READ,
            IOobject::AUTO_WRITE
        ),
        mesh
    );
     Info<< "Reading field Yposition\n" << endl;
    volScalarField Yposition
    (
        IOobject
        (
            "Yposition",
            runTime.timeName(),
            mesh,
            IOobject::MUST_READ,
            IOobject::AUTO_WRITE
        ),
        mesh
    );
Info<< "Reading field solidporosity\n" << endl;
    volScalarField solidporosity
    (
        IOobject
        (
            "solidporosity",
            runTime.timeName(),
            mesh,
            IOobject::MUST_READ,
            IOobject::AUTO_WRITE
        ),
```

```
        mesh
    );
Info<< "Reading field Cps\n" << endl;
    volScalarField Cps
    (
        IOobject
        (
            "Cps",
            runTime.timeName(),
            mesh,
            IOobject::MUST_READ,
            IOobject::AUTO_WRITE
        ),
        mesh
    );
Info<< "Reading field ks\n" << endl;
    volScalarField ks
    (
        IOobject
        (
            "ks",
            runTime.timeName(),
            mesh,
            IOobject::MUST_READ,
            IOobject::AUTO_WRITE
        ),
        mesh
    );

 Info<< "Reading field selectionvalue\n" << endl;
    volScalarField selectionvalue
    (
        IOobject
        (
            "selectionvalue",
            runTime.timeName(),
            mesh,
            IOobject::MUST_READ,
            IOobject::AUTO_WRITE
        ),
        mesh
    );

Info<< "Reading field TotalMass\n" << endl;
    volScalarField TotalMass
    (
        IOobject
        (
            "TotalMass",
            runTime.timeName(),
            mesh,
            IOobject::MUST_READ,
            IOobject::AUTO_WRITE
        ),
        mesh
    );


Info<< "Reading field G\n" << endl;
    volScalarField G
    (
        IOobject
        (
            "G",
            runTime.timeName(),
            mesh,
            IOobject::MUST_READ,
            IOobject::AUTO_WRITE
        ),
        mesh
    );
```

```
 Info<< "Reading field p\n" << endl;
    volScalarField p
    (
        IOobject
        (
            "p",
            runTime.timeName(),
            mesh,
            IOobject::MUST_READ,
            IOobject::AUTO_WRITE
        ),
        mesh
    );

Info<< "Reading field k\n" << endl;
    volScalarField k
    (
        IOobject
        (
            "k",
            runTime.timeName(),
            mesh,
            IOobject::MUST_READ,
            IOobject::AUTO_WRITE
        ),
        mesh
    );

Info<< "Reading field epsilon\n" << endl;
    volScalarField epsilon
    (
        IOobject
        (
            "epsilon",
            runTime.timeName(),
            mesh,
            IOobject::MUST_READ,
            IOobject::AUTO_WRITE
        ),
        mesh
    );

 Info<< "Reading field Tg\n" << endl;
    volScalarField Tg
    (
        IOobject
        (
            "Tg",
            runTime.timeName(),
            mesh,
            IOobject::MUST_READ,
            IOobject::AUTO_WRITE
        ),
        mesh
    );

 Info<< "Reading field Ts\n" << endl;
    volScalarField Ts
    (
        IOobject
        (
            "Ts",
            runTime.timeName(),
            mesh,
            IOobject::MUST_READ,
            IOobject::AUTO_WRITE
        ),
        mesh
    );

Info<< "Reading field mMoisture\n" << endl;
    volScalarField mMoisture_o
```

```
    (
        IOobject
        (
            "mMoisture_o",
            runTime.timeName(),
            mesh,
            IOobject::MUST_READ,
            IOobject::AUTO_WRITE
        ),
        mesh
    );

 Info<< "Reading field mWood_o\n" << endl;
    volScalarField mWood_o
    (
        IOobject
        (
            "mWood_o",
            runTime.timeName(),
            mesh,
            IOobject::MUST_READ,
            IOobject::AUTO_WRITE
        ),
        mesh
    );

Info<< "Reading field mMoisture\n" << endl;
    volScalarField mMoisture
    (
        IOobject
        (
            "mMoisture",
            runTime.timeName(),
            mesh,
            IOobject::MUST_READ,
            IOobject::AUTO_WRITE
        ),
        mesh
    );

 Info<< "Reading field mWood\n" << endl;
    volScalarField mWood
    (
        IOobject
        (
            "mWood",
            runTime.timeName(),
            mesh,
            IOobject::MUST_READ,
            IOobject::AUTO_WRITE
        ),
        mesh
    );

 Info<< "Reading field mchar\n" << endl;
    volScalarField mchar
    (
        IOobject
        (
            "mchar",
            runTime.timeName(),
            mesh,
            IOobject::MUST_READ,
            IOobject::AUTO_WRITE
        ),
        mesh
    );

 Info<< "Reading field mash\n" << endl;
    volScalarField mash
    (
        IOobject
```

```
        (
            "mash",
            runTime.timeName(),
            mesh,
            IOobject::MUST_READ,
            IOobject::AUTO_WRITE
        ),
        mesh
    );

    Info<< "Reading field U\n" << endl;
    volVectorField U
    (
        IOobject
        (
            "U",
            runTime.timeName(),
            mesh,
            IOobject::MUST_READ,
            IOobject::AUTO_WRITE
        ),
        mesh
    );

Info<< "Reading field I\n" << endl;
    volTensorField I
    (
        IOobject
        (
            "I",
            runTime.timeName(),
            mesh,
            IOobject::MUST_READ,
            IOobject::AUTO_WRITE
        ),
        mesh
    );
 Info<< "Reading field mO2\n" << endl;
    volScalarField mO2
    (
        IOobject
        (
            "mO2",
            runTime.timeName(),
            mesh,
            IOobject::MUST_READ,
            IOobject::AUTO_WRITE
        ),
        mesh
    );
 Info<< "Reading field mH2\n" << endl;
    volScalarField mH2
    (
        IOobject
        (
            "mH2",
            runTime.timeName(),
            mesh,
            IOobject::MUST_READ,
            IOobject::AUTO_WRITE
        ),
        mesh
    );
 Info<< "Reading field mCO2\n" << endl;
    volScalarField mCO2
    (
        IOobject
        (
            "mCO2",
            runTime.timeName(),
            mesh,
            IOobject::MUST_READ,
```

```
            IOobject::AUTO_WRITE
        ),
        mesh
    );
  Info<< "Reading field mCO\n" << endl;
    volScalarField mCO
    (
        IOobject
        (
            "mCO",
            runTime.timeName(),
            mesh,
            IOobject::MUST_READ,
            IOobject::AUTO_WRITE
        ),
        mesh
    );
  Info<< "Reading field mH2O\n" << endl;
    volScalarField mH2O
    (
        IOobject
        (
            "mH2O",
            runTime.timeName(),
            mesh,
            IOobject::MUST_READ,
            IOobject::AUTO_WRITE
        ),
        mesh
    );

  Info<< "Reading field mCH4\n" << endl;
    volScalarField mCH4
    (
        IOobject
        (
            "mCH4",
            runTime.timeName(),
            mesh,
            IOobject::MUST_READ,
            IOobject::AUTO_WRITE
        ),
        mesh
    );

  Info<< "Reading field mN2\n" << endl;
    volScalarField mN2
    (
        IOobject
        (
            "mN2",
            runTime.timeName(),
            mesh,
            IOobject::MUST_READ,
            IOobject::AUTO_WRITE
        ),
        mesh
    );

//shrinkage parameters

Info<< "Reading field Vp\n" << endl;
    volScalarField Vp
    (
        IOobject
        (
            "Vp",
            runTime.timeName(),
            mesh,
            IOobject::MUST_READ,
            IOobject::AUTO_WRITE
        ),
```

```
        mesh
    );

    Info<< "Reading field w\n" << endl;
    volScalarField w
    (
        IOobject
        (
            "w",
            runTime.timeName(),
            mesh,
            IOobject::MUST_READ,
            IOobject::AUTO_WRITE
        ),
        mesh
    );
    Info<< "Reading field xx\n" << endl;
    volScalarField xx
    (
        IOobject
        (
            "xx",
            runTime.timeName(),
            mesh,
            IOobject::MUST_READ,
            IOobject::AUTO_WRITE
        ),
        mesh
    );
    Info<< "Reading field yy\n" << endl;
    volScalarField yy
    (
        IOobject
        (
            "yy",
            runTime.timeName(),
            mesh,
            IOobject::MUST_READ,
            IOobject::AUTO_WRITE
        ),
        mesh
    );
    Info<< "Reading field dp\n" << endl;
    volScalarField dp
    (
        IOobject
        (
            "dp",
            runTime.timeName(),
            mesh,
            IOobject::MUST_READ,
            IOobject::AUTO_WRITE
        ),
        mesh
    );
    Info<< "Reading field Lp\n" << endl;
    volScalarField Lp
    (
        IOobject
        (
            "Lp",
            runTime.timeName(),
            mesh,
            IOobject::MUST_READ,
            IOobject::AUTO_WRITE
        ),
        mesh
    );

    Info<< "Reading field Aspec\n" << endl;
    volScalarField Aspec
    (
```

```
        IOobject
        (
            "Aspec",
            runTime.timeName(),
            mesh,
            IOobject::MUST_READ,
            IOobject::AUTO_WRITE
        ),
        mesh
    );
/*****************************************************************************
*****************************************/
#   include "createPhi.H"

surfaceScalarField phis
     (
      "phis",
       fvc::interpolate(solidporosity)*phi
     );

/*****************************************************************************
*****************************************/
    label pRefCell = 0;
    scalar pRefValue = 0.0;
    setRefCell(p, mesh.solutionDict().subDict("PISO"), pRefCell, pRefValue);
```

nut.H

```
volScalarField nut
     (
      "nut",
       0.09*pow(k,2)/epsilon
      );
```

rhosolid.H

```
//Calculate Solid density
volScalarField rhosolid
  (
  "rhosolid",
  (mMoisture+mWood+mchar+mash)/((1-solidporosity)+1e-25)
   );

rhosolid = rhosolid*neg(-(1-solidporosity))+(1-solidporosity)*rhoc;
```

selectionvalue.H

```
volScalarField solidfraction
     (
      "solidfraction",
      neg(0*rhoc-(mMoisture+mWood+mchar))
     );

 volScalarField gasfraction
     (
      "gasfraction",
       1-solidfraction
     );
selectionvalue = 1-pos(gasfraction-0.99);
selectionvalue= selectionvalue*neg(0-selectionvalue)+0*pos(0-selectionvalue);
```

particlesize.H

```
//calculation of particle size

volScalarField reactedmoisturevolume
     (
      "reactedmoisturevolume",
       0.01*selectionvalue*(mMoisture_o-mMoisture)/(6*rhoc)
     );
volScalarField reactedwoodvolume
```

```
      (
       "reactedwoodvolume",
        0.6*selectionvalue*(mWood_o-mWood)/(279*rhoc)
      );
volScalarField reactedcharvolume
      (
       "reactedcharvolume",
        0.3*selectionvalue*(mWood_o*0.145-mchar)*neg(-mchar)/(279*0.145*rhoc)
      );

Vp=selectionvalue*Vptot_init*(1-reactedmoisturevolume-reactedwoodvolume-
reactedcharvolume);
dp=pow(mag(6*Vp/(Foam::constant::mathematical::pi*unitvolume)),0.33)*unitlength;

dp_old=dp.oldTime();
dp=dp*pos(dp_o-dp)*pos(dp-0*unitlength)+dp_o*neg(dp_o-dp)*pos(dp-0*unitlength);
dp=dp*pos(dp_old-dp)*pos(dp-0*unitlength)+dp_old*neg(dp_old-dp)*pos(dp-0*unitlength);
```

variables.H

```
//Gas species mass fraction calculation

volScalarField YMoisture
    (
    "YMoisture",
 mMoisture*selectionvalue/(mWood+mchar+mash+mMoisture+verysmallvaluemass)
    );

volScalarField YWood
    (
    "YWood",
(mWood)*selectionvalue/((mWood+mchar+mash+mMoisture+verysmallvaluemass))
    );

volScalarField Ychar
    (
    "Ychar",
    mchar*selectionvalue/(mWood+mchar+mash+mMoisture+verysmallvaluemass)
    );

volScalarField Yash
    (
    "Yash",
    mash*selectionvalue/(mWood+mchar+mash+mMoisture+verysmallvaluemass)
    );
//Dynamic viscosity mu
    volScalarField mu
      (
       "mu",
        nu*rhog
      );


//saturation temperature for moisture
volScalarField Yfbs
      (
       "Yfbs",
       0.3+0.298-0.001*Ts/Temp
      );
        Yfbs=Yfbs*pos(Yfbs-0.2)+0.2*neg(Yfbs-0.2);
volScalarField PH2O
      (
       "PH2O",
        H2O*p/(H2O+CO+CO2+CH4+H2+N2+smallmolarweight)
      );
volScalarField TT
      (
       "TT",
       1-pow(mag(1-YMoisture/Yfbs),(6.453e-3*(Ts/Tc)))
      );
volScalarField kg
      (
```

```
      "kg",
       (4.8e-4)*kc*pow(mag(Tg/Tc),0.717)
     );
volScalarField Cpg
     (
      "Cpg",
       Cc*(990+0.122*Tg/Tc-(5680e+3)*pow(mag(Tg/Tc),-2))
    );
volScalarField DTg
   (
   "DTg",
   (mag(kg)*solidporosity/rhog/mag(Cpg))
   );


//calculate dimesionless numbers

//Reynolds number
volScalarField Re
   (
   "Re",
   mag(rhog)*mag(U)*(dp_o)/(mag(mu)+smallmu)
   );
//Prandtl number
volScalarField Pr
   (
   "Pr",
   mag(Cpg)*mag(mu)/mag(kg)
    );


// Nusselt Number

volScalarField Nusphere
     (
      "Nusphere",
       2+0.6*pow(Re,0.5)*pow(Pr,0.33)
     );
volScalarField Nu
     (
      "Nu",
       Nusphere
     );

//spherical particles
volScalarField A
     (
      "A",
       6*(1-solidporosity)/ (dp+1e-25*unitlength)
     );

volScalarField h
     (
      "h",
       kg*Nu/(dp+1e-25*unitlength)
     );


//omegac
volScalarField omegac
   (
   "omegac",
   2*(1+4.3*exp(-Tomega/Ts))/(2+4.3*exp(-Tomega/Ts))
   );


//Evaporation heat for bound water

volScalarField FreewaterEvaporationHeat
   (
   "FreewaterEvaporationHeat",
   Cc*(3.179e6*Tc-2.5e3*Ts)
```

```
   );

volScalarField BoundwaterEvaporationHeat
   (
   "BoundwaterEvaporationHeat",
   Cc*(3.179e6*Tc-2.5e3*Ts+Tc*1.1762e6*exp(-15*YMoisture))
   );

volScalarField waterEvaporationHeat
   (
   "waterEvaporationHeat",
  FreewaterEvaporationHeat*pos(YMoisture-
0.18)+BoundwaterEvaporationHeat*neg(YMoisture-0.18)//according to our case FSP is 0.3
moisture on dryfuel
   );

volScalarField Cpparticle
     (
      "Cpparticle",

Cc*(mag(YMoisture)*4200+mag(YWood)*(1500+Ts*Tcinv)+mag(Ychar)*(420+2.09*(Ts*Tcinv)-
6.85e-4*pow(mag(Ts*Tcinv),2))+mag(Yash)*(420+2.09*(Ts*Tcinv)-6.85e-
4*pow(mag(Ts*Tcinv),2)))
     );

//Thermal conductivity of solid

volScalarField nen
     (
      "nen",
   (mWood-mchar)/((mWood_o+1e-25*rhoc)-mWood_o*0.095)
     );

volScalarField kparticle
     (
      "kparticle",
       (nen*0.35+0.071*(1-nen)+mag(Yash)*1.2)*kc
     );
ks=solidporosity*kg+(1-solidporosity)*kparticle ;
volScalarField keffsolid
     (
      "keffsolid",
       ks
     );

volScalarField DTs
   (
   "DTs",
  (keffsolid+ksolid)
   );


 volScalarField OmegaO2
     (
      "OmegaO2",
       pow((44.54*pow(mag(kO2*Tg),-4.909)+1.911*pow(mag(kO2*Tg),-1.575)),0.1)
     );


//Collisional integral calculation
volScalarField OmegaH2O
     (
      "OmegaH2O",
       pow((44.54*pow(mag(kH2O*Tg),-4.909)+1.911*pow(mag(kH2O*Tg),-1.575)),0.1)
     );

volScalarField OmegaH2
     (
      "OmegaH2",
       pow((44.54*pow(mag(kH2*Tg),-4.909)+1.911*pow(mag(kH2*Tg),-1.575)),0.1)
     );
```

```
volScalarField OmegaCH4
     (
      "OmegaCH4",
       pow((44.54*pow(mag(kCH4*Tg),-4.909)+1.911*pow(mag(kCH4*Tg),-1.575)),0.1)
     );

volScalarField OmegaCO
     (
      "OmegaCO",
       pow((44.54*pow(mag(kCO*Tg),-4.909)+1.911*pow(mag(kCO*Tg),-1.575)),0.1)
     );

 volScalarField OmegaCO2
     (
      "OmegaCO2",
       pow((44.54*pow(mag(kCO2*Tg),-4.909)+1.911*pow(mag(kCO2*Tg),-1.575)),0.1)
     );

volScalarField OmegaN2
     (
      "OmegaN2",
       pow((44.54*pow(mag(kN2*Tg),-4.909)+1.911*pow(mag(kN2*Tg),-1.575)),0.1)
     );


//Diffusion coefficients

volScalarField DH2O
     (
      "DH2O",
      Dc*0.0018583e-
4*pow(mag(Tg/Tc),1.5)*0.302*1/(pow(mag(sigmaH2O/sigmac),2)*OmegaH2O)
     );
volScalarField DH2
     (
      "DH2",
      Dc*0.0018583e-
4*pow(mag(Tg/Tc),1.5)*0.732*1/(pow(mag(sigmaH2/sigmac),2)*OmegaH2)
     );
volScalarField DCH4
     (
      "DCH4",
         Dc*0.0018583e-
4*pow(mag(Tg/Tc),1.5)*0.313*1/(pow(mag(sigmaCH4/sigmac),2)*OmegaCH4)
     );
volScalarField DCO
     (
      "DCO",
        Dc*0.0018583e-
4*pow(mag(Tg/Tc),1.5)*0.267*1/(pow(mag(sigmaCO/sigmac),2)*OmegaCO)
     );
volScalarField DCO2
     (
      "DCO2",
       Dc*0.0018583e-
4*pow(mag(Tg/Tc),1.5)*0.242*1/(pow(mag(sigmaCO2/sigmac),2)*OmegaCO2)
     );
volScalarField DO2
     (
      "DO2",
        Dc*0.0018583e-
4*pow(mag(Tg/Tc),1.5)*0.259*1/(pow(mag(sigmaO2/sigmac),2)*OmegaO2)
     );


volScalarField DN2
     (
      "DN2",
        Dc*0.0018583e-
4*pow(mag(Tg/Tc),1.5)*0.267*1/(pow(mag(sigmaN2/sigmac),2)*OmegaN2)
     );
```

```
// Sherwood Number -oxygen

volScalarField ShO2
     (
      "ShO2",
       2+0.6*pow(Re,0.5)*pow(nu/DO2,0.33)
     );

// Sherwood Number -carbon dioxide

volScalarField ShCO2
     (
      "ShCO2",
       2+0.6*pow(Re,0.5)*pow(nu/DCO2,0.33)
     );

// Sherwood Number -water vapour

volScalarField ShH2O
     (
      "ShH2O",
       2+0.6*pow(Re,0.5)*pow(nu/DH2O,0.33)
     );

// Sherwood Number -hydrogen

volScalarField ShH2

     (
      "ShH2",
       2+0.6*pow(Re,0.5)*pow(nu/DH2,0.33)
     );
// Sherwood Number -metahne
volScalarField ShCH4

     (
      "ShCH4",
       2+0.6*pow(Re,0.5)*pow(nu/DCH4,0.33)
     );
// Sherwood Number -carbon monoxide
volScalarField ShCO

     (
      "ShCO",
       2+0.6*pow(Re,0.5)*pow(nu/DCO,0.33)
     );

// Sherwood Number -nytrogen
volScalarField ShN2

     (
      "ShN2",
       2+0.6*pow(Re,0.5)*pow(nu/DN2,0.33)
     );


//MTC -oxygen

volScalarField kmO2
     (
      "kmO2",
       ShO2*DO2/D
     );

//MTC -carbon dioxide

volScalarField kmCO2
     (
      "kmCO2",
       ShCO2*DCO2/D
     );
```

```
//MTC -H2O

volScalarField kmH2O
     (
      "kmH2O",
       ShH2O*DH2O/D
     );

//MTC -H2
volScalarField kmH2
     (
      "kmH2",
       ShH2*DH2/D
     );
volScalarField kmCO
     (
      "kmCO",
       ShCO*DCO/D
     );
volScalarField kmCH4
     (
      "kmCH4",
       ShCH4*DCH4/D
     );
volScalarField kmN2
     (
      "kmN2",
       ShN2*DN2/D
     );
```

Reactionrates.H

```
//Calculation of reaction rates

//calculate drying rate;
volScalarField Rdrying
    (
    "Rdrying",
     -neg(0-selectionvalue)*neg(0*rhoc-mMoisture)*mMoisture*neg(Ts-
1200*Temp)*CpsMoisture*(pos(Ts-373.15*Tc)*(Ts-373.15*Tc)+neg(Ts-
373.15*Tc)*Tc*0)/(Hwater*runTime.deltaT())
    );

//calculate wood pyrolysis rate;
    volScalarField RWood
    (
     "RWood",
    -Awood*selectionvalue*neg(0*rhoc-mWood)*mWood*exp(-
EWood/(universalgasconstant*Ts))
    );


//claculate kinetic rate char combustion;
volScalarField charO2_rkinetic
    (
    "charO2_rkinetic",
    AcharO2*exp(-EcharO2/universalgasconstant/Ts)
    );

volScalarField charO2_rdiffusion
    (
    "charO2_rdiffusion",
    hmO2
    );

//calculate char combustion rate;
volScalarField Rcombustion
    (
    "Rcombustion",
    -Ap_init/Vptot_init*neg(0*rhoc-
mchar)*Mchar*omegac*O2*charO2_rkinetic*charO2_rdiffusion/(charO2_rkinetic+charO2_rdif
fusion)
    );
```

```
//claculate kinetic rate char&CO2 gasification;
volScalarField charCO2_rkinetic
    (
    "charCO2_rkinetic",
    AcharCO2*exp(-EcharCO2/universalgasconstant/Ts)
    );
//claculate diffusion rate char&CO2 gasification;
volScalarField charCO2_rdiffusion
    (
    "charCO2_rdiffusion",
    hmCO2
    );
//calculate char&CO2 gaification rate;
volScalarField charCO2_rgasification
    (
    "charCO2_rgasification",
    -Ap_init/Vptot_init*neg(0*rhoc-
mchar)*Mchar*CO2*charCO2_rkinetic*charCO2_rdiffusion/(charCO2_rkinetic+charCO2_rdiffu
sion)
    );
//calculate kinetic rate char&H2O gaification;
volScalarField charH2O_rkinetic
    (
    "charH2O_rkinetic",
    AcharH2O*exp(-EcharH2O/universalgasconstant/Ts)
    );
//claculate diffusion rate char&H2O gasification;
volScalarField charH2O_rdiffusion
    (
    "charH2O_rdiffusion",
    hmH2O
    );
//calculate char&H2O gaification rate;
volScalarField charH2O_rgasification
    (
    "charH2O_rgasification",
    -Ap_init/Vptot_init*neg(0*rhoc-
mchar)*Mchar*H2O*charH2O_rkinetic*charH2O_rdiffusion/(charH2O_rkinetic+charH2O_rdiffu
sion)
    );
//calculate kinetic rate char&H2 gaification;
volScalarField charH2_rkinetic
    (
    "charH2_rkinetic",
    AcharH2*exp(-EcharH2/universalgasconstant/Ts)
    );
//claculate diffusion rate char&H2 gasification;
volScalarField charH2_rdiffusion
    (
    "charH2_rdiffusion",
    hmH2
    );
//calculate char&H2 gaification rate;
volScalarField charH2_rgasification
    (
    "charH2_rgasification",
    -Ap_init/Vptot_init*neg(0*rhoc-
mchar)*Mchar*H2*charH2_rkinetic*charH2_rdiffusion/(charH2_rkinetic+charH2_rdiffusion)
    );
//claculate diffusion rate char&CH4 ;
volScalarField charCH4_rdiffusion
    (
    "charCH4_rdiffusion",
   hmCH4
    );
//claculate diffusion rate char&CO ;
volScalarField charCO_rdiffusion
    (
    "charCO_rdiffusion",
     hmCO
```

```
    );
//claculate diffusion rate char&N2 ;
volScalarField charN2_rdiffusion
    (
    "charN2_rdiffusion",
     hmN2
    );
//calculate overall char gasification rate;
volScalarField Rgasification
    (
    "Rgasification",
    charCO2_rgasification+charH2O_rgasification+charH2_rgasification
    );

volScalarField gasgeneration
       (
       "gasgeneration",
       Rdrying
       +0.9*Rpyrolysis
       );


//Gaseous reaction rates
//CO2&H2 kinetic reaction rate;
volScalarField rkCO2_H2
    (
    "rkCO2_H2",
    ACO2_H2*exp(-ECO2_H2/Tg)*CO2*H2
    );


//CO&O2 kinetic reaction rate;
volScalarField rkCO_oxidation
    (
    "rkCO_oxidation",
    ACO_O2*exp(-ECO_O2/Tg)*CO*pow(mag(O2),0.5)*pow(mag(H2O),0.5)
    );
//CO&H2O kinetic reaction rate;
volScalarField rkCO_H2O
    (
    "rkCO_H2O",
    ACO_H2O*exp(-ECO_H2O/Tg)*CO*H2O
    );


//H2&O2 kinetic reaction rate;
volScalarField rkH2_oxidation
    (
    "rkH2_oxidation",
    AH2_O2*exp(-EH2_O2/Tg)*CH4*pow(mag(O2),0.5)
    );

//CH4 kinetic reaction rate;
volScalarField rkCH4_oxidation
    (
    "rkCH4_oxidation",
    ACH4_O2*exp(-ECH4_O2/Tg)*pow(mag(CH4),0.5)*O2
    );
```

kepsilon.H

```
//Solve k-epsilon model

fvScalarMatrix kEqn
        (
            fvm::ddt(bedporosity, k)
          + fvm::div(phis, k)
          - fvm::laplacian(nutporosity, k)
        );
solve(kEqn == 2*nut*SintoS*bedporosity-epsilon*bedporosity);
```

```
fvScalarMatrix epsilonEqn
        (
            fvm::ddt(bedporosity, epsilon)
          + fvm::div(phis, epsilon)
          - fvm::laplacian(0.77*nutporosity, epsilon)
        );
solve(epsilonEqn == 2*1.44*epsilon/k*nut*SintoS*bedporosity-
1.92*pow(epsilon,2)/k*bedporosity);
```

heatrelease.H

```
//Calculation of heat generation from reactions

//heat required for evaporation
volScalarField Dryingheat
    (
    "Dryingheat",
    -Rdrying*waterEvaporationHeat
    );

//char reactions//

//char and O2
volScalarField HC_O2
   (
   "HC_O2",
   (2*(omegac-1)*deltaHC_O2A+(2-omegac)*deltaHC_O2B)*Rcombustion/omegac
   );
//char and CO2//
volScalarField HC_CO2
  (
   "HC_CO2",
   -deltaHC_CO2*charCO2_rgasification
   );
//char and H2O//
volScalarField HC_H2O
  (
   "HC_H2O",
   -deltaHC_H2O*charH2O_rgasification
   );
//char and H2
volScalarField HC_H2
   (
   "HC_H2",
   -deltaHC_H2*charH2_rgasification
   );


//gas phase reactions//

//CO with O2;
; volScalarField HCO_O2
   (
   "HCO_O2",
   -deltaHCO_O2*rCO_oxidation
   );
//H2 with O2
 volScalarField HH2_O2
   (
   "HH2_O2",
   -deltaHH2_O2*rH2_oxidation
   );
//CH4 with O2
 volScalarField HCH4_O2
   (
   "HCH4_O2",
   -deltaHCH4_O2*rCH4_oxidation
   );
//CO with H2O
```

```
 volScalarField HCO_H2O
   (
   "HCO_H2O",
   -deltaHCO_H2O*rCO_H2O
   );
//CO2 with H2
 volScalarField HCO2_H2
   (
   "HCO2_H2",
   deltaHCO2_H2*rCO2_H2
   );
```

radiation.H

```
//Solve radiation model

// Calculate radiation intensity

fvScalarMatrix GEqn
        (
          fvm::laplacian((1.0/(3.0*((abscoeff/sigmac)+(abscoeffsolid/sigmac))+
sigmarad*(3-C))),G)
         - fvm::Sp(((abscoeff/sigmac)+(abscoeffsolid/sigmac)), G)
        );

solve(GEqn==-4*(((abscoeff/sigmac)+(abscoeffsolid/sigmac))*sigma*pow(Tg,4)+
Econt+Esolid));
```

mass.H

```
TotalMass=fvc::domainIntegrate(mMoisture+mWood+mchar+mash);

volScalarField normalisedmass
     (
      "normalisedmass",
       (TotalMass)/fvc::domainIntegrate(mWood_o+mMoisture_o)
     );
```

Gasdiffusioninsideparticle.H

```
volScalarField  Ash_layer_thickness=0.5*mag(dp_o-dp)*Ychar*mchar/((mash+1e-
25*rhoc)*0.6);


//Effective diffusion coefficient in packedbed
//Diffusivity unit m2s-1
volScalarField Deff_O2bed
    (
    "Deff_O2bed ",
    (DO2*0.8+0.5*mag(U)*D)*bedporosity*selectionvalue
    );
volScalarField Deff_CO2bed
    (
    "Deff_CO2bed ",
    (DCO2*0.8+0.5*mag(U)*D)*selectionvalue
    );
volScalarField Deff_CObed
    (
    "Deff_CObed",
    (DCO*0.8+0.5*mag(U)*D)*selectionvalue
    );
volScalarField Deff_H2Obed
    (
    "Deff_H2Obed",
     (DH2O*0.8+0.5*mag(U)*D)*selectionvalue
    );
volScalarField Deff_H2bed
    (
    "Deff_H2bed",
   (DH2*0.8+0.5*mag(U)*D)*selectionvalue
    );
```

```
volScalarField Deff_CH4bed
    (
    "Deff_CH4bed",
    (DCH4*0.8+0.5*mag(U)*D)*selectionvalue
    );
 volScalarField Deff_N2bed
    (
    "Deff_N2bed",
    (DN2*0.8+0.5*mag(U)*D)*selectionvalue
    );


//calculate effective diffusion coefficient through ash layer
volScalarField Deff_O2_2
    (
    "Deff_O2_2",
    Deff_O2bed*pow(0.9,2)*selectionvalue/(Ash_layer_thickness+1e-25*unitlength)
    );
volScalarField Deff_CO2_2
    (
    "Deff_CO2_2",
    Deff_CO2bed*pow(0.9,2)*selectionvalue/(Ash_layer_thickness+1e-25*unitlength)
    );
volScalarField Deff_CO_2
    (
    "Deff_CO_2",
    Deff_CObed*pow(0.9,2)*selectionvalue/(Ash_layer_thickness+1e-25*unitlength)
    );
volScalarField Deff_H2O_2
    (
    "Deff_H2O_2",
    Deff_H2Obed*pow(0.9,2)*selectionvalue/(Ash_layer_thickness+1e-25*unitlength)
    );
volScalarField Deff_H2_2
    (
    "Deff_H2_2",
    Deff_H2bed*pow(0.9,2)*selectionvalue/(Ash_layer_thickness+1e-25*unitlength)
    );
 volScalarField Deff_CH4_2
    (
    "Deff_CH4_2",
    Deff_CH4bed*pow(0.9,2)*selectionvalue/(Ash_layer_thickness+1e-25*unitlength)
    );
volScalarField Deff_N2_2
    (
    "Deff_N2_2",
    Deff_N2bed*pow(0.9,2)*selectionvalue/(Ash_layer_thickness+1e-25*unitlength)
    );

//MTC -oxygen
volScalarField kmO2
     (
      "kmO2",
       ShO2*Deff_O2bed/D+1e-25*unitlength/Time
     );

//MTC -carbon dioxide
volScalarField kmCO2
     (
      "kmCO2",
       ShCO2*Deff_CO2bed/D+1e-25*unitlength/Time
     );

//MTC -H2O
volScalarField kmH2O
     (
      "kmH2O",
       ShH2O*Deff_H2Obed/D+1e-25*unitlength/Time
     );
//MTC -H2
volScalarField kmH2
     (
```

```
      "kmH2",
       ShH2*Deff_H2bed/D+1e-25*unitlength/Time
     );
volScalarField kmCO
     (
      "kmCO",
       ShCO*Deff_CObed/D+1e-25*unitlength/Time
     );
volScalarField kmCH4
     (
      "kmCH4",
       ShCH4*Deff_CH4bed/D+1e-25*unitlength/Time
     );
volScalarField kmN2
     (
      "kmN2",
       ShN2*Deff_N2bed/D+1e-25*unitlength/Time
     );

volScalarField SCH2O
     (
      "SCH2O",
       mu/(rhog*DH2O)
     );

volScalarField ShH2O_2
     (
      "ShH2O_2",
       (0.35+0.34*pow(Re,0.5)+0.15*pow(Re,0.58))*pow(SCH2O,0.3)
     );
volScalarField kmH2O_2
     (
      "kmH2O_2",
       ShH2O_2*DH2O/D
     );
//kmiH2O
volScalarField kmiH2O
     (
      "kmiH2O",
       1.932e-5*pow(Ts/Temp,0.5)*unitlength/Time
     );

volScalarField hmiH2O
     (
      "hmiH2O",
      kmH2O_2*kmiH2O/(kmH2O_2+kmiH2O)
     );
volScalarField Dk_O2
    (
    "Dk_O2",

2*dpore*pow((2*universalgasconstant*Tg/((Foam::constant::mathematical::pi)*MO2)),0.5)
/3
    );

volScalarField Dk_CO2
    (
    "Dk_CO2",

2*dpore*pow((2*universalgasconstant*Tg/(Foam::constant::mathematical::pi*MCO2)),0.5)/
3
    );

volScalarField Dk_CO
    (
    "Dk_CO ",

2*dpore*pow((2*universalgasconstant*Tg/(Foam::constant::mathematical::pi*MCO)),0.5)/3
    );
volScalarField Dk_H2O
    (
    "Dk_H2O",
```

```
2*dpore*pow((2*universalgasconstant*mag(Tg)/(Foam::constant::mathematical::pi*MH2O)),
0.5)/3
    );

volScalarField Dk_H2
    (
    "Dk_H2",

2*dpore*pow((2*universalgasconstant*mag(Tg)/(Foam::constant::mathematical::pi*MH2)),0
.5)/3
    );
volScalarField Dk_CH4
    (
    "Dk_CH4",

2*dpore*pow((2*universalgasconstant*mag(Tg)/(Foam::constant::mathematical::pi*MCH4)),
0.5)/3
    );
volScalarField Dk_N2
    (
    "Dk_N2",
2*dpore*pow((2*universalgasconstant*mag(Tg)/(Foam::constant::mathematical::pi*MN2)),0
.5)/3
    );

volScalarField Deff_O2_3
    (
    "Deff_O2_3",
    ((DO2*Dk_O2*selectionvalue/(DO2+Dk_O2))+DO2*(1-
selectionvalue))*pow(solidporosity,2)/((Ash_layer_thickness)+1e-25*unitlength)
    );

volScalarField Deff_CO2_3
    (
    "Deff_CO2_3",
    ((DCO2*Dk_CO2/(DCO2+Dk_CO2)*selectionvalue)+DCO2*(1-
selectionvalue))*pow(solidporosity,2)/(Ash_layer_thickness+1e-25*unitlength)
    );

volScalarField Deff_CO_3
    (
    "Deff_CO_3",
    ((DCO*Dk_CO/(DCO+Dk_CO)*selectionvalue)+DCO*(1-
selectionvalue))*pow(solidporosity,2)/(Ash_layer_thickness+1e-25*unitlength)
    );

volScalarField Deff_H2O_3
    (
    "Deff_H2O_3",
    ((DH2O*Dk_H2O/(DH2O+Dk_H2O)*selectionvalue)+DH2O*(1-
selectionvalue))*pow(solidporosity,2)/(Ash_layer_thickness+1e-25*unitlength)
    );

volScalarField Deff_H2_3
    (
    "Deff_H2_3",
    ((DH2*Dk_H2/(DH2+Dk_H2)*selectionvalue)+DH2*(1-
selectionvalue))*pow(solidporosity,2)/(Ash_layer_thickness+1e-25*unitlength)
    );

volScalarField Deff_CH4_3
    (
    "Deff_CH4_3",
    ((DCH4*Dk_CH4/(DCH4+Dk_CH4)*selectionvalue)+DCH4*(1-
selectionvalue))*pow(solidporosity,2)/(Ash_layer_thickness+1e-25*unitlength)
    );

volScalarField Deff_N2_3
    (
    "Deff_N2_3",
    ((DN2*Dk_N2/(DN2+Dk_N2)*selectionvalue)+DN2*(1-
```

```
selectionvalue))*pow(solidporosity,2)/(Ash_layer_thickness+1e-25*unitlength)
    );


volScalarField hmO2
   (
   "hmO2",
   kmO2*Deff_O2_3/(kmO2+(Deff_O2_3))
   );

//hmCO2
volScalarField hmCO2
   (
   "hmCO2",
   kmCO2*Deff_CO2_3/(kmCO2+(Deff_CO2_3))
   );

//hmCO
volScalarField hmCO
   (
   "hmCO",
   kmCO*Deff_CO_3/(kmCO+(Deff_CO_3))
   );
//hmH2
volScalarField hmH2
   (
   "hmH2",
  kmH2*Deff_H2_3/(kmH2+(Deff_H2_3))
   );

//hmH2O
volScalarField hmH2O
   (
   "hmH2O",
   kmH2O*Deff_H2O_3/(kmH2O+(Deff_H2O_3))
   );

//hmCH4
volScalarField hmCH4
   (
   "hmCH4",
  kmCH4*Deff_CH4_3/(kmCH4+(Deff_CH4_3))
   );

//hmN2
volScalarField hmN2
   (
   "hmN2",
 kmN2*Deff_N2_3/(kmN2+(Deff_N2_3))
   );


//Effective Diffusion coefficient

volScalarField Deff_O2
    (
    "Deff_O2 ",
    Deff_O2bed+DO2*(1-selectionvalue)
    );

volScalarField Deff_CO2
    (
    "Deff_CO2",
    Deff_CO2bed+DCO2*(1-selectionvalue)
    );

volScalarField Deff_CO
    (
    "Deff_CO",
   Deff_CObed+DCO*(1-selectionvalue)
    );
```

```
volScalarField Deff_H2O
    (
    "Deff_H2O",
    Deff_H2Obed+DH2O*(1-selectionvalue)
    );

volScalarField Deff_H2
    (
    "Deff_H2",
   Deff_H2bed+DH2*(1-selectionvalue)
    );

volScalarField Deff_CH4
    (
    "Deff_CH4",
    Deff_CH4bed+DCH4*(1-selectionvalue)
    );

volScalarField Deff_N2
    (
    "Deff_N2",
     Deff_N2bed+DN2*(1-selectionvalue)
    );
```

shrinkage.H

```
//calculation packed bed shrinkage
dimensionedScalar
Vbed_o=fvc::domainIntegrate(mMoisture_o+mWood_o)/((2.595*(dp_o*1000/unitlength)+137.0
8)*rhoc);

bulkdensityfactor2=fvc::domainIntegrate(mMoisture+mWood+mchar+mash)/(fvc::domainInteg
rate(pos(mWood+mMoisture+mchar+mash-95*rhoc))+1e-10*unitvolume);


bulkdensityfactor2=bulkdensityfactor2*pos(2500*rhoc-
bulkdensityfactor2)+2500*rhoc*neg(2500*rhoc-bulkdensityfactor2);


Vbed=TotalMass/(bulkdensityfactor2+1e-10*rhoc);
Vbedlimit=Vbed.oldTime();
Vbed=Vbed*pos(Vbedlimit-Vbed)+Vbedlimit*neg(Vbedlimit-Vbed);


Ub=-(Vbed.oldTime()-Vbed)*(Vbed_o/(0.09*unitvolume)-
(ydistance/unitlength))*shrinkagevector*selectionvalue*1.3/((Vbed+1e-
10*unitvolume)*(runTime.deltaT()/Time))*neg(mag(Ub)-0.1*unitlength/Time);
Ubed=Ub*neg(mag(Ub)-0.1*unitlength/Time);
```

phibed.H

```
//calculation of face flux
surfaceScalarField phibed
     (
      "phibed",
       linearInterpolate(Ubed) & mesh.Sf()
     );
surfaceScalarField phimass
     (
      "phimass",
       fvc::interpolate(solidwetmass)*phibed
     );
surfaceScalarField phicp
     (
      "phicp",
       fvc::interpolate(rhosolid*Cps*(1-bedporosity))*phibed
     );
```

Reactionrates.H

```
//Mixing rates of gases in packed bed

volScalarField rCO_oxidationmix
   (
   "rCO_oxidationmix",
    0.63*1.75*(1-bedporosity)*mag(U)/(0.5*0.025*unitlength)*(CO*MCO*neg(CO-
O2/2)+O2*MO2/2*pos(CO-O2/2))
   );

volScalarField rCO_H2Omix
   (
   "rCO_H2Omix",
    0.63*1.75*(1-bedporosity)*mag(U)/(0.5*0.025*unitlength)*(CO*MCO*neg(CO-
H2O)+H2O*MH2O*pos(CO-H2O))
   );

volScalarField rCO2_H2mix
   (
   "rCO2_H2mix",
    0.63*1.75*(1-bedporosity)*mag(U)/(0.5*0.025*unitlength)*(CO2*MCO2*neg(CO2-
H2)+H2*MH2*pos(CO2-H2))
   );

volScalarField rCH4_oxidationmix
   (
   "rCH4_oxidationmix",
    0.63*1.75*(1-bedporosity)*mag(U)/(0.5*0.025*unitlength)*(CH4*MCH4*neg(CH4-
O2/1.5)+O2*MO2/1.5*pos(CH4-O2/1.5))
   );

volScalarField rH2_oxidationmix
   (
   "rH2_oxidationmix",
    0.63*1.75*(1-bedporosity)*mag(U)/(0.5*0.025*unitlength)*(H2*MH2*neg(H2-
O2/2)+O2*MO2*pos(H2-O2/2))
   );

//selection of minimum reaction rates for gases

volScalarField rCO_oxidation
   (
   "rCO_oxidation",
   -rCO_oxidationmix*pos(mag(rkCO_oxidation)-mag(rCO_oxidationmix))+(-
rkCO_oxidation)*neg(mag(rkCO_oxidation)-mag(rCO_oxidationmix))
   );

volScalarField rCO_H2O
   (
   "rCO_H2O",
   -rCO_H2Omix*pos(mag(rkCO_H2O)-mag(rCO_H2Omix))+(-rkCO_H2O)*neg(mag(rkCO_H2O)-
mag(rCO_H2Omix))
   );

volScalarField rCO2_H2
   (
   "rCO2_H2",
   -rCO2_H2mix*pos(mag(rkCO2_H2)-mag(rCO2_H2mix))+(-rkCO2_H2)*neg(mag(rkCO2_H2)-
mag(rCO2_H2mix))
   );

volScalarField rCH4_oxidation
   (
   "rCH4_oxidation",
   rCH4_oxidationmix*pos(mag(rkCH4_oxidation)-mag(rCH4_oxidationmix))+(-
rkCH4_oxidation)*neg(mag(rkCH4_oxidation)-mag(rCH4_oxidationmix))
   );

volScalarField rH2_oxidation
   (
   "rH2_oxidation",
```

```
  -rH2_oxidationmix*pos(mag(rkH2_oxidation)-mag(rH2_oxidationmix))+(-
rkH2_oxidation)*neg(mag(rkH2_oxidation)-mag(rH2_oxidationmix))
   );
```

TsEqn.H

```
//Solid phase energy equation:

fvScalarMatrix TsEqn
    (
       fvm::ddt((rhosolid*Cps*(1-bedporosity))+x,Ts)

    + fvm::div(phicp,Ts)

       - fvc::laplacian(DTs,Ts)
    );

solve(TsEqn==-h*(Ts-Tg)*A*selectionvalue-Dryingheat-woodheat+HC_O2-HC_CO2-
HC_H2O+HC_H2+ignitionarea*ignitionheat*pos(1200-
shrinkagetemperature)+(abscoeffsolid*G-
4*abscoeffsolid*sigma*pow(Ts,4))*selectionvalue/unitlength);
Ts = Ts*pos(Ts-300*Temp)+300*Temp*neg(Ts-300*Temp);
Ts = Ts*pos(selectionvalue-1)+300*Temp*pos(-selectionvalue);
```

solidmassconservationEqn.H

```
//solve equations for solid species conservation//


//solve wood conservation equation;
 fvScalarMatrix mWoodEqn
        (
           fvm::ddt(mWood)
        +fvm::div(phibed, mWood)
        );
solve (mWoodEqn == RWood);



//solve char conservation equation;
fvScalarMatrix mcharEqn
        (
           fvm::ddt(mchar)
        +fvm::div(phibed, mchar)
        );
solve (mcharEqn == -0.145*(RWood)+Rgasification+Rcombustion);


//solve Ash conservation equation;
fvScalarMatrix mashEqn
        (
            fvm::ddt(mash)
            +fvm::div(phibed, mash)
        );
solve (mashEqn == -0.005*(RWood));


//solve moisture conservation equation;
 fvScalarMatrix YMoistureEqn
        (
           fvm::ddt(solidwetmass,YMoisture)
       +fvm::div(phimass, YMoisture)
        );
solve (YMoistureEqn==Rdrying);


mWood = pos(mWood-0*rhoc)*mWood+neg(mWood-0*rhoc)*0*rhoc;
YMoisture=pos(YMoisture-0)*YMoisture+neg(YMoisture-0)*0;
mMoisture=YMoisture*solidwetmass;
mchar = pos(mchar-0*rhoc)*mchar+neg(mchar-0*rhoc)*0*rhoc;
mash = pos(mash-0*rhoc)*mash+neg(mash-0*rhoc)*0*rhoc;
```

APPENDIX B - OpenFoam Programme for Moving Grate Combustion

```
/*---------------------------------------------------------------------------*\
  =========                 |
  \\      /  F ield         | OpenFOAM: The Open Source CFD Toolbox
   \\    /   O peration     |
    \\  /    A nd           | Copyright (C) 2011-2013 OpenFOAM Foundation
     \\/     M anipulation  |
-------------------------------------------------------------------------------
License
    This file is part of OpenFOAM.

    OpenFOAM is free software: you can redistribute it and/or modify it
    under the terms of the GNU General Public License as published by
    the Free Software Foundation, either version 3 of the License, or
    (at your option) any later version.

    OpenFOAM is distributed in the hope that it will be useful, but WITHOUT
    ANY WARRANTY; without even the implied warranty of MERCHANTABILITY or
    FITNESS FOR A PARTICULAR PURPOSE.  See the GNU General Public License
    for more details.

    You should have received a copy of the GNU General Public License
    along with OpenFOAM.  If not, see <http://www.gnu.org/licenses/>.

Application
    movinggrateFoam

Description
    Transient solver for incompressible, laminar flow of Newtonian fluids.

\*---------------------------------------------------------------------------*/

#include "fvCFD.H"
#include "fvcVolumeIntegrate.H"
#include "pisoControl.H"
#include "OFstream.H"
#include "wallDist.H"
#include "fvOptions.H"

// * * * * * * * * * * * * * * * * * * * * * * * * * * * * * * * * * * * * //

int main(int argc, char *argv[])
{
    #include "setRootCase.H"
    #include "createTime.H"
    #include "createMesh.H"
    pisoControl piso(mesh);
    #include "createFields.H"
    #include "nut.H"
    #include "initContinuityErrs.H"


    // * * * * * * * * * * * * * * * * * * * * * * * * * * * * * * * * * * * //

    Info<< "\nStarting time loop\n" << endl;

    while (runTime.loop())
    {
        Info<< "Time = " << runTime.timeName() << nl << endl;


   volScalarField nu
     (
      "nu",
       (1.98e-5)*nu_c*(Tg/(300*Tc))/(rhog/rhoc)
     );
```

```
      volScalarField nuporosity
      (
       "nuporosity",
        nu*bedporosity
      );
      volScalarField nutporosity
      (
       "nutporosity",
        nut*bedporosity
      );
     volTensorField velocityGradient
      (
       "velocityGradient",
        fvc::grad(U)
      );
     volTensorField S
      (
       "S",
        0.5*(velocityGradient+T(velocityGradient))
      );
       volScalarField SintoS
      (
       "SintoS",
        S && S
      );
   volTensorField turbulance
      (
       "turbulance",
        2*nut*S-2/3*(k+ksmall)*I
      );

volVectorField momentumresistance
      (
       "momentumresistance",
    ( selectionvalue*150*(1-0.5)*(1-0.5)*nu/((dp_o)*(dp_o)*0.5*0.5)*mag(U)*(-
shrinkagevector)+1.75*(1-0.5)/((dp_o)*0.5)*mag(U)*mag(U)*(-
shrinkagevector))*(Time/unitlength)
      );


   #include "particlesize.H"
   #include "variables.H"
   #include "Gasdiffusioninsideparticle.H"
   #include "shrinkagenew.H"
   #include "phibed.H"
   #include "solid.H"
   #include "Reactionrates.H"

// Solve Gas Phase Velocity and Pressure Equations:

  fvVectorMatrix UEqn
        (
            fvm::ddt(bedporosity, U)
          + fvm::div(phis, U)
          - fvm::laplacian(nuporosity, U)
        );

      solve(UEqn ==-fvc::grad(p)*bedporosity-fvc::div(turbulance)-
momentumresistance);


        // --- PISO loop

        while (piso.correct())
        {
            volScalarField rAU(1.0/UEqn.A());
            volVectorField HbyA(constrainHbyA(rAU*UEqn.H(), U, p));
            surfaceScalarField phisHbyA
            (
                "phisHbyA",
                fvc::flux(HbyA)
              + fvc::interpolate(rAU)*fvc::ddtCorr(U, phis)
```

```
            );

            adjustPhi(phisHbyA, U, p);

            // Update the pressure BCs to ensure flux consistency
            constrainPressure(p, U, phisHbyA, rAU);

            // Non-orthogonal pressure corrector loop
            while (piso.correctNonOrthogonal())
            {
                // Pressure corrector

                fvScalarMatrix pEqn
                (
                    fvm::laplacian(rAU, p)==
(1/bedporosity)*fvc::div(phisHbyA)+gasgeneration/rhog
                );

                pEqn.setReference(pRefCell, pRefValue);

                pEqn.solve(mesh.solver(p.select(piso.finalInnerIter())));

                if (piso.finalNonOrthogonalIter())
                {
                    phis = phisHbyA - pEqn.flux();
                }
            }

            #include "continuityErrs.H"

            U = HbyA - rAU*fvc::grad(p);
            U.correctBoundaryConditions();
        }
// --End Piso loop


#include "kepsilon.H"
#include "heatrelease.H"
#include "radiation2.H"
#include "phicp.H"
#include "TgEqn.H"
#include "TsEqn.H"
#include "TgrateEqn.H"
#include "gasspeciesconservationEqn.H"
#include "solidmassconservationEqn.H"


     runTime.write();


        Info<< "ExecutionTime = " << runTime.elapsedCpuTime() << " s"
            << "  ClockTime = " << runTime.elapsedClockTime() << " s"
            << nl << endl;
    }

    Info<< "End\n" << endl;

    return 0;
}
// ************************************************************************* //
```

phibed.H

```
//calculation of face fluxes due to bed shrinkage and grate movement

surfaceScalarField phibed
     (
      "phibed",
       linearInterpolate(Ubed) & mesh.Sf()
     );
surfaceScalarField phimass
     (
      "phimass",
```

```
       fvc::interpolate(solidwetmass25*rhoc)*phibed
     );
surfaceScalarField phimassx
     (
      "phimassx",
linearInterpolate(Ugrate*(solidwetmass25*rhoc)) & mesh.Sf()
        //fvc::interpolate(ttsolidwetmass)*phigrate
     );
surfaceScalarField phicp
     (
      "phicp",
      linearInterpolate((mWood+mchar+mash+mMoisture)*Cps*Ubed) & mesh.Sf()
     );
surfaceScalarField phigratecp
     (
      "phigratecp",
      fvc::interpolate((mWood+mchar+mash+mMoisture)*Cps)*phigrate
     );
```

TsEqn.H

```
//Solid phase energy equation:

fvScalarMatrix TsEqn
    (
       (fvm::ddt(((mWood+mchar+mash+mMoisture)*Cps)+x,Ts)

     +fvm::div(phicp,Ts)
     +fvc::div(phigratecp,Ts)
        -fvc::laplacian(DTs,Ts)
     +h*(Ts-Tg)*A*neg(0-selectionvalue)+Dryingheat+woodheat-HC_O2+HC_CO2+HC_H2O-
HC_H2-(abscoeffsolid*G-4*abscoeffsolid*sigma*pow(Ts,4))*neg(0-
selectionvalue)/unitlength)
    );
TsEqn.solve();
TsEqn.setValues(removedCells, valuesToImpose);
Ts = Ts*pos(Ts-300*Temp)+300*Temp*neg(Ts-300*Temp);
Ts=Ts*pos(1500*Temp-Ts)+1500*Temp*neg(1500*Temp-Ts);
```

solidmassconservationEqn.H

```
//solve equations for solid species conservation//


//solve wood conservation equation;
 fvScalarMatrix mWoodEqn
        (
           fvm::ddt(mWood)
        +fvm::div(phibed, mWood)
        +fvc::div(phigrate, mWood)
        -RWood
        );
mWoodEqn.solve();


//solve char conservation equation;

fvScalarMatrix mcharEqn
        (
           fvm::ddt(mchar)
        +fvm::div(phibed, mchar)
        +fvc::div(phigrate, mchar)
        +0.15*(RWood)-Rgasification-Rcombustion
        );
mcharEqn.solve();


//solve Ash conservation equation;

fvScalarMatrix mashEqn
        (
            fvm::ddt(mash)
            +fvm::div(phibed, mash)
      +fvc::div(phigrate, mash)
```

```
         +0.034*(Rgasification+Rcombustion)
        );
mashEqn.solve();


//solve moisture conservation equation;
fvScalarMatrix YMoistureEqn
        (
           fvm::ddt(YMoisture)
        +fvm::div(phibed, YMoisture)
        +fvc::div(phigrate, YMoisture)
         -Rdrying/(solidwetmass+1e-25*rhoc)
        );
YMoistureEqn.solve();

dimensionedScalar moisturefactor=(sum(YMoisture_o))/sum(one*neg(0-
selectionvalue_o))*rhoc;
dimensionedScalar woodfactor=(sum(mWood_o))/sum(one*neg(0-selectionvalue_o));
mWood = pos(mWood-0*rhoc)*mWood+neg(mWood-0*rhoc)*0*rhoc;
YMoisture=pos(YMoisture-0)*YMoisture+neg(YMoisture-0)*0;
YMoisture=pos(0*rhoc-mWood)*0+neg(0*rhoc-mWood)*YMoisture;
YMoisture=pos(moisturefactor-YMoisture)*YMoisture+neg(moisturefactor-
YMoisture)*moisturefactor*pos(mWood-mWood_o)+neg(moisturefactor-YMoisture)*neg(mWood-
mWood_o)*0;
mMoisture=YMoisture*solidwetmass;
mchar = pos(mchar-0*rhoc)*mchar+neg(mchar-0*rhoc)*0*rhoc;
mash = pos(mash-0*rhoc)*mash+neg(mash-0*rhoc)*0*rhoc;
```

APPENDIX C - List of Papers

Journal Papers published

Paper I - **Perera K.U.C.**, Narayana M., Kissinger method: the sequential approach and DAEM for kinetic study of rubber and gliricidia wood, *J.National Science Foundation Sri Lanka 2018 46 (2): 187 - 196 DOI: http://dx.doi.org/10.4038/jnsfsr.v46i2.8419*- Indexed in Science Citation Index Expanded

Paper II - Perera **K.U.C.**, Narayana M., Modelling of Particle Size Effect on Equivalence Ratio Requirement for Wood Combustion in Fixed Beds, *Biomass Conversion and Biorefinery*, 2018,- Indexed in Science Citation Index Expanded

Conference papers presented

Paper III - **Perera K.U.C.**, Narayana M., Finite Volume Analysis of Biomass Particle Pyrolysis, *2017 Moratuwa Engineering Research Conference (MERCon)*- Indexed in SCOPUS

Conference papers accepted

Paper IV- **Perera K.U.C.**, Narayana M., Witharana S. Numerical Modelling of Biomass Combustion on Moving Grates, *Renewable and Sustainable Energy Conference,(ASET 2019)*- Indexed in SCOPUS

Papers presented in IESL conference

Paper V- **Perera K.U.C.**, Narayana M., Numerical Simulation of Carbon Dioxide Capture in Rubber Wood Gasification, *112th Annual sessions IESL, 2018.*